Volume 2, Number 1
March 1987

ISSN: 0127-7065

JOURNAL OF NATURAL RUBBER RESEARCH

Continuation of the Journal of the Rubber Research Institute of Malaysia

Price: Malaysia: 30 Ringgit Per Issue
100 Ringgit Per Volume
Overseas: US$15 Per Issue
US$50 Per Volume

JOURNAL OF NATURAL RUBBER RESEARCH

Rubber Research Institute of Malaysia (RRIM)
Malaysian Rubber Research and Development Board (MRRDB)
Malaysian Rubber Producers' Research Association (MRPRA)

Each volume of the Journal of Natural Rubber Research constitutes four issues published quarterly in March, June, September and December each year.

Published by the Rubber Research Institute of Malaysia
(A Statutory Agency under the Ministry of Primary Industries)
Printed by Percetakan Sinar Suria
March 1987

Contents

J. nat. Rubb. Res.
2(1), March 1987

J. nat. Rubb. Res., **2(1)**, 1-14

Rubber Friction Dependence on Roughness and Surface Energy

S.P. ARNOLD*, A.D. ROBERTS* AND A.D. TAYLOR*

When a smooth surfaced rubber sphere slides on glass relative motion between surfaces may be only due to 'waves of detachment' (Schallamach waves) crossing the contact region. Remarkably enough, the observed friction scarcely depends on sliding speed, temperature or rubber type of similar hardness, despite rubber being a viscoelastic material. This is in sharp contrast to the 'classical results' of Grosch. His friction data for a wide range of speeds and temperatures showed a pronounced maximum in the friction with increasing rate, a characteristic to be expected if viscoelastic processes are involved. New measurements are helping to resolve the paradox. Schallamach waves act as a stress relieving mechanism which prevents a substantial rise in friction with rate.

If smooth surfaced rubber samples are deliberately roughened with abrasive, then the friction varies with speed and temperature in a manner more in accord with Grosch's data. Apparently, surface roughness is important to an overtly viscoelastic response. It also seems to suppress the generation of Schallamach waves, and cause the track surface energy to be reflected in the level of friction.

It is difficult to predict the likely level of friction of rubber components in engineering practice. Model experiments must often be carried out and sometimes full-scale tests are the only acceptable way, such as in tyre skid resistance. Many factors contribute to the friction of a rubber surface, and the topology of the track may matter as much as the rubber. Grosch[1] suggested ideas for prediction when he found, at least in his laboratory tests, that the frictional behaviour of different rubber vulcanisates could be anticipated according to their viscoelastic properties. In general it is observed that the frictional force F for a given load W rises with increasing sliding speed[2]. Grosch showed that there was a characteristic peak to the friction of a particular rubber and beyond that the friction fell with increasing speed. The effect of temperature could also be related through the WLF[3] shift factor a_T so that under certain circumstances Grosch was able to obtain his classical 'master curves' of friction coefficient μ ($=F/W$) against reduced rate $lg\ a_T V$. In this notation V is the sliding speed and $lg\ a_T = -8.86\ (T - Tg - 50) / (51.5 + T - Tg)$, where T is the test temperature and Tg is the glass transition temperature of the particular rubber under test. The master curves were subsequently employed to predict, for example, tyre tread skid performance and have enjoyed a considerable measure of success.

The discovery of Schallamach waves[4] initiated new investigations into friction mechanics with a view to predicting the level of rubber friction in terms of viscoelastic and surface properties. It soon emerged that under circumstances where Schallamach waves were generated the sliding friction was surprisingly invariant with speed[5,6], with vulcanisate[7] and with temperature[8]. Apparently the rubber was not behaving in a viscoelastic manner. How can this be explained and how does it affect friction prediction?

It is now appreciated that Schallamach waves arise as an elastic instability in the rubber[4,5,9] and consequently the level of friction is determined by its elastic modulus[10]. One of these

*Malaysian Rubber Producers' Research Association, Brickendonbury, Hertford SG13 8NL, United Kingdom

studies[9] agreed that in general the sliding friction was constant with speed and temperature; in sharp contrast to Grosch's data.

More recently this apparent contradiction was investigated in a systematic way by repeating the experiments of Grosch using the same rubber compound, pad dimensions and wavy glass[11]. It was still not possible to reproduce the Grosch data. In this latest study smooth rubber surfaces were employed, in common with many earlier studies. At the time of the study it came to light[12] that in his earlier work Grosch[1] had used rubber samples deliberately roughened in order to avoid complications due to surface oxidation. A few experiments were carried out at room temperature[11] in which rubber samples were deliberately roughened but surprisingly there was only a modest fall in friction. This made it difficult to rationalise with the earlier Grosch data. However, because the effect of roughness was only studied at room temperature, we decided to mount a more complete examination of the friction of surface roughened rubber samples over a broad range of temperatures.

In this paper we report measurements of the friction of smooth and roughened rubber samples against wavy glass. These will show how, with changing surface roughness, the master curve changes towards that obtained by Grosch. We also note that with rough surfaces, not only is there a more pronounced viscoelastic behaviour but also a response to track surface energy.

EXPERIMENTAL

The investigation consists of three distinct experiments. A 'deep freeze' apparatus[8,11] was used for the friction of rubber on wavy glass, with varied temperature and sliding speed. A cantilever apparatus was used for the frictional shear strength of rubber against a flat track, with varied speed and normal load. A simple rolling apparatus was employed to examine the variation in peel energy with speed.

Friction of Flat Rubber Against Wavy Glass

The experiments were carried out inside a deep freeze cabinet, covering temperatures from $-45°C$ to $+60°C$; with dry ice to take it below $-35°C$ and electric light bulbs to heat it above room temperature. The temperature could be maintained to $\pm 2°C$ using a mercury contact thermometer installed through the lid.

The wavy glass track was supported on a turntable driven by an electrically powered hydraulic motor *via* a five speed gearbox. Speeds from 0.01 mm per second to 10 mm per second were used. The rubber pad was attached to the end of a lever arm on which a chosen load was applied to press it down on the wavy grass track *(Figure 1a)*. The normal load was 57 N unless otherwise stated. The tangential force between the rubber and the glass was measured using a load cell transducer fixed to the other end of the lever arm. Full details of the apparatus have been given previously[8,11].

The rubber pads were made from a natural rubber (NR) specimen whose rate of crystallisation had been considerably decreased by an isomerisation process which reduces the *cis*-double bond content of the rubber by about one-half. This material is subsequently referred to as isomerised natural rubber (INR), see *Table 1*. This compound is very similar to the rubber *Type E* used by Grosch[1], and has the advantage of crystallising slowly at low temperatures, which helps to minimise complications in the frictional behaviour of NR. Its glass transition temperature was measured by differential scanning calorimetry (DSC) and is $-72°C \pm 1°C$. Its hardness was measured using an indentation hardness meter (reading accuracy ± 2) and the mean of many readings was 43.3 IRHD at 20°C. This corresponds to a Young's modulus of 1.72 MPa. The rubber pads were 10 mm thick and had a sliding area of 645 mm^2. For rough rubber the pads were roughened by rubbing with 180 grade emery paper (Tri-M-ite). This was done by hand in a controlled manner using both circular (swirling) and linear motion. The surface roughness was measured with a Talysurf 10. Smooth rubber gave 0.23 μm CLA (± 0.17 μm) after cleaning; 0.34 μm CLA (± 0.22 μm) before the bloom was removed. The roughened rubber had roughnesses of 4 μm CLA (± 0.2 μm). There was an intermediate pad with a roughness of

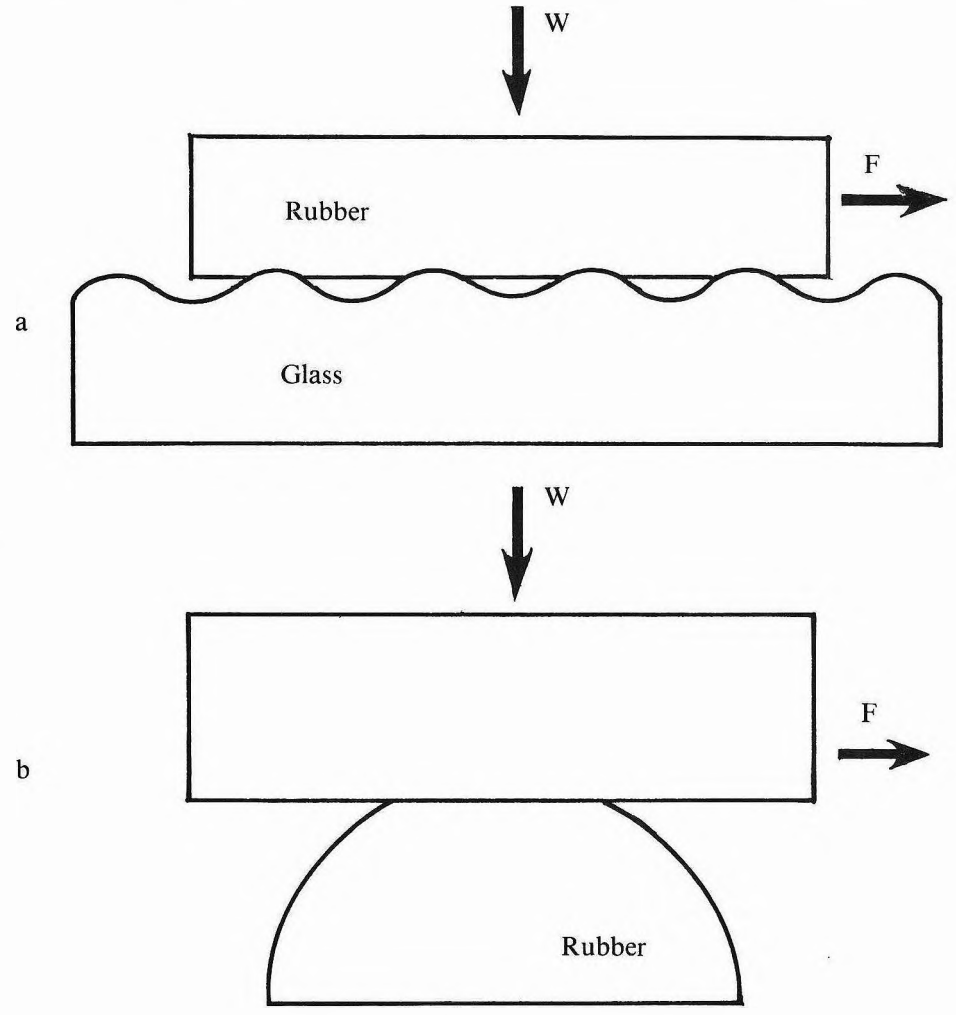

Figure 1. Contact geometries.

1.5 μm CLA (± 0.9 μm). It is noted that most of the roughness measurements were distributed reasonably closely to the mean. The glass surface is made up of gentle adjacent individual bumps and gives a roughness value of 125 μm CLA.

Just before friction tests were carried out the rubber was cleaned with a variety of solvents to remove bloom and dust. The solvents were acetone, isopropanol and 10% acetylacetone in isopropanol. The glass was cleaned with acetone followed by isopropanol.

Friction of Rubber Hemisphere Against Flat Rigid Track

The apparatus consisted of a rubber hemisphere fixed to the stage of a microscope which was driven by an electric motor *via* a gear box. The travel distance available was 27 mm. Sliding speeds between 0.0019 mm per second and 17 mm per second could be achieved. The rigid track was part of a balanced arm and rested under an applied load on the rubber hemisphere *(Figure 1b)*. When transparent, the

TABLE 1. RUBBER COMPOUND FORMULATIONS (PARTS BY WEIGHT)

Compound	INR	NR
NR (SMR L)		100
INR (59% trans)	100	
Stearic acid	1	2
Zinc oxide	5	5
Sulphur	1.45	2.5
N-isopropyl-N-phenyl-p-p-phenylenediamine (Nonox ZA)		1
N-tert-butylbenzothiazole-2-sulphenamide		0.5
N-cyclohexylbenzothiazole-2-sulphenamide (Santocure CBS)	0.4	
Poly-2,2,4-trimethyl-1, 2-dihydroquinoline	1	
Cure time/temperature (min/°C)	35/140	40/140
Hardness (IRHD)	43.3	42.5
Young's modulus (MPa)	1.72	1.65
Glass transition temperature	−72	−69

IRHD = International Rubber Hardness Degrees

contact area could be viewed through it from above, using a low power microscope and normally incident illumination for good optical contrast.

The contact area could be measured using a scale in the microscope eyepiece and for static contact it was generally found to agree well with the Hertz theory[13]. For the sake of consistency the Hertzian area was used in all calculations. It was not possible to measure the area accurately when the rubber was moving. The traction force applied by the rubber on the rigid surface in the driven direction (horizontal) was detected by a cantilever arrangement *(Figure 2)* on the balanced arm. The bending of the leaf springs under an applied force was measured by a four arm strain gauge bridge, the output of which was amplified and recorded on a chart recorder.

The rubber vulcanisate used was sulphur cured NR *(Table 1)*. Its glass transition temperature was measured by DSC to be −69°C. Its modulus, deduced from measurements in IRHD was 1.65 MPa. The rubber hemispheres were either smooth or deliberately roughened by hand with 180 grade emery paper (Tri-M-ite). The roughnesses correspond to those of the pads above for smooth and fully roughened rubber respectively.

If there appeared to be bloom on the hemisphere it was cleaned once with 10% acetylacetone in isopropanol before being used for experiments. Before each experiment (a change in surface or speed) both surfaces were cleaned with isopropanol and allowed to dry for at least 20 minutes.

Adhesion of Rubber to Different Flat Tracks

Rolling experiments were completed for the NR vulcanisates on a series of flat tracks as used for friction experiments in friction of rubber hemisphere against flat rigid track. A sheet of 2 mm thick rubber was stuck around a 'Perspex' roller, total weight 0.5 N and radius 35.5 mm. The rubber roller thus formed was rested gently at the top of the sloping rigid track and released, the time between two fixed points being recorded[14]. Both surfaces were cleaned with isopropanol and allowed to dry for 20 min before each roll.

RESULTS

Friction of Flat Rubber Against Wavy Glass

Figure 3 shows the results as a coefficient of friction against reduced rate, using the Williams-Landel-Ferry equation[1,3,5,11] with a standard reference temperature of $Tg + 50°C$. Starting with the smooth rubber (0.2 μm CLA) good agreement is seen with a previous study[11] under identical conditions. The friction varies little with speed and temperature. For the slightly rough rubber (1.49 μm CLA) (a smooth sample that became worn) the friction characteristic shows more variation with rate, rising from $\mu = 0.5$ at low rates to a peak of around $\mu = 2.4$ and then falling again. The roughened rubber (4.1 μm CLA) gives even lower (as low as 0.3) friction coefficients at low rates. However the coefficient rises steeply to a plateau and where $l_g a_T V$ is above 1, $\mu = 2.5$ in the absence of stick-slip motion.

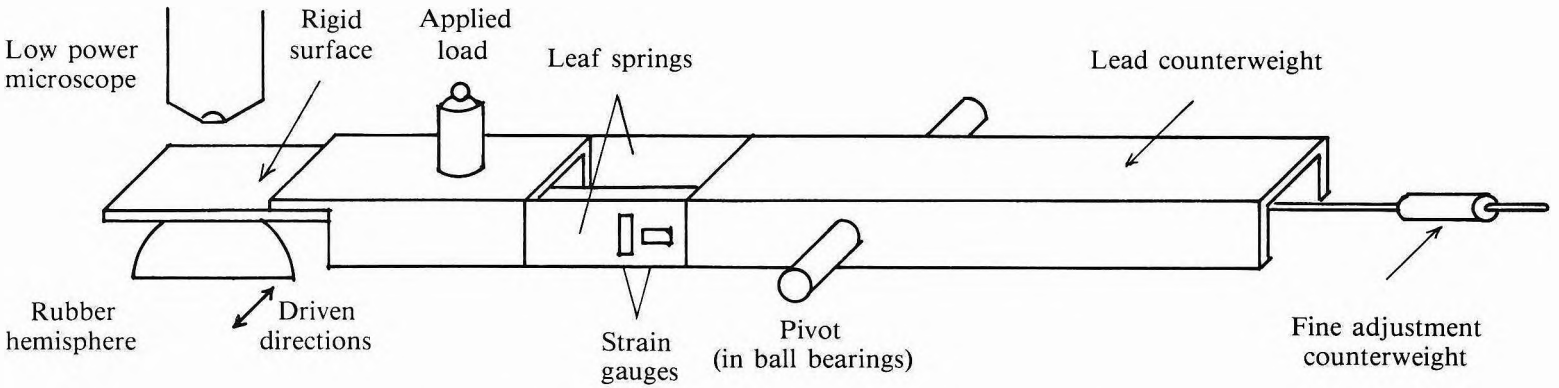

Figure 2. Apparatus for measuring interfacial shear strength.

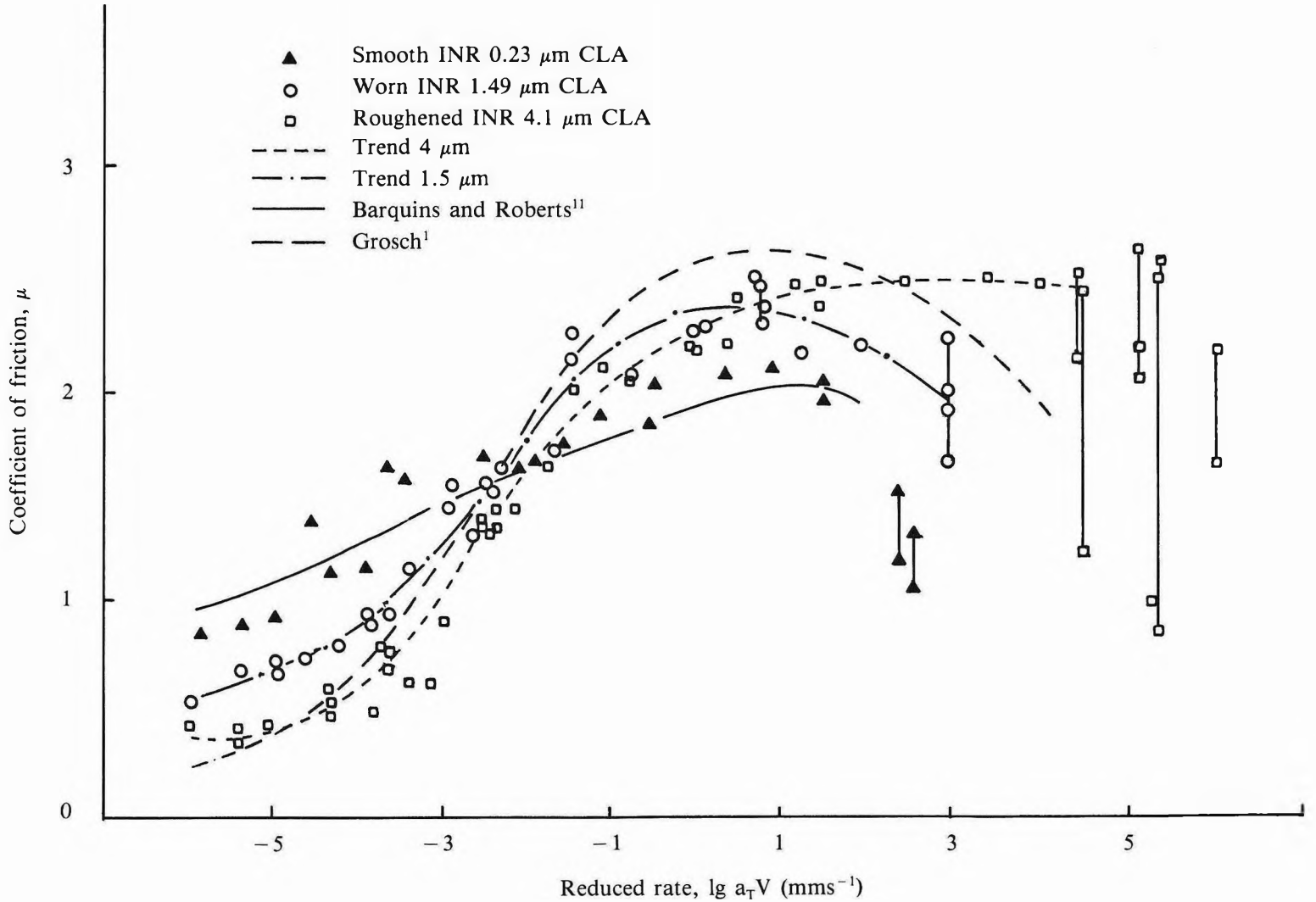

Figure 3. Friction of flat rubber against wavy glass.

Comparing the results obtained for three different levels of roughness reveals a clear pattern, the shape of the friction characteristic changing and becoming more rate sensitive with increased roughness.

Friction of Rubber Hemisphere Against Flat Rigid Track

Dependence on sliding speed. The variation of friction coefficient μ with speed, lgV, is shown in *Figure 4*. For smooth rubber against glass, well-defined Schallamach waves were observed over the whole range of speeds for which μ is constant. At lower speeds the waves diminish in size and frequency and the coefficient drops. Increasing the speed causes the waves to become stationary ridges[4] so that the relative motion is due to true sliding, and μ increases. The pattern is essentially the same for smooth rubber against polytetrafluoroethylene (PTFE) except that the interface adhesion is lower and so Schallamach waves do not occur until the speed is 0.2 mm per second. Below this speed true sliding probably occurs and the speed dependence of friction is obvious. At and above 0.2 mm per second the friction mechanism is dominated by the waves, and there is no difference in friction level between PTFE and glass.

For roughened rubber Schallamach waves were not observed, though individual asperity tips in contact with the glass plate were seen to 'twitch' from time to time. The friction coefficient showed a steady increase with speed. The contrast between this and smooth rubber suggests that the Schallamach waves are a stress relieving mechanism that limit the build up of friction with speed.

Dependence on track surface. Some measurements were carried out using six different tracks; these were smooth, flat and effectively rigid and had different surface energies. They were glass, nylon, polyethylene (PE), polypropylene (PP), polymethylmethacrylate (PMMA) and polytetrafluoroethylene (PTFE).

Figure 5 shows the friction of a smooth rubber hemisphere against these and is expressed as a shear strength τ (friction force/contact area) plotted against mean contact pressure P (normal load/contact area). Five of the surfaces give plots effectively coincident, and in these cases waves were observed if the track was transparent. Once again it is apparent that Schallamach waves act to mask differences, in this case differences between track surface energies. In the case of PTFE the friction was too low to produce waves and true sliding probably took place, except for the lowest load where a dual reading was obtained. There appeared to be two stable levels of friction and when plotted one agreed with the Schallamach wave motion associated with the first five tracks whilst the other agreed with the rest of the PTFE results. This bifurcation indicates that under these conditions the mechanism is close to the point at which true sliding ceases and waves begin. Barquins and Roberts[11] confirm that the production of waves is more likely at lower loads.

Figure 6 is the equivalent plot for roughened rubber, where Schallamach waves have not been observed. Here a wide range of friction levels is found for the six surfaces. For each, the friction increases with contact pressure producing a distinct line of data. The levels of friction appear to reflect the variation in levels of the surface energies of the tracks. Previously published measurements of rubber peel adhesion[14] show a similar pattern of behaviour. This prompted some rolling experiments to discover whether a link could be found between peel energy and the friction of roughened rubber.

Correlation with peel energy. Figure 7 shows the results of rolling experiments using the same rubber and tracks as for the friction measurements above. The data points for each track are reasonably consistent. The gradients of plots for different tracks are similar because they depend on the viscoelastic properties of the rubber. The most striking result is that these distinct lines of data fall in exactly the same order of level as the data for the shear strength of roughened rubber *(Figure 6)*. This is strong evidence for a link between the friction of roughened rubber and peeling adhesion, a link noticeably absent from the friction of smooth rubber.

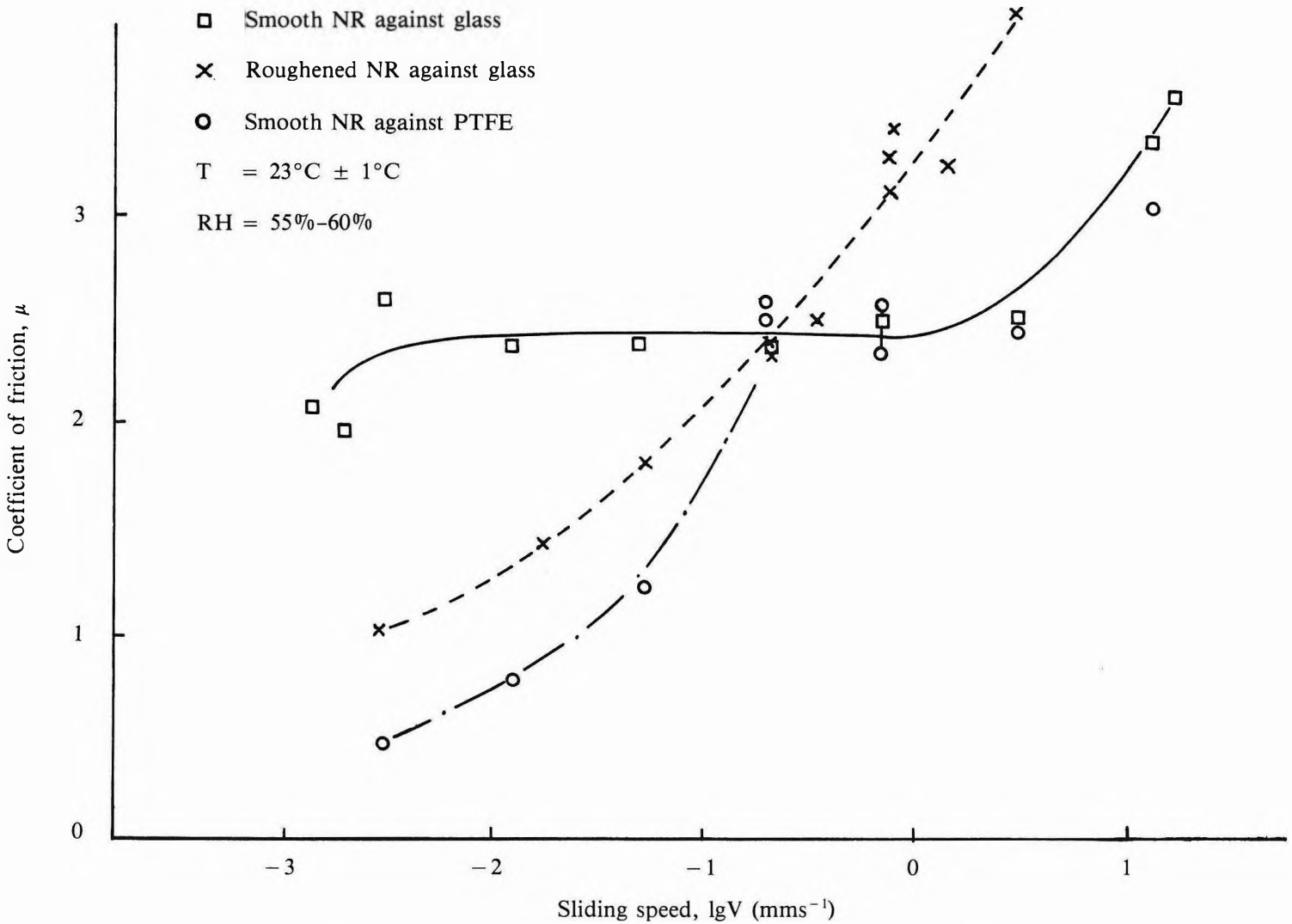

Figure 4. Speed dependence of smooth and roughened rubber.

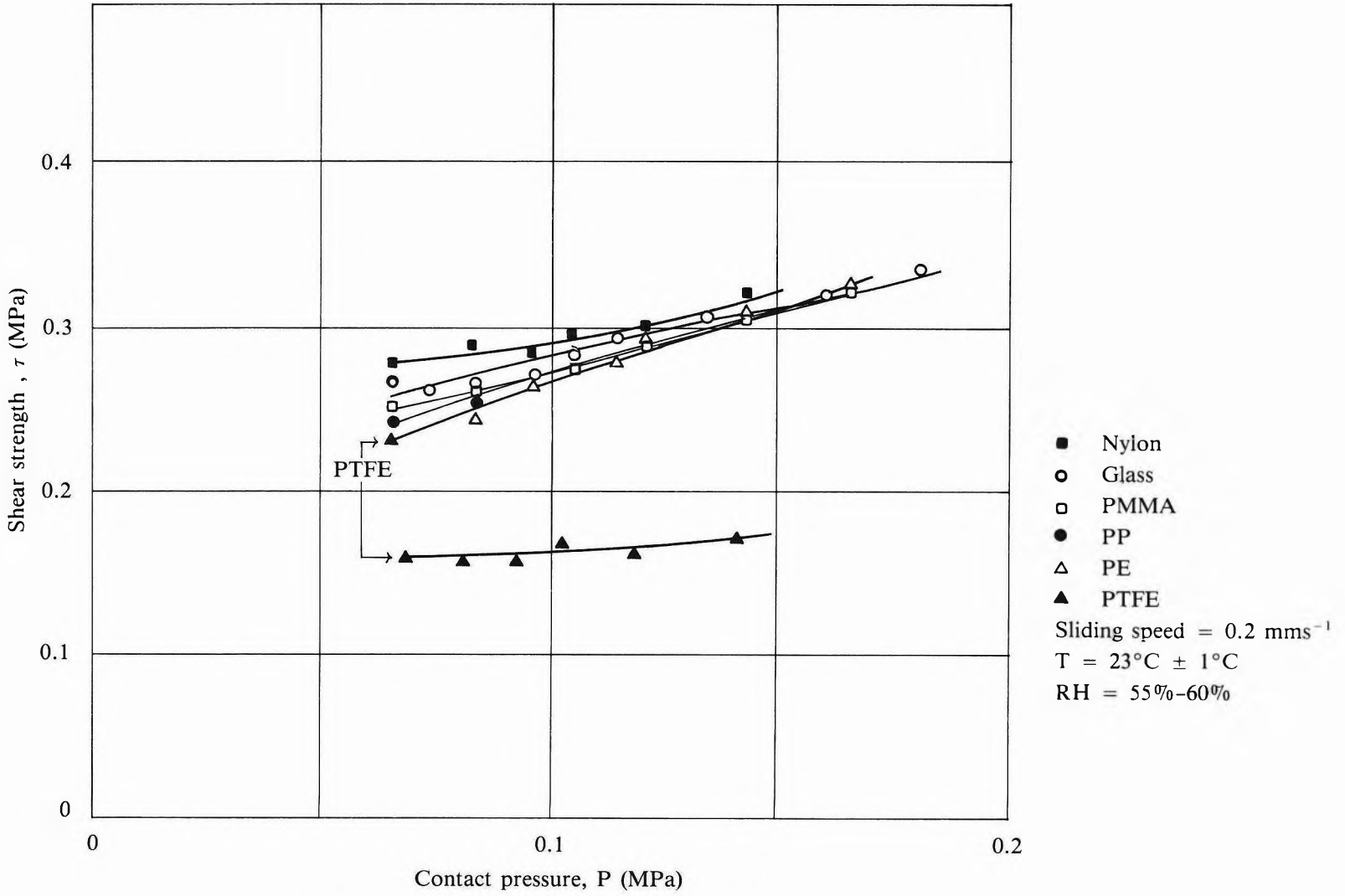

Figure 5. Smooth rubber against various substrates.

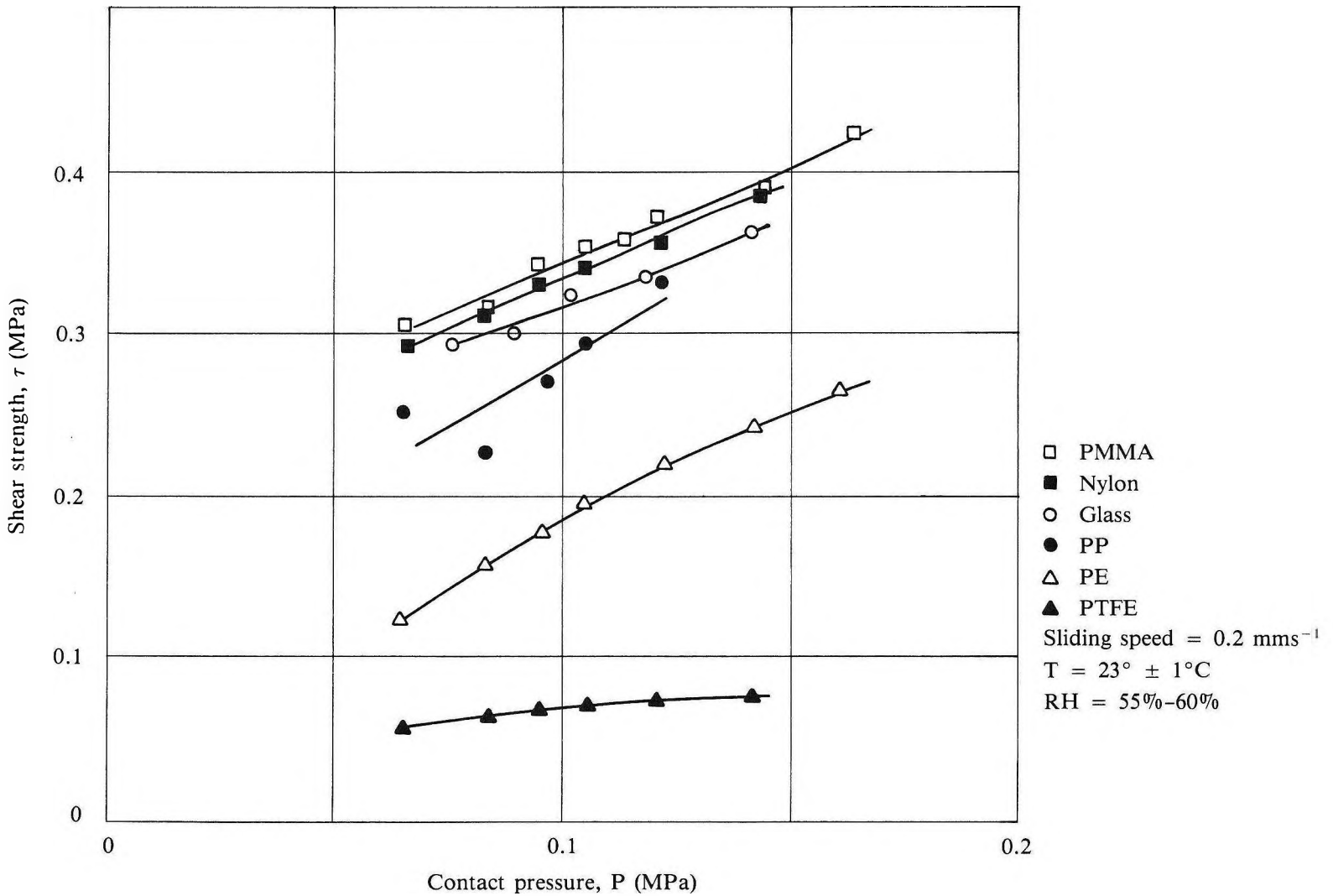

Figure 6. Roughened rubber against various substrates.

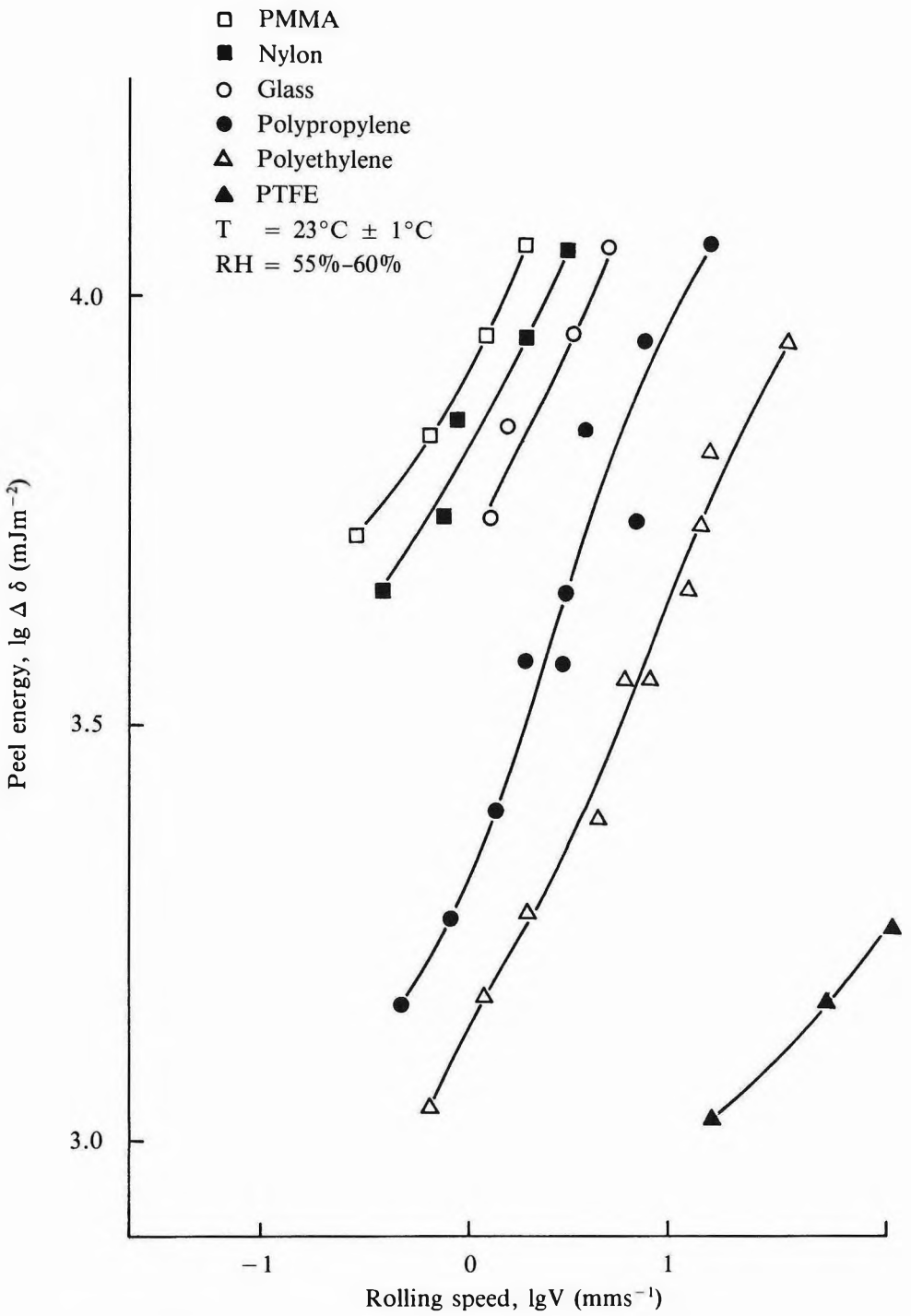

Figure 7. Variation in peel energy with speed obtained by rolling measurements. The peel energy, $\Delta\delta$, is given by mg sin θ/L where m *is roller mass of axial length* L, *and* θ *is track angle*[14].

DISCUSSION

These results for the friction of NR show a variation in the friction coefficient according to the roughness of the rubber. The wavy glass track or the hemispherical rubber slider ensure that the nominal contact area is well-defined. Schallamach waves do not appear to form on a roughened rubber surface and so what is observed may reflect the 'true' frictional nature of the contact pair. True sliding appears to take place though the mechanism for this awaits clarification. One possibility is that actual peeling takes place, on a microscopic scale, support for this idea coming from the link between frictional stress and track surface energy. However, the relationship between the sliding friction and rolling adhesion measurements may be more subtle. An effect of surface energy on rubber friction has been previously reported[15]. The coefficient of friction for a series of rigid indentors sliding on rubber was correlated with the contact angle for a liquid drop on the indentor. This correlation was made without invoking peeling.

Schallamach waves have been studied in detail[4-11] and a predictive criterion for the frictional force has been sought. Following many contact area observations the relationship $F = Yw/lV$ was suggested[7] where a rubber slab is pulled at a velocity V over a hard track by a tangential stress F. The waves move with a velocity w and their spacing apart is l. Y is the rate dependent surface energy. We find, however, that in the presence of waves F is independent of sliding speed, and also independent of the track surface energy. The waves appear to be part of a relaxation mechanism which responds to keep the friction at a level determined by elastic properties[10]. So the relationship predicts the product of the number and speed of the waves rather than the level of friction.

Although this investigation has revealed a change in the friction-rate characteristic with increased roughness, the results do not entirely agree with the appropriate 'master curve' reported by Grosch[1]. Further experiments were carried out, using roughened rubber against wavy glass as above, and they reveal changes in friction level with normal load. Grosch[1] stated that the coefficient of friction was substantially independent of load up to 0.55 kg per square centimetre, his highest experimental normal pressure. This pressure corresponds to a normal load of 34.8 N, whereas the normal load used here to obtain the data in *Figure 3* was 57 N. Trend lines from further experiments show the change in friction coefficient with reduced rate *(Figure 8)* for loads of 3.7 N, 13.2 N and 57 N (repeat measurements). It would seem that the friction coefficient is not independent of load but that given the right combination of normal load and rubber roughness one might be able to reproduce Grosch's 'master curves.'

The contrast between the behaviour of smooth and roughened rubber suggests a difference in friction mechanisms. It is clearly vital, when reporting on the friction of rubber, to specify the operating conditions and likely mechanism involved.

When looking for reference measurements appropriate to applications such as vehicle tyres or windscreen wipers, the rough rubber friction value should normally be used. This means that minor distinctions between different rubbers, tracks or surface treatments will affect the friction both as measured in the laboratory and in practice. On the other hand, reference measurements appropriate to rubber seals will probably call for the use of 'smooth rubber' friction values that are less dependent on rubber hysteresis or tracks surface energy, being mainly governed by the bulk elastic modulus of the rubber[10].

CONCLUSION

The main outcome of this investigation is a clear indication of the importance of rubber roughness to the sliding friction of rubber against a rigid track. With smooth rubber when waves are not present true sliding appears to take place. Increasing the sliding speed or the track surface energy increases the friction coefficient and may initiate the propagation of Schallamach waves. In the presence of waves, the friction coefficient is independent of sliding speed and track surface energy. Waves were not

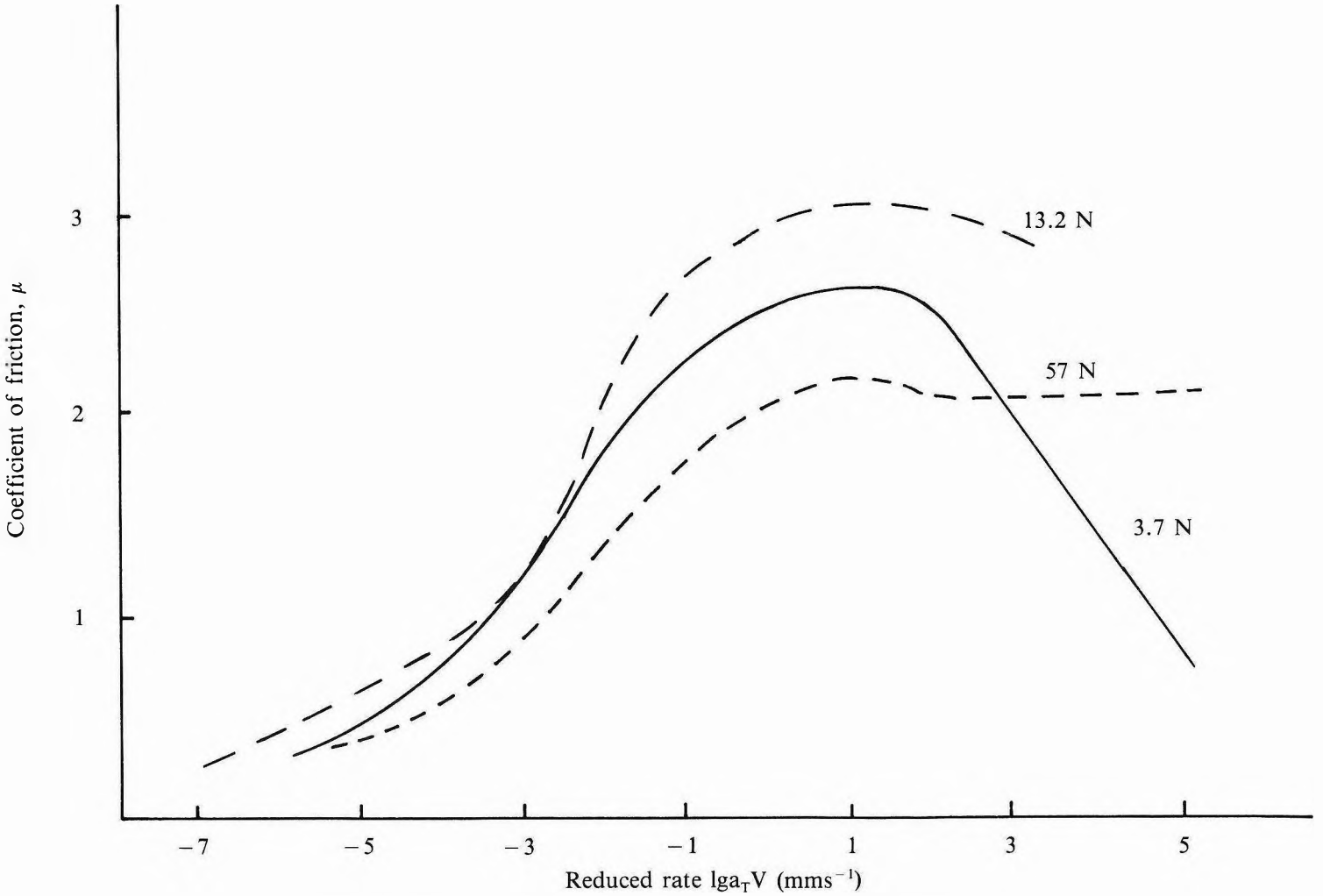

Figure 8. Friction of INR flat on wavy glass for different normal loads.

observed for roughened rubber. The friction of roughened rubber is strongly rate dependent and for the right combination of load and roughness Grosch's 'master curves' would not seem unlikely. The level of friction is seen to reflect the track surface energy, as measured by rolling experiments.

ACKNOWLEDGEMENT

The authors thank Mrs C.A. Brackley for experimental assistance, and Dr A Schallamach for comments on the manuscript.

REFERENCES

1. GROSCH, K.A. (1963) The Relation between the Friction and Visco-elastic Properties of Rubber. *Proc. Royal Soc.*, **A274,** 21.
2. ROTH, F.L., DRISCOLL, R.L. AND HOLT, W.L. (1942) Frictional Properties of Rubber. *J. Res. Natl Bur. Std USA,* **28,** 439.
3. WILLIAMS, M.L., LANDEL, R.F. AND FERRY, J.D. (1955) The Temperature Dependence of Relaxation Mechanisms in Amorphous Polymers and Other Glass-forming Liquids. *J. Am. Chem. Soc.*, **77,** 3701.
4. SCHALLAMACH, A. (1971) How Does Rubber Slide. *Wear,* **17,** 301.
5. BARQUINS, M. AND COURTEL, R. (1975) Rubber Friction and the Rheology of Viscoelastic Contact. *Wear,* **32,** 133.
6. ROBERTS, A.D. (1978) Friction of Rubber. *Progress Rubb. Technol.*, **41,** 121.
7. ROBERTS, A.D. AND JACKSON, S.A. (1975) Sliding Friction of Rubber. *Nature, Lond.*, **257,** 118.
8. ROBERTS, A.D. AND RICHARDSON, J.C. (1981) Interface Study of Rubber-ice Friction. *Wear,* **67,** 55.
9. BRIGGS, G.A.D. AND BRISCOE, B.J. (1978) The Dissipation of Energy in the Friction of Rubber. *Phil. Mag. A.*, **38,** 387.
10. ROBERTS, A.D. AND THOMAS, A.G. (1976) Static Friction of Smooth Clean Vulcanized Rubber. *Nat. Rubb. Technol,* **7,** 38.
11. BARQUINS, M. AND ROBERTS, A.D. (1986) Rubber Friction Variation With Rate and Temperature: Some New Observations. *J. Phys. D.: Appl. Phys.*, **19,** 547.
12. GROSCH, K.A. (1984) Private communication. Uniroyal, European Tire Development Centre, Germany.
13. HERTZ, H. (1896) *Miscellaneous Papers,* p. 146. London: Macmillan.
14. ROBERTS, A.D. (1985) Physico-chemical Aspects of Rubber Adhesion. *Proc. Int. Rubb. Conf. 1985 Kuala Lumpur,* **2,** 111.
15. SAVKOOR, A.R. (1974) Adhesion and Deformation Friction of Polymer on Hard Solids. *Advances in Polymer Friction and Wear (Lee, L.H. ed).* New York: Plenum press.

J. nat. Rubb. Res., **2(1)**, 15-26

The Use of Novel Parameters in the Assessment of Natural Rubber Processability

G.M. BRISTOW* AND A.G. SEARS*

A number of parameters related to rheological behaviour of natural rubber (NR) may be obtained from unconventional measurements using the Mooney viscometer. These parameters have been measured on commercial samples of the major available grades of SMR. Discrimination between grades is better than for more conventional parameters. The significance of the measurements in terms of consistent processability of NR is discussed.

Technically specified rubber (TSR) was first introduced by Malaysia under the Standard Malaysian Rubber (SMR) Scheme, and its characteristics and advantages are now familiar to all NR consumers. Marketed in polyethylene-wrapped bales packaged in unit containers, SMR conforms to technical, rather than visual, specifications. Levels or ranges of ash, nitrogen, dirt, volatile matter, plasticity (P_0) and resistance to oxidative breakdown (PRI) are guaranteed. Similar schemes, with a number of differences, are operated by other NR producing territories. The SMR Scheme provides additional information on cure rate for latex grades, and two viscosity-stabilised grades, SMR CV and SMR GP, are produced to declared ranges of Mooney viscosity.

Over the last few years, consumers have increasingly emphasised the need for improved consistency in processing behaviour of both natural and synthetic rubbers. Many of the parameters specified in the current SMR Scheme relate more to the purity of the rubber than to its processability. Only the information on Mooney viscosity provided for SMR CV and SMR GP and the P_0 and PRI values for all grades relate directly to processability. A further factor often overlooked is the grade effect: the source materials and production route used have a considerable influence so that, for example, SMR L differs characteristically in processability from SMR 20. The customary selection of a single SMR grade for a given application automatically imposes some constraint on processing behaviour. However, there is growing need for processability parameters suitable for inclusion in the SMR Scheme. Such parameters should ideally be obtained from well-proven and generally-available instruments known to be suitable for use under quality control conditions rather than from sophisticated and expensive 'processability testers', though the latter may give data which are more readily interpreted in terms of rheology. Also, unless the consumer is prepared to accept the producers' assessment of processability, whether expressed numerically or in terms of sub-grades, there must be agreement on test procedures and knowledge of testing errors. This is more readily achieved for well-tried and generally-available equipment.

Attention has recently been drawn to the potential use of the Brabender *Plasticorder* to assess susceptibility to mechano-chemical breakdown, which is a major factor in the processing behaviour of natural rubber[1]. A processability specification based upon the use of this instrument may be possible but little information on this has yet been published. The *Plasticorder,* or a more recently developed processability tester, may ultimately give the best approach to the production of NR having consistent processing behaviour. Nevertheless, it seems desirable that the maximum information should be obtained from equipment already in use, even if this involves the use of non-

*Malaysian Rubber Producers' Research Association, Brickendonbury, Hertford SG13 8NL, United Kingdom

standard test procedures. In this context it is important to note that there is no *necessity* for a processability test to predict particular aspects of processing behaviour since the basic aim is only to provide raw NR which behaves consistently when processed by the consumer.

As noted above, NR grade, or more correctly source material and production procedure, are in fact parameters affecting processability. This is, of course, recognised by consumers and such differences in processability are probably partly the basis of the long-standing controversy over the relative merits of sheet and crumb rubber. For the producer, the knowledge that inadvertent variations in procedure during rubber production result in changes in processability may inhibit deliberate changes aimed at improving product quality or production economics. A good example of this is seen in the coagulation of latex by heat gelation rather than acidification to give a latex quality rubber which, in terms of processability, is manifestly not SMR L[2].

In the longer term, a fully technical SMR Scheme can be envisaged where all reference to source material and production procedure is replaced by specified parameters. This paper presents an evaluation of the information on processability given by non-standard procedures using the Mooney viscometer, and analyses the data in terms of possible contributions to a processability specification.

EXPERIMENTAL

Materials

Fifteen to twenty samples of each of the current major SMR grades were obtained from typical commercial production of different SMR factories. The data obtained therefore give some indication of the expected within-grade variability for each grade. Before use, all samples were blended on a 300 × 150 mm two-roll mill. The SMR test procedure[3] was used, *i.e.* six passes with a nip setting of 1.65 mm, but with a roll temperature of 40°C rather than 'ambient temperature (with water cooling)' as specified (See *Appendix*).

Wallace plasticity measurements. Wallace plasticity values, P_0, were determined using the Plastimeter under the conditions specified for SMR testing[3], except that the required smooth sheet was prepared by three passes through mill rolls at 20°C rather than two passes through cool rolls. ISO 2390:1981 specifies three passes through mill rolls at ambient temperature (See *Appendix*).

Mooney viscometer measurements. A range of 'non-standard' parameters was obtained using the Mooney viscometer at 100°C. In the standard ML 1 + 4 test, initial maximum torque, ML_{max}, was recorded as well as the normal reading at 4 minutes. As the rubber temperature after preheating for 1 min is still below 100°C, longer preheating reduces ML_{max} *(Figure 1)*. ML_{max} is essentially constant for preheat periods of 5 min or greater *(Figure 1)*, and 5 min preheat was therefore adopted for routine testing. As might be expected, the viscosity value after 4 min is far less dependent on preheat time over the same range.

A further feature of the torque *versus* time relation observed with the Mooney viscometer is shown in *Figure 2*. The torque often falls from the initial maximum before rising to the 'equilibrium value' at *ca.* 4 minutes. The exact minimum torque value is rather difficult to determine; as a compromise the value of the torque at 1 min, *i.e.* ML'1 = ML 5 + 1, was recorded.

While the torque observed after 4 min is normally considered to be the characteristic 'viscosity' of the rubber, it is not in fact an equilibrium value as, owing to chemical (oxidative) and/or rheological factors, the torque decreases more or less slowly after this time. The rate of this decrease was characterised in a ML 5 + 60 test by the values of the ML 5-ML 60 and ML 10-ML 60.

The relaxation of torque following cessation of rotor movement, first studied by Mooney[4] and later considered by Blow[5] as a means of characterising GR-S, was also studied. On completion of a ML 5 + 4 measurement the rotor drive was switched off and torque recorded every 10 s for 90 seconds. The data

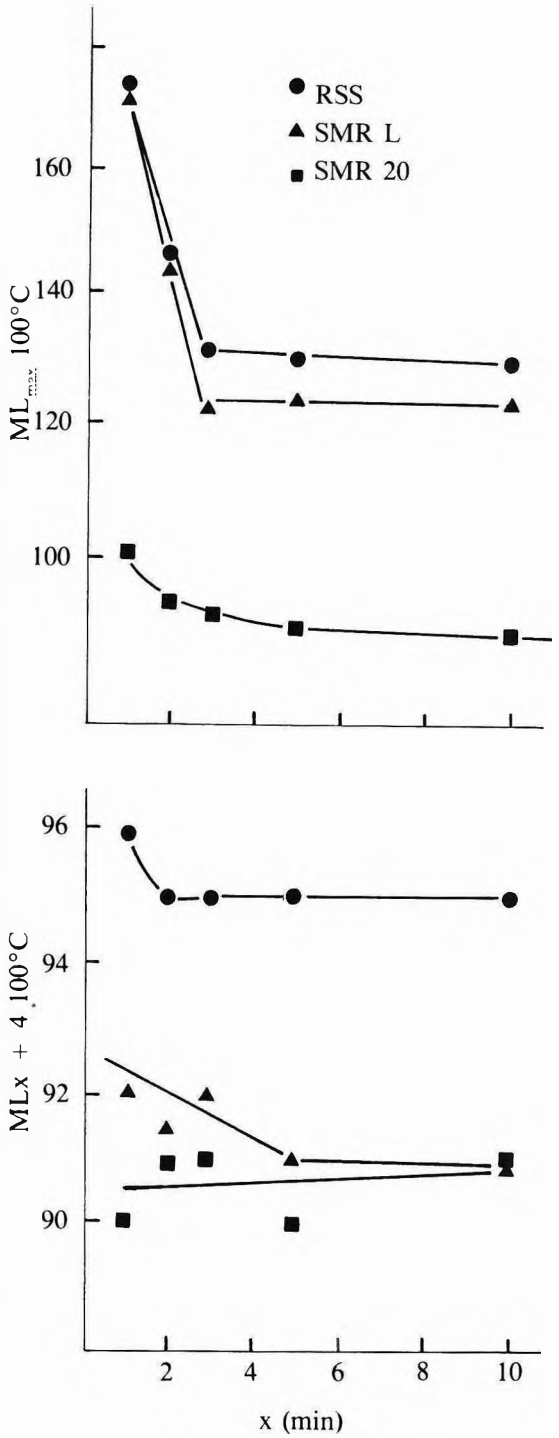

Figure 1. Dependence of initial maximum and 4-min viscosity on preheat time.

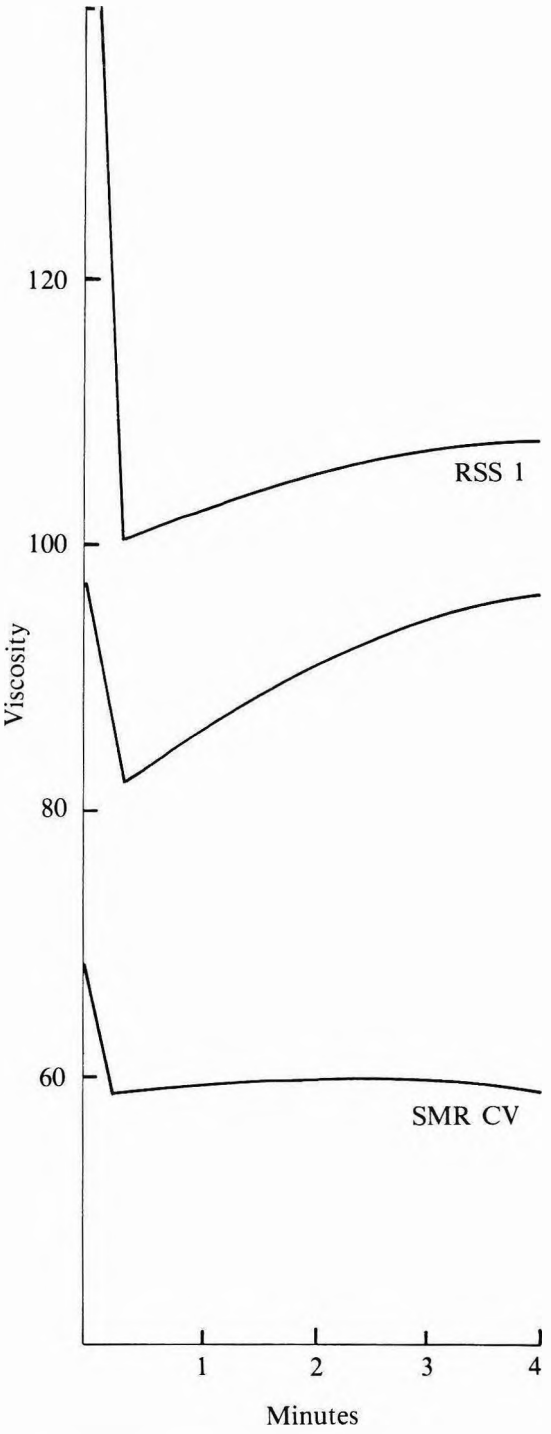

Figure 2. Typical torque/time relations observed with the Mooney viscometer.

obtained were found to conform to the relation

$$\text{torque} = kt^{-a}$$

where k = torque after relaxation for 1 second. A parameter based on k or, more significantly, on the rate of relaxation a can therefore be obtained. However, the form of the expression makes k and, particularly, a rather sensitive to timing errors, especially to systematic errors arising from imprecision in timing the start of relaxation. For example, an observed relationship

$$\text{torque} = 99.3t^{-0.224}$$

becomes

$$\text{torque} = 103.2t^{-0.233}$$

or

$$\text{torque} = 95.5t^{-0.215}$$

if undetected systematic timing errors of + 1 s or − 1 s, respectively, are present. The relaxation has therefore also been characterised more simply by the change in torque after fixed times of relaxation,

D_1 = torque at 4 min − torque after 20 s relaxation

D_2 = torque at 4 min − torque after 90 s relaxation.

The test procedures, test data recorded and parameters utilised are summarised in *Table 1*. Details of within-sample reproducibility, *i.e.* experimental error, are given in *Table 2*.

RESULTS

Table 3 gives data for the existing tests for processability in the SMR Scheme: ML 1 + 4, 100°C; P_0; and PRI.

Grade mean values and standard deviations for the application of the test procedures summarised in *Table 1* are given in *Tables 4–10*. In view of disparities in the number of samples of each grade and in particular of the extent to

TABLE 1. SUMMARY OF TEST MEASUREMENTS AND DERIVED PARAMETERS

Test	Value measured	Derived parameters
ML 1 + 4, 100°C	Maximum viscosity, ML_{max}	ML_{max}-ML 4
	Viscosity at 4 min, ML 4	ML_{max}/ML 4
		ML 4/P_0
ML 5 + 4, 100°C	Maximum viscosity, ML'$_{max}$	ML'$_{max}$-ML'4
	Viscosity at 1 min, ML'1	ML'$_{max}$/ML'4
	Viscosity at 4 min, ML'4	ML'4-ML'1
	Torque after 20 s relaxation, ML_R20	k (see text)
	Torque after 90 s relaxation, ML_R90	a (see text)
		a (ML'4) (see text)
		D_1 (see text)
		D_3 (see text)
		ML'$_{max}$/P_0
		ML'4/P_0
ML 5 + 60, 100°C	Viscosity at 5 min, ML 5	ML 5-ML 60
	Viscosity at 10 min, ML 10	ML 10-ML 60
	Viscosity at 60 min, ML 60	

TABLE 2A. REPRODUCIBILITY OF TESTING: WALLACE PLASTICITY (FIVE TEST PIECES FROM A SINGLE SHEET)

Grade	Initial plasticity, P_0		
	Mean	sd	CV (%)
SMR L	60.4	0.9	1.5
SMR 20	52.6	1.3	2.6

which the samples are sufficiently representative of the grade, the significance of the between-grade difference has not been assessed by variance analysis. As an alternative and admittedly very approximate arbiter, the maximum difference in grade means has been compared with the typical or average scatter within a grade. Such comparisons are included for each parameter in *Tables 4–10.*

Comparison of maximum and 4-min viscosities (Tables 4 and 5). Since maximum viscosity will clearly depend on the value at 4 min, the data are assessed as the difference and as the ratio of these values. The latter apparently gives less within-grade scatter. Maximum viscosity is relatively high for the latex grades, and as expected, the effect is greater in absolute terms for the ML 1 + 4 test *(Table 4)* than for ML 5 + 4 *(Table 5).* However, discrimination between the grades, especially between the several latex grades, is greater for the parameters based upon ML 5 + 4.

Relation between P_0 *and Mooney viscosity* (Table 6). In terms of experimental procedure, P_0 is more akin to maximum viscosity than to the value after 4 minutes. It is not surprising therefore that relatively low values of ML $4/P_0$ and ML'$4/P_0$ are associated with latex grades and that ML'$_{max}/P_0$ does not discriminate between grades. Again, as might

TABLE 2B. REPRODUCIBILITY OF TESTING: MOONEY VISCOMETRY (FIVE TESTS ON A SINGLE BLENDED SAMPLE)

Parameter	RSS			SMR 20			SMR 10		
	Mean	sd	CV (%)	Mean	sd	CV (%)	Mean	sd	CV (%)
ML'$_{max}$	145.2	1.5	1.0	100.6	1.1	1.1	—	—	—
ML'1	102.1	0.7	0.6	90.9	0.4	0.5	—	—	—
ML'4	104.1	0.2	0.2	94.6	0.5	0.6	—	—	—
ML'$_{max}$-ML'4	41.1	1.4	3.5	6.0	1.2	20.4	—	—	—
ML'$_{max}$/ML'4	1.394	0.011	0.8	1.063	0.013	1.2	—	—	—
ML'4-ML'1	2.0	0.6	30.6	3.7	0.6	15.4	—	—	—
ML_R20	60.3	1.1	1.8	42.6	0.5	1.3	—	—	—
ML_R90	46.3	0.6	1.2	28.8	0.4	1.6	—	—	—
D_1	43.8	1.2	2.6	52.0	1.0	1.9	—	—	—
D_2	57.8	0.6	1.0	65.8	0.8	1.3	—	—	—
k	101.4	1.5	1.5	91.7	2.5	2.7	—	—	—
a	0.176	0.004	2.4	0.256	0.007	2.9	—	—	—
ML 5	103.4	0.5	0.5	—	—	—	86.6	0.5	0.6
ML 10	101.3	0.3	0.3	—	—	—	84.3	0.4	0.5
ML 60	101.3	2.0	2.0	—	—	—	66.4	0.4	0.6
ML 5-ML 60	2.1	1.8	84.9	—	—	—	20.2	0.6	2.8
ML 10-ML 60	0.0	1.7	—	—	—	—	17.9	0.2	1.2

TABLE 3. CONVENTIONAL PROCESSABILITY PARAMETERS

Grade	No. of samples	ML 1 + 4, 100°C			P_0			PRI		
		Mean	sd	CV (%)	Mean	sd	CV (%)	Mean	sd	CV (%)
SMR 5	17	96.0	4.7	4.9	50.6	6.4	12.7	74.1	4.9	6.6
SMR 10	17	94.9	3.4	3.5	46.5	3.2	7.0	66.5	6.6	9.9
SMR 20	19	89.7	8.3	9.2	44.3	5.9	13.4	67.5	8.8	13.0
SMR CV	21	64.4	4.6	7.1	34.0	2.7	8.0	83.8	5.5	6.6
SMR WF/L	18	90.3	7.1	7.8	53.5	4.0	7.4	80.0	4.8	6.0
RSS	10	90.8	4.5	4.9	58.6	4.1	7.1	78.8	4.2	5.3

TABLE 4. PARAMETERS DERIVED FROM ML_{max} AND ML 4

Grade	No. of samples	ML_{max}-ML 4			ML_{max}/ML 4		
		Mean	sd	CV (%)	Mean	sd	CV (%)
SMR 5	17	49.3	29.1	59	1.512	0.303	20
SMR 10	17	25.7	10.3	40	1.270	0.105	8
SMR 20	19	27.2	15.2	56	1.299	0.152	12
SMR CV	21	26.5	6.3	24	1.415	0.103	7
SMR L/WF	18	64.6	17.1	27	1.713	0.174	10
RSS	10	64.8	15.8	24	1.175	0.177	10
Average sd of grade means, S			15.6			0.169	
Max difference in grade means, Δ			39.1			0.445	
S/Δ			2.5			2.6	

TABLE 5. PARAMETERS DERIVED FROM ML'_{max} AND ML'4

Grade	No. of samples	ML'_{max}-ML'4			ML'_{max}/ML'4		
		Mean	sd	CV (%)	Mean	sd	CV (%)
SMR 5	17	10.6	10.2	96	1.110	0.104	9
SMR 10	17	2.7	5.5	209	1.026	0.056	6
SMR 20	19	3.2	5.5	181	1.033	0.063	6
SMR CV	21	15.2	5.2	34	1.238	0.087	7
SMR L/WF	18	18.4	7.0	38	1.207	0.086	70
RSS	10	26.0	7.2	28	1.289	0.084	7
Average sd of grade means, S			6.8			0.080	
Max difference in grade means, Δ			22.8			0.2576	
S/Δ			2.5			2.6	

TABLE 6. RELATIONS BETWEEN P_0 AND MOONEY VISCOSITY

Grade	No. of samples	ML $4/P_0$			ML'_{max}/P_0			ML'$4/P_0$		
		Mean	sd	CV (%)	Mean	sd	CV (%)	Mean	sd	CV (%)
SMR 5	17	1.92	0.21	11	2.13	0.08	4	1.94	0.20	10
SMR 10	17	2.05	0.11	5	2.12	0.09	4	2.07	0.12	6
SMR 20	19	2.04	0.13	6	2.12	0.07	3	2.05	0.13	6
SMR CV	21	1.90	0.13	7	2.36	0.07	3	1.91	0.15	8
SMR L/WF	18	1.69	0.09	5	2.04	0.12	6	1.70	0.09	5
RSS	10	1.56	0.09	6	1.99	0.09	5	1.55	0.09	6
Average sd of grade means, S			0.127			0.087			0.130	
Max difference in grade means, Δ			0.49			0.37			0.52	
S/Δ			3.9			4.3			4.0	

be anticipated, the time of preheat in the Mooney test is unimportant.

Short-time Mooney tests (Table 7). The rather more limited data for ML'4–ML'1 also show characteristic differences between latex and field coagulum grades. However, the absolute value of ML'4–ML'1 is rather small and the within-grade variation proportionately large, so that discrimination is poor. Further work is necessary to investigate the full potential of this procedure.

Extended Mooney viscosity tests (Table 8). One of the factors leading to a progressive decrease in torque over the period 5–60 min must be susceptibility to oxidative degradation, and a correlation between the extended test and PRI might be anticipated. As shown in *Figure 3,* such a correlation does exist if mean values for the various grades are considered, but the individual sample data show no correlation. The scatter is far greater than would be expected from the precision of the data *(cf. Table 2)* so that other factors must be involved. Once again there are clear indications of between-grade differences.

*Relaxation tests (*Tables 9 *and* 10*).* Grade mean values for the relaxation rate parameter *a* are given in *Table 9.* Within-grade variability

TABLE 7. PARAMETERS FROM SHORT-TIME MOONEY TESTS, ML 5 + 4, 100°C

Grade	No. of samples	ML'4–ML'1		
		Mean	sd	CV (%)
SMR 5	8	+3.3	1.3	39
SMR 10	10	+4.5	1.8	41
SMR 20	10	+4.3	1.9	44
SMR CV	10	0.0	1.5	—
SMR L	10	+1.0	1.0	107
RSS	10	−1.2	1.8	153
Average sd of grade means, S			1.6	
Max difference in grade means, Δ			5.7	
S/Δ			3.6	

is relatively high; only for SMR CV and possibly RSS are there any indications of significant differences between the various grades. However, general experience of relaxation phenomena and tests with masticated rubbers *(Figure 4)* indicate that *a* is very dependent on the stress level before relaxation, *i.e.* the ML 5 + 4 value. The relatively high value of *a* for SMR CV is therefore probably associated

TABLE 8. VISCOSITY CHANGES IN EXTENDED MOONEY TEST, ML 5 + 60, 100°C

Grade	No. of samples	ML 5-ML 60			ML 10-ML 60		
		Mean	sd	CV (%)	Mean	sd	CV (%)
SMR 5	8	13.5	2.7	20	11.4	2.6	23
SMR 10	10	18.2	3.1	17	15.3	3.4	22
SMR 20	10	15.0	4.6	31	13.0	4.5	35
SMR CV	8	5.6	0.8	14	3.4	0.9	25
SMR L	10	9.5	1.6	17	8.3	2.0	24
RSS	10	7.4	1.7	23	5.7	2.2	39
Average sd of grade means, S			2.4			2.6	
Max difference in grade means, Δ			12.6			11.9	
S/Δ			5.3			6.0	

TABLE 9. MOONEY RELAXATION TEST, ML_R90: ANALYSIS BY RELAXED TORQUE = kt^{-a}

Grade	No. of samples	a			a (ML'4)		
		Mean	sd	CV (%)	Mean	sd	CV (%)
SMR 5	17	0.242	0.045	19	23.3	3.1	14
SMR 10	17	0.246	0.023	9	23.5	1.7	7
SMR 20	19	0.276	0.049	18	24.5	2.3	10
SMR CV	21	0.356	0.034	10	23.0	2.0	9
SMR L/WF	18	0.259	0.030	12	23.3	1.7	8
RSS	10	0.200	0.016	8	18.1	1.5	8
Average sd of grade means, S			0.030			2.1	
Max difference in grade means, Δ			0.156			6.4	
S/Δ			5.2			3.0	

with the relatively low viscosity of the grade. This explanation is supported by the virtual identity of mean values of *a* (ML'4) for the other grades except RSS. It should be noted that this approach does *not* compensate for viscosity variation within a grade, since the coefficients of variation for *a* (ML'4) are not greatly less than those for *a* itself. Whether *a* or *a* (ML'4) is considered, RSS shows a lower relaxation rate.

Data for the assessment of relaxation directly by the decrease in viscosity are given in *Table 10.* SMR CV again shows a lesser extent of relaxation, though the effect is not so marked as with the *a* value. In this case no attempt was made to correct D_1 and D_2 for any dependence on initial stress. RSS again shows a lower relaxation rate, but the values of D_1 and D_2 appear less discriminating in this respect than *a* or, better, *a* (ML'4).

TABLE 10. MOONEY RELAXATION TEST, ML 5 + 4, 100°C: ANALYSIS BY D_1 = ML'4-ML_R20 AND D_2 = ML'4-ML_R90

Grade	No. of samples	D_1			D_2		
		Mean	sd	CV (%)	Mean	sd	CV (%)
SMR 5	10	49.7	2.5	5	64.2	2.4	4
SMR 10	13	49.7	1.5	3	63.6	1.6	3
SMR CV	15	43.1	2.0	5	52.1	2.4	5
SMR L	19	46.4	1.7	4	59.0	2.9	5
RSS	15	44.0	2.8	6	57.2	3.3	6
Average sd of grade means, S			2.1			2.5	
Max difference in grade means, Δ			6.6			12.1	
S/Δ			3.1			4.8	

TABLE 11. SUMMARY OF GRADE MEAN VALUES OF PROCESSABILITY PARAMETERS

Parameter	SMR CV	SMR L/WF	RSS	SMR 5	SMR 10	SMR 20
ML 1 + 4, 100°C	64.4	90.3	90.8	96.0	94.9	89.7
P_0	34.0	53.5	58.6	50.6	46.5	44.3
PRI	83.8	80.0	78.8	74.1	66.5	67.5
ML 1 + 4/P_0	1.90	1.69	1.56	1.92	2.05	2.04
ML'$_{max}$/ML'4	1.238	1.207	1.289	1.110	1.026	1.033
ML'4-ML'1	0.0	1.0	−1.2	3.3	4.5	4.3
ML 5-ML 60	5.6	9.5	7.4	13.5	18.2	15.0
a (ML'4)	23.0	23.3	18.1	23.3	23.5	24.5
D_2	52.1	59.0	57.2	64.2	63.6	—

TABLE 12. SUMMARY OF RELATIVE GRADE MEAN VALUES OF PROCESSABILITY PARAMETERS

Parameter	SMR CV	SMR L/WF	RSS	SMR 5	SMR 10	SMR 20
ML 1 + 4	71	100	101	106	105	99
P_0	64	100	110	95	87	83
PRI	105	100	99	93	83	84
ML 1 + 4/P_0	112	100	92	114	121	121
ML'$_{max}$/ML'4	103	100	107	92	85	86
ML'4-ML'1	—	100	−120	330	450	430
ML 5- ML 60	59	100	78	142	192	158
a (ML'4)	99	100	78	100	101	105
D_2	88	100	97	109	108	—

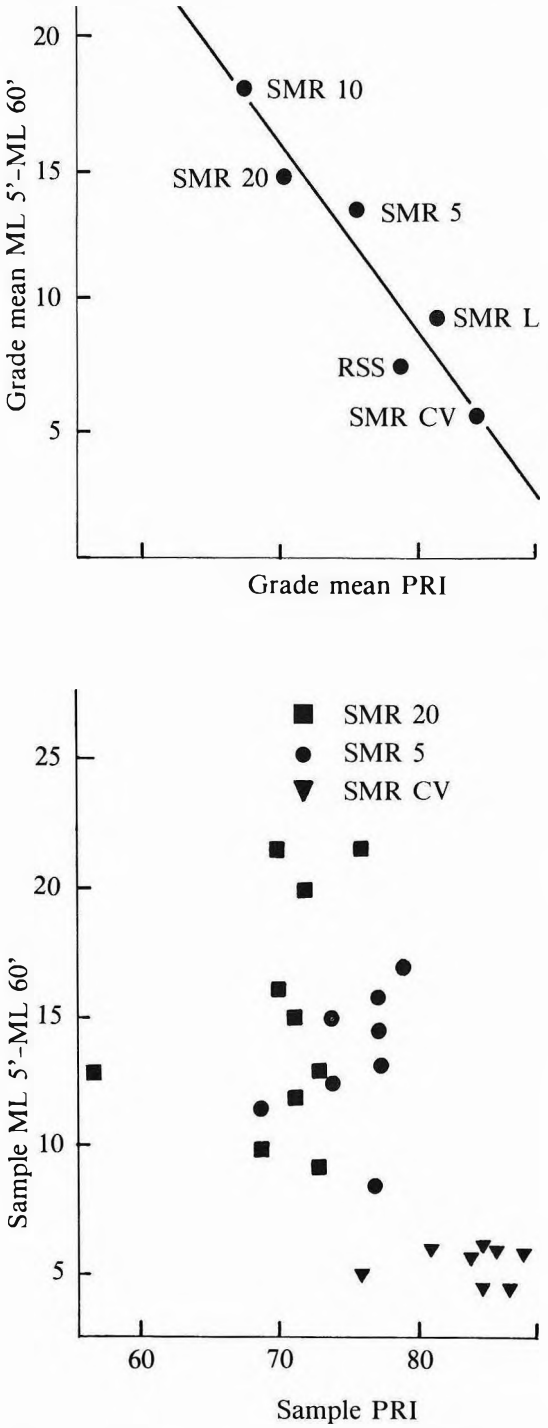

Figure 3. Relation between PRI and torque change in the extended Mooney viscosity test.

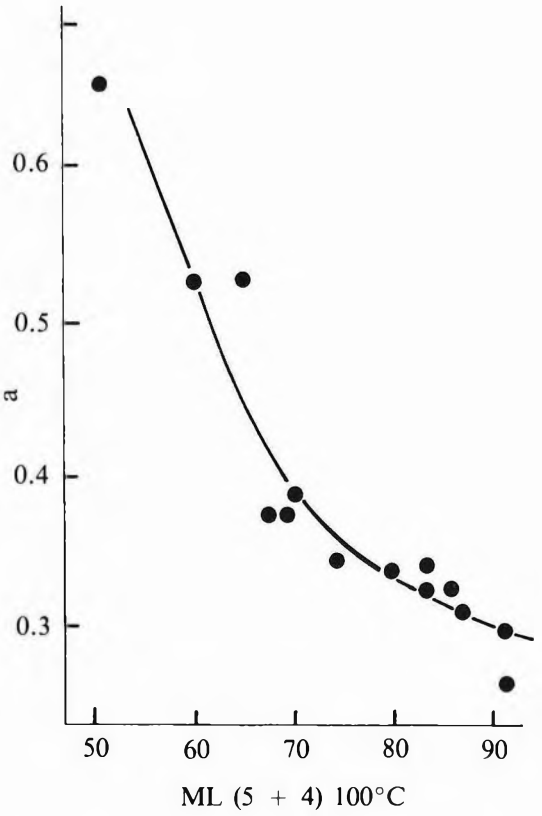

Figure 4. Dependence of the relaxation parameters a *on the degree of mastication of a sample of SMR 10.*

CONCLUSIONS

Grade mean values for all the various test parameters are given in *Table 11* and summarised relative to the values for SMR L in *Table 12*. Of the conventional parameters, ML 1 + 4 or P_0 identify the low-viscosity, easy-processing quality of SMR CV, while PRI indicates the greater susceptibility to oxidative breakdown of SMR 10 and SMR 20. Most of the more novel parameters show greater discimination between grades. Tests of this type would identify the grade of, or perhaps more correctly the source material used for, a given sample of raw rubber, and go some way to eliminating the need for these factors to be detailed in SMR specifications. In this context it should perhaps be stressed that the samples studied were com-

mercial materials; while conforming to the SMR specifications they did not, with the possible exception of RSS, originate from rigidly controlled source materials and/or production procedures. Any variability in this respect would be a factor in the significant *within-grade* variability of most of the properties measured.

It is not suggested that any of the novel parameters identified here indicate any particular aspect of processability as it may be measured by the consumer. Indeed, this is not an essential requirement of a 'processability parameter': uniform processing in the consumer's factory must depend on consistent rheological behaviour from the NR, and the need is for a parameter which, directly or indirectly, measures this consistency in a reliable and reproducible way. Despite such considerations, it should be noted however, that recent attempts to interpret consumer problems with NR have shown $ML'_{max}/ML'4$ and $ML'4/P_0$ to be the parameters of greatest utility.

REFERENCES

1. ONG, E.L. AND LIM, C.L. (1985) Brabender Plasticorder and Breakdown Index. *Proc. SMR Revision Wkshop Kuala Lumpur 1985.*

2. CHEONG, S.F. AND LIM, F.P. (1976) Continuous Heat Gelation of Latex — a Potentially Cost-effective Processing Technique for SMR. *Proc. Int. Rubb. Conf. 1975 Kuala Lumpur,* **IV**, 295.

3. RUBBER RESEARCH INSTITUTE OF MALAYSIA (1973) RRIM Test Methods for Standard Malaysian Rubbers. *SMR Bull. No. 7.*

4. MOONEY, M. (1934) A Shearing Disk Plastometer for Unvulcanized Rubber. *Ind. Eng. Chem. (Analyt.),* **6**, 147.

5. BLOW, C.M. AND SCHOFIELD, J.R. (1950) The Measurement of Stress Relaxation of Unvulcanized Rubber by Means of the Mooney Shearing-disc Viscometer. *Rubb. Chem. Technol.,* **23**, 601.

APPENDIX

Conditions specified for the preparation of rubber samples for SMR viscosity and plasticity tests are imprecise, particularly in respect of mill roll temperatures. In practice, ML 1 + 4, 100°C and P_0 are little affected by variations in roll temperature in initial blending *(Table A1)* or in sheeting for Wallace plasticity tests *(Table A2).* The effect of P_0 on three rather than two mill passes in the sheeting operation is hardly greater than the expected experimental error *(Table A3).*

TABLE A1. MOONEY VISCOSITY AS A FUNCTION OF BLENDING TEMPERATURE
Blend procedure: 300 × 150 mm mill; nip 1.65 mm; six passes
Viscosity: four tests per batch

Roll temperature (°C)	Mooney viscosity, ML 1 + 4, 100°C				Mean
20	88	87	88	85	87.0
30	87	83.5	85	86.5	85.5
34	85	87.5	85	86	85.9
43	86	84	83	86	84.8
52	84.5	84	83	84	83.9
63	83	85	84	87	84.8

Variance analysis, all data: F ratio 2.49, significant at 90%-95%.

If data for 20°C omitted: F ratio 1.3, not significant at 99%.

TABLE A2. EFFECT OF MILL ROLL TEMPERATURE ON INITIAL WALLACE PLASTICITY
Blend procedure: 300 × 150 mm mill; three passes
Viscosity: ten test pieces per sheet or three test pieces selected at random

Roll temperature (°C)	Wallace plasticity P_0							
	SMR L				SMR 20			
	10 tests		3 tests		10 tests		3 tests	
	Mean	sd	Mean	sd	Mean	sd	Mean	sd
21	60.7	1.1	61.3	0.6	52.8	1.2	52.0	1.7
30	59.7	1.3	59.0	1.0	53.6	0.8	53.7	0.6
41	62.0	0.8	61.3	1.1	52.4	1.1	53.0	0
49	59.9	0.9	60.3	0.6	51.6	0.8	51.0	1.0

TABLE A3. EFFECT OF NUMBER OF MILL PASSES ON INITIAL WALLACE PLASTICITY
Blend procedure: 300 × 150 mm mill, roll temperature 20°C
Viscosity: ten test pieces per sheet or three test pieces selected at random.

Mill passes	Wallace plasticity P_0							
	SMR L				SMR 20			
	10 tests		3 tests		10 tests		3 tests	
	Mean	sd	Mean	sd	Mean	sd	Mean	sd
1	65.1	2.3	63.3	0.6	61.4	2.1	62.3	1.2
2	60.7	1.1	59.8	1.3	55.0	1.7	54.7	2.1
3	59.9	1.3	59.8	1.9	53.2	0.7	53.7	0.6
4	58.0	0.8	58.0	1.0	50.1	1.0	50.2	0.7
5	55.9	1.3	56.0	1.0	48.0	0.8	47.8	0.8

J. nat. Rubb. Res., **2(1)**, 27–45

A Comparative Study of the Combustion Characteristics of Rubberwood and Some Malaysian Wood Species

A.G. TAN* AND J.B. STOTT**

The combustion characteristics of rubberwood and eighteen common Malaysian wood species were examined and compared using two complementary methods of analysis, namely differential thermal analysis (DTA) and thermogravimetry (TG). The DTA experiments were carried out in fluidised beds, as opposed to static beds in the conventional method. The results obtained indicate that rubberwood is relatively easy to burn and that, in general, the lighter a wood species, the easier it is to burn. Increasing the oxygen supply to the combustion chamber resulted in the wood burning faster but did not seem to have a major effect on its relatively combustibility. The effects of ash and moisture content of the wood on its combustion were discussed.

Wood is composed of three basic polymers, namely cellulose, the hemicelluloses and lignin. Added to these are the extractives which may be extracted from the wood using water or organic solvents. In general, hardwoods contain around 40% cellulose, 33% hemicelluloses, 20% lignin and 7% extractives, on a weight basis[1]. Elementally, wood consists of around 52% carbon, 41% oxygen, 6% hydrogen and 1% ash[2].

The combustion of wood begins with pyrolysis during which it is decomposed into gases and vapours (known as the volatiles) and a solid residue called char. In the presence of oxygen, the volatiles burn with a flame while the char burns by glowing combustion without flame. Cellulose and the hemicelluloses promote flaming combustion as their degradation products consist mainly of the volatiles while the lignin fraction supports glowing combustion as it contributes the most to char formation[1].

Although different wood species have only a minor difference in their elemental compositions[3], they vary considerably in their combustion characteristics. Some wood species burn easily while others burn less readily. The thermal behaviour of wood may be studied using several methods[4,5], including differential thermal analysis (DTA) and thermogravimetry (TG). In DTA, the difference in temperature between a sample and an inert reference material is recorded as a function of temperature while in TG the weight of a sample is recorded as a function of temperature. These two techniques are, therefore, complementary to each other.

A study using DTA and TG was carried out to compare the combustion characteristics of rubberwood, which is widely used as fuelwood in this country, with those of some common Malaysian wood species whose off-cut timbers are also being used as fuel. The DTA experiments were conducted in fluidised beds instead of in static beds as in the conventional method. This was to overcome the problem of non-uniformity of bed temperature and also to allow larger testpieces to be used. The results of this study are presented here.

*Rubber Research Institute of Malaysia, P.O. Box 10150, 50908 Kuala Lumpur, Malaysia

**Department of Chemical and Process Engineering, University of Canterbury, Christchurch 1, New Zealand

EXPERIMENTAL

Apparatus

A reactor and a furnace were used. The reactor was made up of three components, namely a pair of reaction tubes, a stainless steel block and a stand as illustrated in *Figure 1*. The two reaction tubes were connected to a common gas coil of 10 mm internal diameter by a 'T'. An orifice plug inserted at the entrance of each tube ensured that the gas flow rates in both the tubes were uniform. The gas distributor consisted of a circular piece of ceramic fibre ('Kaowool') of 13 mm thickness. It was supported by a 125 mm high stainless steel frame placed at the bottom of each tube. The stainless steel block served as a heat sink and sat on a steel stand with a 19 mm thick base. The reactor was placed inside an electrically heated furnace of 576 mm height, with 66 mm of each reaction tube protruding out of the lid. The lid and the reactor could be lifted out of the furnace with the aid of a crane for fan cooling at the end of each run.

Materials

Nineteen wood species, including rubberwood, were used. These are listed in *Table 1*, in order of density. All of them are hardwoods, except oil palm wood and coconut wood which are obtained from 'palms' and not 'trees'. Oil palm wood and coconut wood are agricultural by-products and are presently not used for sawn timber production in Malaysia.

The testpieces were of 5 mm diameter and 11 mm height. A uniform sample size of 1 g (oven-dried wood) was used in the DTA runs. The number of wood pieces in a sample varied from species to species as it was dependent on the density of the wood; in the case of rubberwood, there were seven pieces. In TG analysis, a sample size of 1 g was used in runs carried out in an inert atmosphere (to compare the char yields of different wood species) and 0.6 g in those conducted in an oxidative environment. The test samples of rubberwood, oil palm wood and coconut wood were obtained from trunk sections of 5 cm thickness and 20-30 cm diameter. Those of the other wood species were derived from hand samples measuring 75 × 100 × 18 mm prepared by the Forest Research Institute of Malaysia.

Differential Thermal Analysis

Thirty grammes of sand of particle size −85 + 100 mesh was poured down each tube onto the gas distributor. The static height of each bed was 40 millimetres. The test sample was dropped into the sample tube, after which both the beds were fluidised by the desired fluidising medium. The gas flow rate in each tube was adjusted at 2 litres per minute to give a gas velocity of around three times the minimum value required for fluidisation of the sand, *i.e.* 0.02 m per second. Following this, the reactor was heated at a constant rate of around 5.5°C per minute. The temperature difference between the two beds and the reference bed temperature were measured using 1 mm diameter chromel/alumel thermocouples and were recorded on a Watanabe hot-pen recorder. The experiment was terminated when all the testpieces had been burnt and the DTA trace had returned to the base line.

Two sets of experiment were carried out, the first using air and the second using a mixture of oxygen (80% volume/volume) and nitrogen (20% volume/volume) as the fluidising medium.

Thermogravimetry

The experimental set-up for TG analysis is shown in *Figure 2*. The sample holder consisted of a cylindrical basket of 16 mm diameter and depth made from 100-mesh stainless steel screen. It was suspended at the end of a long wire, the other end of which was hooked onto the bottom of a digital balance which read up to three decimal places. After the test sample had been loaded, the carrier gas was passed through the two tubes with a combined flow rate of 0.8 litre per minute in the case of nitrogen gas and 0.4 litre per minute in the case of air. The reactor was then heated at around 5.5°C per minute, as in the DTA runs. Readings on the balance were recorded from the time the sample began to lose weight, at intervals varying from 1 min (at the height of pyrolysis) to 5 min until they remained constant or nearly constant. The actual heating

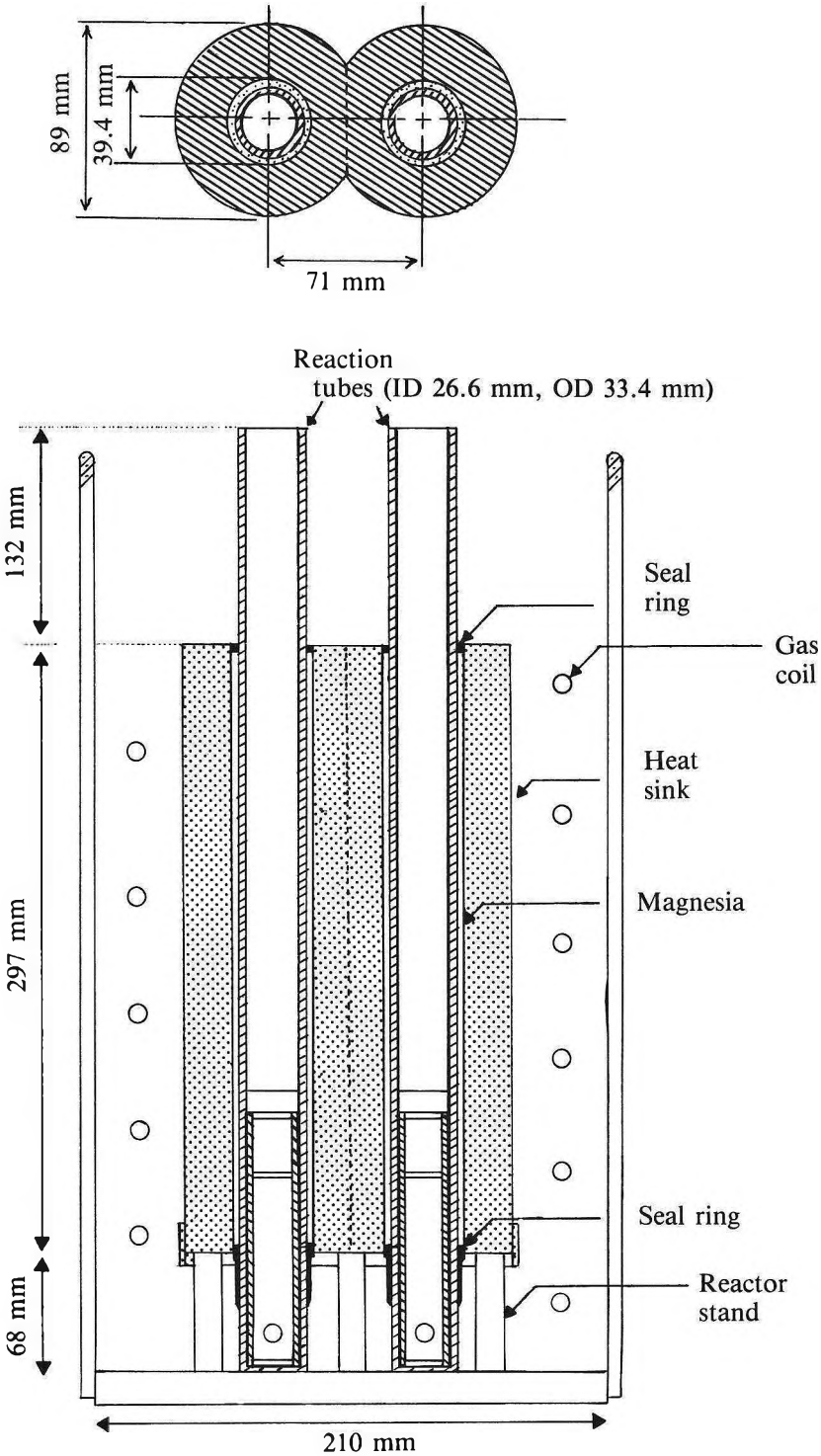

Figure 1. Schematic representation of reactor.

TABLE 1. WOOD SPECIES USED IN THE STUDY

Common name	Botanical name	Density at 15% moisture content[a] (kg/m^3)
Oil palm wood[b]	*Elaies guineensis*	196
Jelutong	*Dyera costulata*	445
Mengkulang	*Heritiera* spp.	490
Pulai	*Alstonia* spp.	505
Mersawa	*Anisoptera* spp.	557
Meranti, light red	*Shorea* spp.	610
Meranti, dark red	*Shorea* spp.	643
Sepetir	*Sindora* spp.	675
Rubberwood	*Hevea brasiliensis*	698
Nyatoh	Spp. of *Sapotaceae*	732
Keruing	*Dipterocarpus* spp.	796
Tualang	*Koompassia excelsa*	810
Ramin	*Gonystylus* spp.	822
Tembusu	*Fagraea* spp.	833
Merbau	*Intsia palembanica*	871
Kempas	*Koompassia malaccensis*	873
Chengal	*Balanocarpus heimii*	920
Coconut wood[b]	*Cocos nucifera*	1 004
Balau	*Shorea* spp.	1 005

[a]Determined from testpieces

[b]Outer wood

rate was determined from the temperature curve, after which the TG curve was plotted as a function of the reference temperature.

RESULTS AND DISCUSSION

Differential Thermal Analysis Curves of Rubberwood

The DTA curve in air of rubberwood contained two overlapping exotherms *(Figure 3)*, with peak temperatures of 343°C and 426°C and a dip at 372°C*. The first exotherm, which began at around 270°C, was attributed to oxidative degradation of the volatiles while the second exotherm was attributed to both oxidative degradation of the volatiles (released at higher temperatures) and decomposition of the residual char. The heights of the two peaks, measured on a temperature scale, were: first peak, 8.9°C and second peak, 16.3°C. No flaming or glowing combustion occurred during the run, *i.e.* the volatiles did not burst into flame, neither did the char turn 'red hot'.

In the run in 80% oxygen, ignition of the volatiles occurred at 285°C, resulting in flaming combustion which lasted for less than 1 minute. When ignition took place, there was quite a loud explosion in the sample tube. It was observed that the wood pieces burnt at almost

*Unless otherwise stated, all temperatures referred to hereafter are those of the reference bed. The corresponding sample bed temperatures, in the case of DTA, can be deduced from the DTA curves.

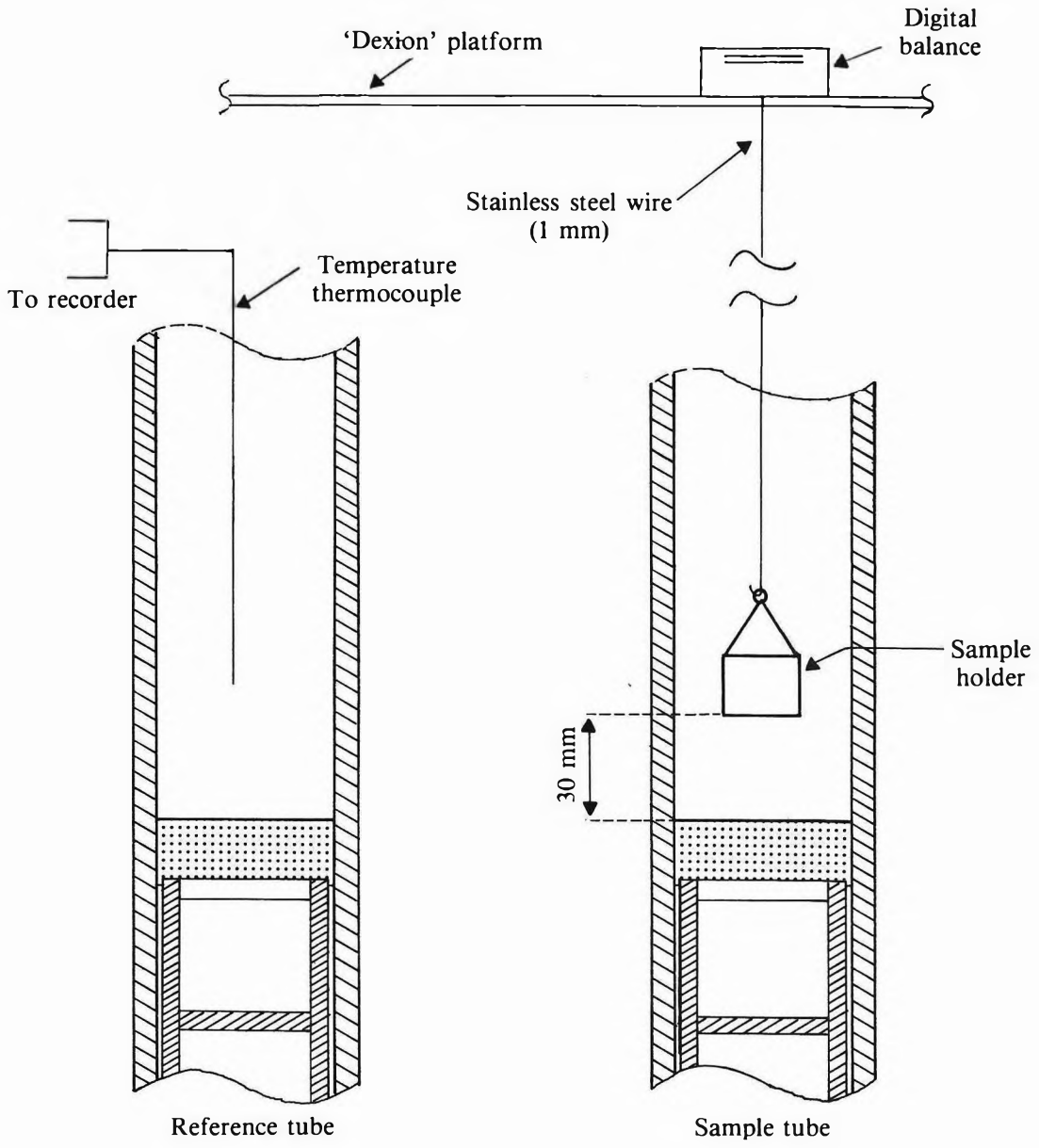

Figure 2. Experimental set-up for TG analysis.

the same time but independently, *i.e.* each of them had its own flame front. The flaming combustion was rather noisy, like the firing of crackers, and this is believed to be due to the volatiles being released in 'bursts'. All the char pieces began to burn by glowing combustion as soon as the flaming combustion had subsided and before the DTA trace had made its way down. This resulted in only one peak being formed, at 295°C, with a height of 54°C *(Figure 4)*. These results appear to show that it is possible to burn off the pyrolysis products

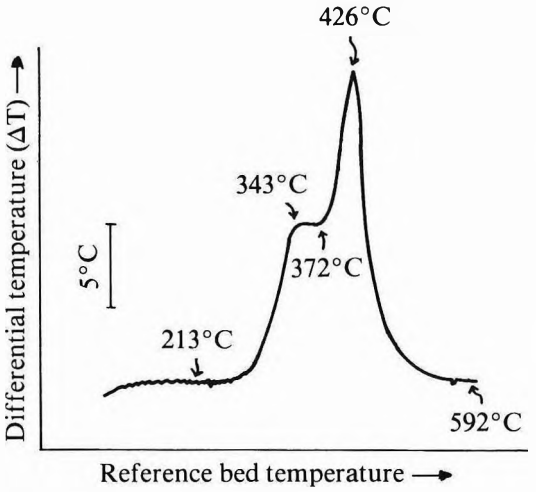

Figure 3. DTA curve in air of rubberwood.

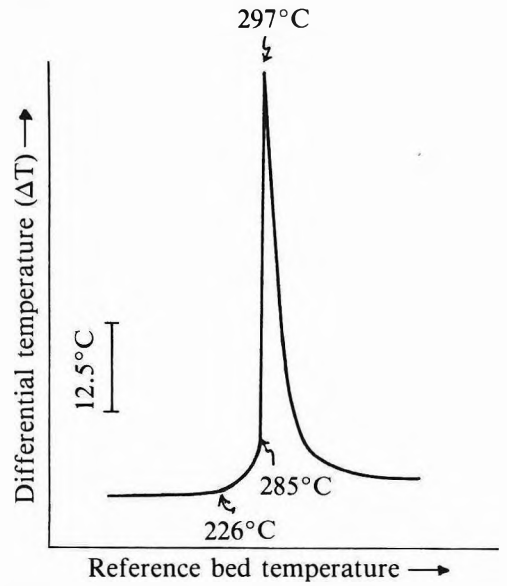

Figure 4. DTA curve in 80% oxygen of rubberwood.

at a lower temperature with an increased oxygen supply. Similar observations have been made by Stott and Baker[6] in studies on coal pyrolysis and combustion.

Besides oxygen supply, the shape of a DTA curve is also influenced by other factors, including the heating rate and the particle size of the wood[7,8].

Comparison with Other Wood Species

The DTA curves in air and in 80% oxygen of the other wood species are given in *Appendix A* while particulars of their respective reaction peaks are presented in *Tables 2* and *3*.

No flaming or glowing combustion occurred in any of the runs in air of the other wood species. Each of the resultant DTA curves contained two overlapping exotherms, as in the case of rubberwood. However, the first exotherm of some of the wood species appeared more like a shoulder than a peak. Except for oil palm wood, the second exotherm was considerably larger than the first. The first peak temperature varied from 302°C for oil palm wood to 364°C for Nyatoh, Tembusu and Chengal and the second from 401°C for oil palm wood to 501°C for Chengal. The heights of the two peaks also varied from species to species, the first from 3.9°C for Balau to 12.5°C for oil palm wood and the second from 13.3°C for dark red Meranti to 24.0°C for Nyatoh. As the first peak is attributed to the volatiles, its height gives an indication of the rate of pyrolysis of the sample, *i.e.* the higher the peak, the faster the wood pyrolyses and the better the resolution of the two peaks, as in the case of oil palm wood. Since the first peak of rubberwood's DTA curve is the fourth highest of all the wood species tested, the inference is that it is relatively easy to pyrolyse.

It was rather difficult to determine the combustion time of each sample as its DTA trace did not immediately return to the base line when it was completely burnt. For this reason, the location of the second peak was used as the basis for comparing the combustion times of different wood species since the farther it was from the origin, the longer the wood took to burn to completion. Thus, since the second peak temperature of oil palm wood was the lowest of all the wood species tested, its combustion time was the shortest. The difference between the second peak temperatures of two test samples divided by the heating rate gave approximately the difference in their burning times. Based on this criterion, the burning times of the various wood samples relative to that of oil palm wood were calculated

TABLE 2. PEAK TEMPERATURES AND HEIGHTS (DIFFERENTIAL THERMAL ANALYSIS IN AIR)

Species	First peak		Second peak	
	Temp. (°C)	Height (°C)	Temp. (°C)	Height (°C)
Oil palm wood	302	12.5	401	14.2
Jelutong	338	10.7	432	16.5
Mengkulang	353	6.3	435	22.5
Pulai	347	9.8	436	16.5
Mersawa	351	4.6	458	21.0
Meranti, light red	348	6.0	463	13.9
Meranti, dark red	363	5.0	472	13.3
Sepetir	339	8.9	428	18.0
Rubberwood	343	8.9	426	17.0
Nyatoh	364	4.7	449	24.0
Keruing	356	4.7	478	17.5
Tualang	359	5.7	464	19.0
Ramin	341	7.1	426	18.5
Tembusu	364	4.6	490	13.4
Merbau	356	5.9	451	19.5
Kempas	356	5.0	480	14.8
Chengal	364	4.0	501	15.7
Coconut wood	360	4.9	474	18.8
Balau	361	3.9	498	16.0

and presented in *Table 4*. It is noted that, compared with oil palm wood, the other wood species took between 4.5 min and 18.2 min longer to burn. The results show that, in general, the greater the density of a wood species, the longer it takes to burn. Rubberwood was ranked second, together with Ramin, in terms of ease of burning.

In the runs of the other wood species in 80% oxygen, ignition occurred in only four of them, *i.e.* in those of oil palm wood, Jelutong, Pulai and Sepetir. This brings to five the number of wood species whose samples burnt with a flame in runs in 80% oxygen. Each of their DTA curves contained only one peak, as in that of rubberwood. The DTA curve of Ramin also contained a single peak although no flaming combustion occurred in its run. This was because its char began to burn at a relatively low temperature (around 310°C), resulting in the two reaction peaks merging into one. The DTA curves of the other wood species exhibited the usual two reaction peaks which were higher and also located at lower temperatures compared with those resulted from the first set of runs. In all the runs in 80% oxygen, the residual char burnt by glowing combustion. Again oil palm wood was the first to burn to completion. The combustion times of the other wood species relative to that of this wood were determined in the same way as before. As shown in *Table 5*, the other wood species took between 4 min and 34 min longer to burn compared with oil palm wood. Again, with a few exceptions, the lighter species burnt faster. This time rubberwood was ranked fourth, in terms of rate of burning. The order of the various wood species in combustion time obtained from the second set of experiments was about the same as that obtained from the first. This indicates that, for the majority of the wood species tested, an increase in the oxygen supply merely resulted

TABLE 3. PEAK TEMPERATURES AND HEIGHTS (DIFFERENTIAL THERMAL ANALYSIS IN 80% OXYGEN)

Species	First peak		Second peak	
	Temp. (°C)	Height (°C)	Temp. (°C)	Height (°C)
Oil palm wood	263	85.0	—	—
Jelutong	284	64.0	—	—
Mengkulang	310	8.3	362	54.0
Pulai	287	65.0	—	—
Mersawa	322	7.9	385	48.0
Meranti, light red	321	8.5	406	27.0
Meranti, dark red	338	7.6	409	36.0
Sepetir	295	59.5	—	—
Rubberwood	295	54.0	—	—
Nyatoh	350	6.5	393	55.0
Keruing	354	6.2	425	37.0
Tualang	340	9.0	408	36.0
Ramin	316	42.0	—	—
Tembusu	360	5.5	449	28.0
Merbau	325	9.5	375	44.0
Kempas	335	9.3	411	28.5
Chengal	357	5.2	438	39.5
Coconut wood	330	5.7	402	37.0
Balau	358	4.5	449	39.0

in the wood burning faster and did not alter its relative combustibility.

In *Table 6,* the various wood species are listed in descending order of their first peak heights from the first set of runs. It is noted that the first five slots are occupied by species whose samples burnt with a flame in the runs in 80% oxygen. This is not surprising since the height of the first peak is related to the rate of pyrolysis and the higher the peak, the faster is the evolution of the volatiles and the greater is the tendency for ignition to take place.

If desired, the heat released by each test sample can be determined by first performing an internal calibration involving the insertion of a heating coil into one of the beds in a blank run and noting the area under curve of the resultant peak for a certain power input. This is another advantage of performing the DTA experiments in fluidised beds[9].

Thermogravimetry

The TG curves in nitrogen gas and in air of rubberwood are shown in *Figure 5.* It can be seen that although each of the test samples began to lose weight at around 130°C, the bulk of the weight loss occurred above 200°C. Pyrolysis of the wood *(Portion I)* took place mainly between 300°C and 370°C in nitrogen gas and below 300°C in air. It is clear that the rate of pyrolysis of the wood was faster in air than in nitrogen gas. The char yield at a particular temperature may be determined from *Portion II* of *Curve (a).* At 500°C, for example, it amounted to 27.8%. In an oxidative environment, the char is decomposed or burnt, leaving behind ash. *Portion II of Curve (b)* corresponds to decomposition of the char.

As in the case of rubberwood, the rate of pyrolysis of the other wood species was higher in air than in nitrogen gas, as shown in their

TABLE 4. BURNING TIMES RELATIVE TO THAT OF OIL PALM WOOD (DIFFERENTIAL THERMAL ANALYSIS IN AIR)

Species	Ranking in density	Extra burning time (min)
Oil palm wood	19	.0
Rubberwood	11	4.5
Ramin	7	4.5
Sepetir	12	4.9
Jelutong	18	5.1
Mengkulang	17	6.2
Pulai	16	6.4
Nyatoh	10	8.7
Merbau	5	9.1
Mersawa	15	10.4
Meranti, light red	14	11.3
Tualang	8	11.5
Meranti, dark red	13	12.9
Coconut wood	2	13.3
Keruing	9	14.0
Kempas	4	14.4
Tembusu	6	16.2
Balau	1	17.6
Chengal	3	18.2

TABLE 5. BURNING TIMES RELATIVE TO THAT OF OIL PALM WOOD (DIFFERENTIAL THERMAL ANALYSIS IN 80% OXYGEN)

Species	Ranking in density	Extra burning time (min)
Oil palm wood	19	.0
Jelutong	18	3.8
Pulai	16	4.4
Rubberwood	11	5.8
Sepetir	12	5.8
Ramin	7	9.6
Mengkulang	17	18.0
Merbau	5	20.4
Mersawa	15	22.2
Nyatoh	10	23.6
Coconut wood	2	25.3
Meranti, light red	14	26.0
Tualang	8	26.4
Meranti, dark red	13	26.5
Kempas	4	26.9
Keruing	9	29.5
Chengal	3	31.8
Tembusu	6	33.8
Balau	1	33.8

TG curves in *Appendix B.* The char yield at 500°C varied from 26.6% for oil palm wood to 39.5% for Merbau *(Table 7)* and did not appear to be related to the density of the wood. Except for Sepetir, those species which burst into flame in the DTA runs recorded the lowest char yields. This is to be expected in view of the fact that the lower the char yield, the higher is the amount of volatiles produced and the greater is the tendency for ignition to occur. It is necessary to add that besides yield, the rate of production of the volatiles is also important. This is because if the volatiles are released slowly over a wide temperature range, the likelihood of the fuel mixture being rich enough for ignition to take place becomes less.

In the runs conducted in an oxidative environment, oil palm wood was the first to burn to completion, as in the case of DTA. The combustion times of the other wood species relative to that of this species were calculated, using the 5% weight mark as the end point since the exact end point could not be ascertained. As shown in *Table 8,* the other wood species took between 4 min and 33 min longer to burn compared with oil palm wood. Only three of the wood species tested burnt faster than rubberwood, namely oil palm wood, Jelutong and Pulai. With one or two exceptions, the order of the wood species in combustion time obtained from the TG runs was about the same as that obtained from the DTA runs. This shows that the two methods gave fairly similar results.

It needs to be mentioned that in the DTA and TG experiments, the ash formed did not

TABLE 6. FIRST PEAK HEIGHTS (DIFFERENTIAL THERMAL ANALYSIS IN AIR)

Species	Ranking in density	Height of first peak (°C)
Oil palm wood	19	12.5
Jelutong	18	10.7
Pulai	16	9.8
Rubberwood	11	8.9
Sepetir	12	8.9
Ramin	7	7.1
Mengkulang	17	6.3
Meranti, light red	14	6.0
Merbau	5	5.9
Tualang	8	5.7
Kempas	4	5.0
Meranti, dark red	13	5.0
Coconut wood	2	4.9
Keruing	9	4.7
Nyatoh	10	4.7
Mersawa	15	4.6
Tembusu	6	4.6
Chengal	3	4.0
Balau	1	3.9

TABLE 7. CHAR YIELDS AT 500°C

Species	Ranking in density	Char yield (%)
Oil palm wood	19	26.6
Jelutong	18	27.1
Rubberwood	11	27.8
Pulai	16	28.4
Ramin	7	30.2
Tembusu	6	30.2
Keruing	9	31.0
Meranti, light red	14	31.2
Kempas	4	32.6
Sepetir	12	32.9
Coconut wood	2	33.2
Mengkulang	17	33.2
Mersawa	15	33.7
Tualang	8	34.2
Nyatoh	10	35.2
Balau	1	36.1
Meranti, dark red	13	36.7
Chengal	3	38.8
Merbau	5	39.5

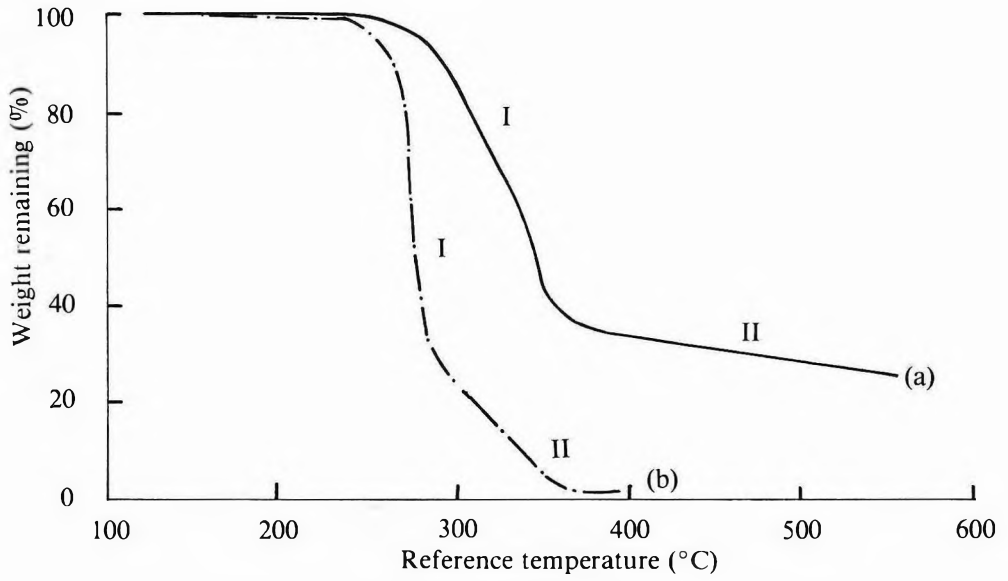

Figure 5. TG curves of rubberwood: (a) in nitrogen gas and (b) in air.

TABLE 8. BURNING TIMES RELATIVE TO THAT OF OIL PALM WOOD (THERMOGRAVIMETRY IN AIR)

Species	Ranking in density	Extra burning time (min)
Oil palm wood	19	.0
Jelutong	18	3.7
Sepetir	12	4.7
Rubberwood	11	5.3
Pulai	16	6.5
Ramin	7	8.2
Mengkulang	17	11.1
Tualang	8	11.8
Merbau	5	12.7
Mersawa	15	14.4
Nyatoh	10	16.2
Meranti, light red	14	17.1
Meranti, dark red	13	17.4
Kempas	4	17.4
Tembusu	6	19.1
Coconut wood	2	23.3
Keruing	9	24.7
Chengal	3	32.4
Balau	1	32.9

adversely affect combustion of the test samples as it was either removed automatically or small in quantity. In practice, especially in static beds, the ash formed around the wood or on top of the fuel bed, if not removed constantly, may impede the flow of oxygen into the wood and adversely affect its combustion. The problem is usually greater for species which have a high ash content. Thus, the results obtained from the DTA and TG studies are more applicable for combustion of wood in systems where the ash formed is removed constantly, either naturally such as in fluidised beds or by some device.

The test samples used in the experiments were oven-dried for uniformity of moisture contents. This is not normally done for fuelwoods which are mostly air-dried. The purpose of drying the wood is to reduce its moisture content so as to improve its combustion efficiency. If the wood is too wet, combustion becomes unstable and the flame may be extinguished. Rubberwood, Pulai and Jelutong, besides being relatively easy to burn, are also comparatively easy to dry[10], which gives them an added advantage over the other wood species for use as fuel. The air-drying characteristics of oil palm wood, another of the species which burns easily, are not available.

CONCLUSIONS

Fluidised-bed DTA appears to be a suitable technique for the study of wood combustion. The rapid transfer of the heat of combustion from the sample bed to the surrounding walls results in a fairly good separation of the reaction peaks of the different pyrolysis products. The variation in the shapes of the DTA curves of different wood species provides a means for comparing their combustion characteristics.

The lighter wood species are generally easier to burn than the denser ones. Rubberwood, although of average density among the wood species tested, appears to be relatively easy to burn. The results of TG analysis on the order of combustibility of the various wood species were in good agreement with those of DTA.

ACKNOWLEDGEMENT

The apparatus used was built in the Chemical and Process Engineering Department of the University of Canterbury, New Zealand while the test materials were provided by the Rubber Research Institute of Malaysia. The authors would like to thank all those concerned for the assistance provided.

REFERENCES

1. SHAFIZADEH, F. AND DEGROOT, W.F. (1976) Combustion Characteristics of Cellulosic Fuels. *Thermal Uses and Properties of Carbohydrates and Lignin (Shafizadeh, F., Sarkenan, K.V. and Tillman, D.A. ed).* New York: Academic Press.

2. TILLMAN, D.A. (1978) *Wood as an Energy Resource.* New York: Academic Press.

3. WENZL, H.F.J. (1970) *The Chemical Technology of Wood* (Translated from German by Brauns, F.E. and Brauns, D.A.). New York: Academic Press.

4. SHAFIZADEH, F. AND DEGROOT, W.F. (1977) Thermal Analysis of Forest Fuels. *Fuels and Energy from Renewable Resources (Tillman, D.A., Sarkanen, K.V. and Anderson, L.L. ed).* New York: Academic Press.

5. NGUYEN, T., ZAVARIN, E. AND BARRALL II, E.M. (1981) Thermal Analysis of Cellulosic Materials. Part I. Unmodified Materials. *J. Macromol. Sci — Rev. Macromol. Chem.,* **C20(1),** 1.

6. STOTT, J.B. AND BAKER, O.J. (1953) Differential Thermal Analysis of Coal. *Fuel,* **32,** 415.

7. TANG, W.K. (1972) Forest Products. *Differential Thermal Analysis (MacKenzie, R.C. ed),* Vol II. New York: Academic Press.

8. TAN, A.G. (1986) The Combustion of Wood, Mainly as Assessed by Fluidised-bed Differential Thermal Analysis, with Particular Reference to Rubberwood. Doctor of Philosophy Thesis, University of Canterbury, New Zealand.

9. BASDEN, K.S. (1967) A Fluidised-bed Differential Thermal Calorimeter. *Physical Aspects of Coal Carbonisation (Kirov, N.Y. and Stephens, J.N. ed).* Research Monograph, Department of Fuel Technology, University of New South Wales, Sydney.

10. GREWAL, G.S. (1979) Air-seasoning Properties of Some Malaysian Timbers. *Malaysian Forest Service Trade Leaflet No. 41.* Kuala Lumpur: The Malaysian Timber Industry Board.

APPENDIX A

DIFFERENTIAL THERMAL ANALYSIS CURVES OF SOME MALAYSIAN WOOD SPECIES: (a) IN AIR AND (b) IN 80% OXYGEN

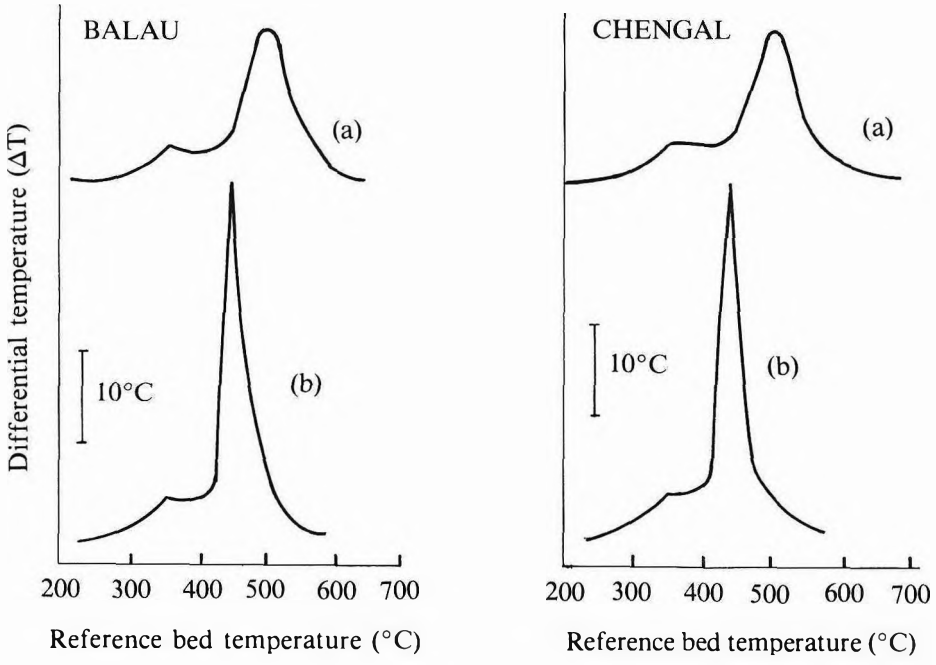

APPENDIX A (CONTD)

DIFFERENTIAL THERMAL ANALYSIS CURVES OF SOME MALAYSIAN WOOD SPECIES: (a) IN AIR AND (b) IN 80% OXYGEN

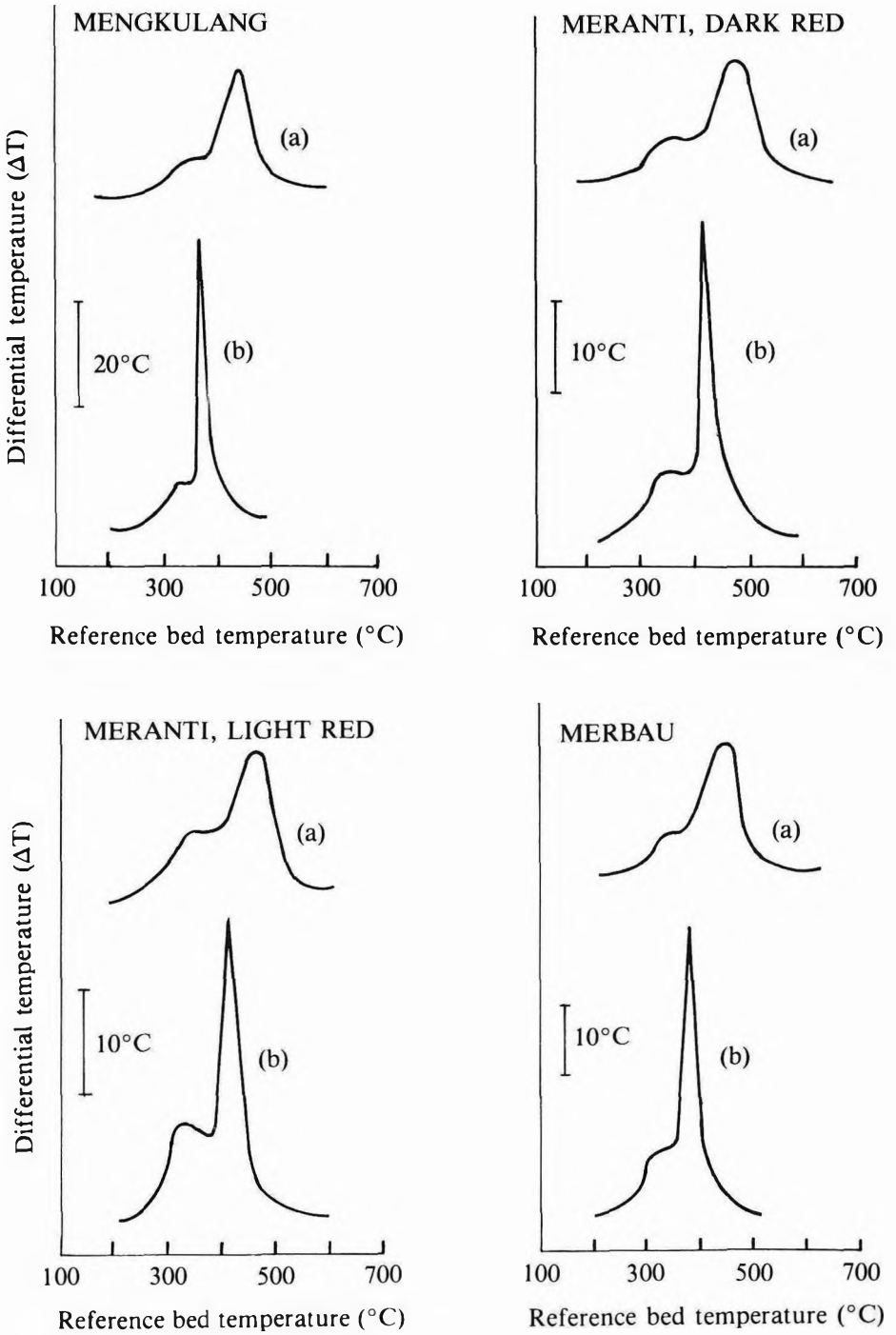

APPENDIX A (CONTD)

DIFFERENTIAL THERMAL ANALYSIS CURVES OF SOME MALAYSIAN WOOD SPECIES: (a) IN AIR AND (b) IN 80% OXYGEN

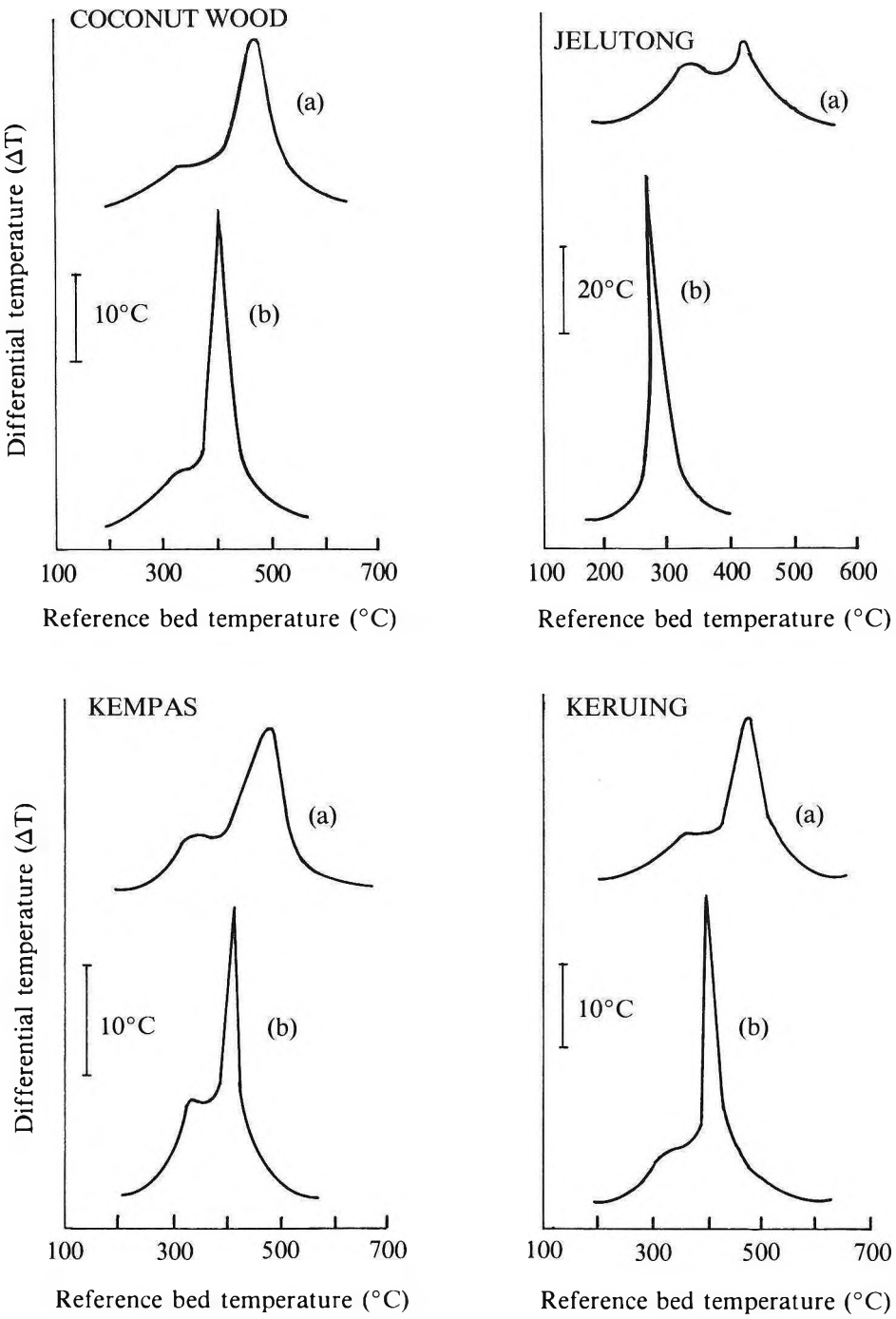

APPENDIX A (CONTD)

DIFFERENTIAL THERMAL ANALYSIS CURVES OF SOME MALAYSIAN WOOD SPECIES: (a) IN AIR AND (b) IN 80% OXYGEN

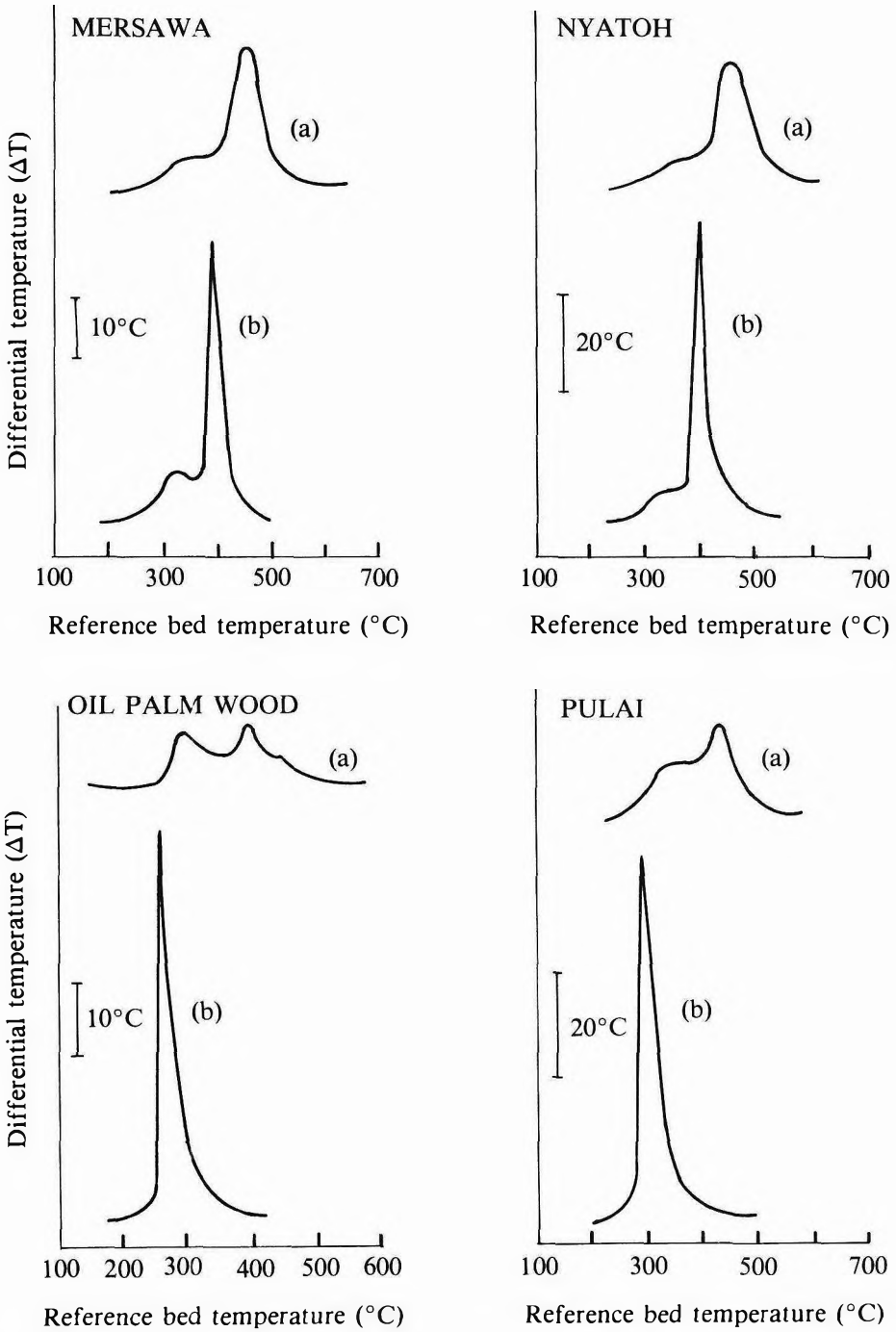

APPENDIX A (CONTD)

DIFFERENTIAL THERMAL ANALYSIS CURVES OF SOME MALAYSIAN WOOD SPECIES: (a) IN AIR AND (b) IN 80% OXYGEN

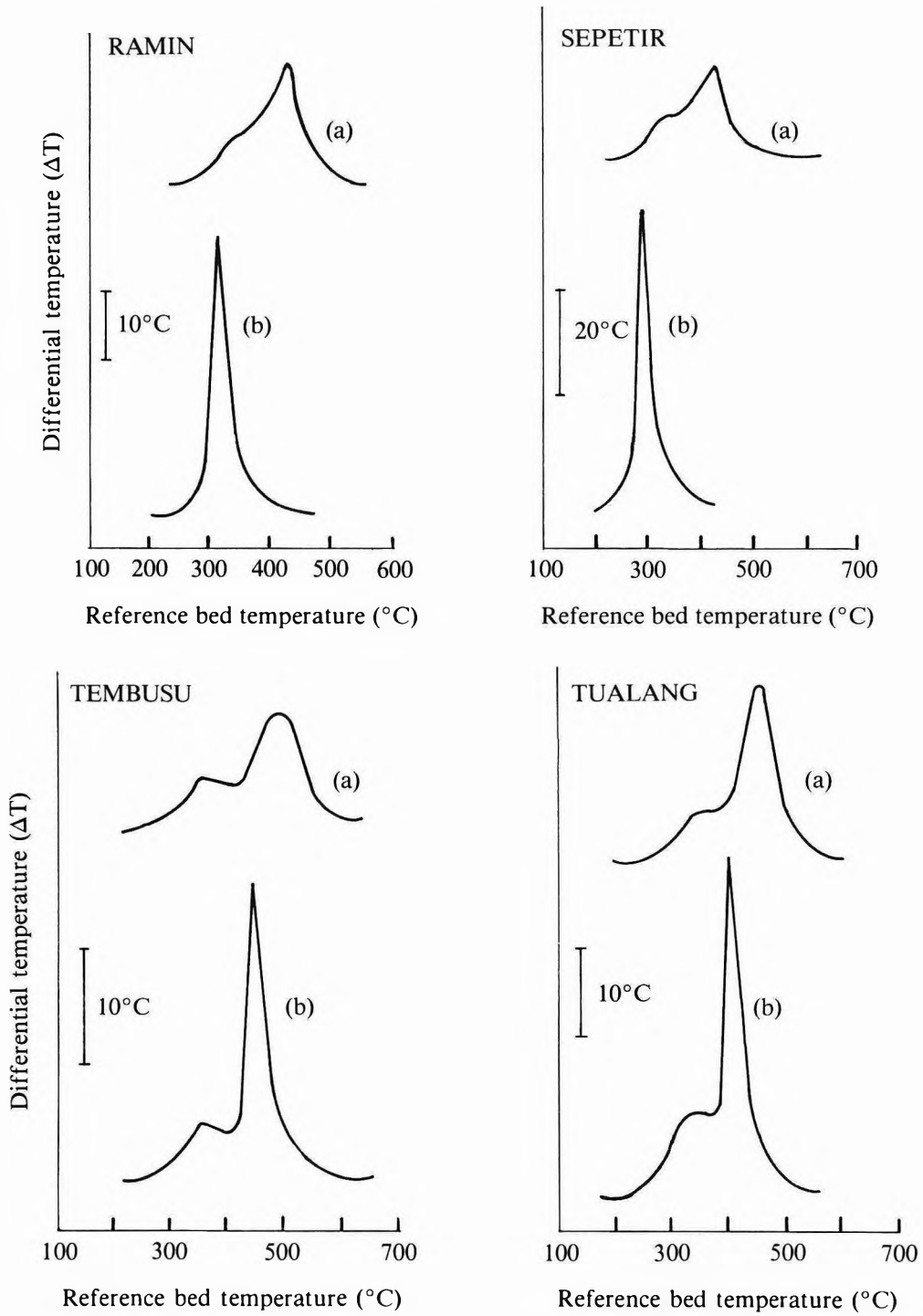

APPENDIX B

THERMOGRAVIMETRY CURVES OF SOME MALAYSIAN WOOD SPECIES: (a) IN NITROGEN GAS AND (b) IN AIR

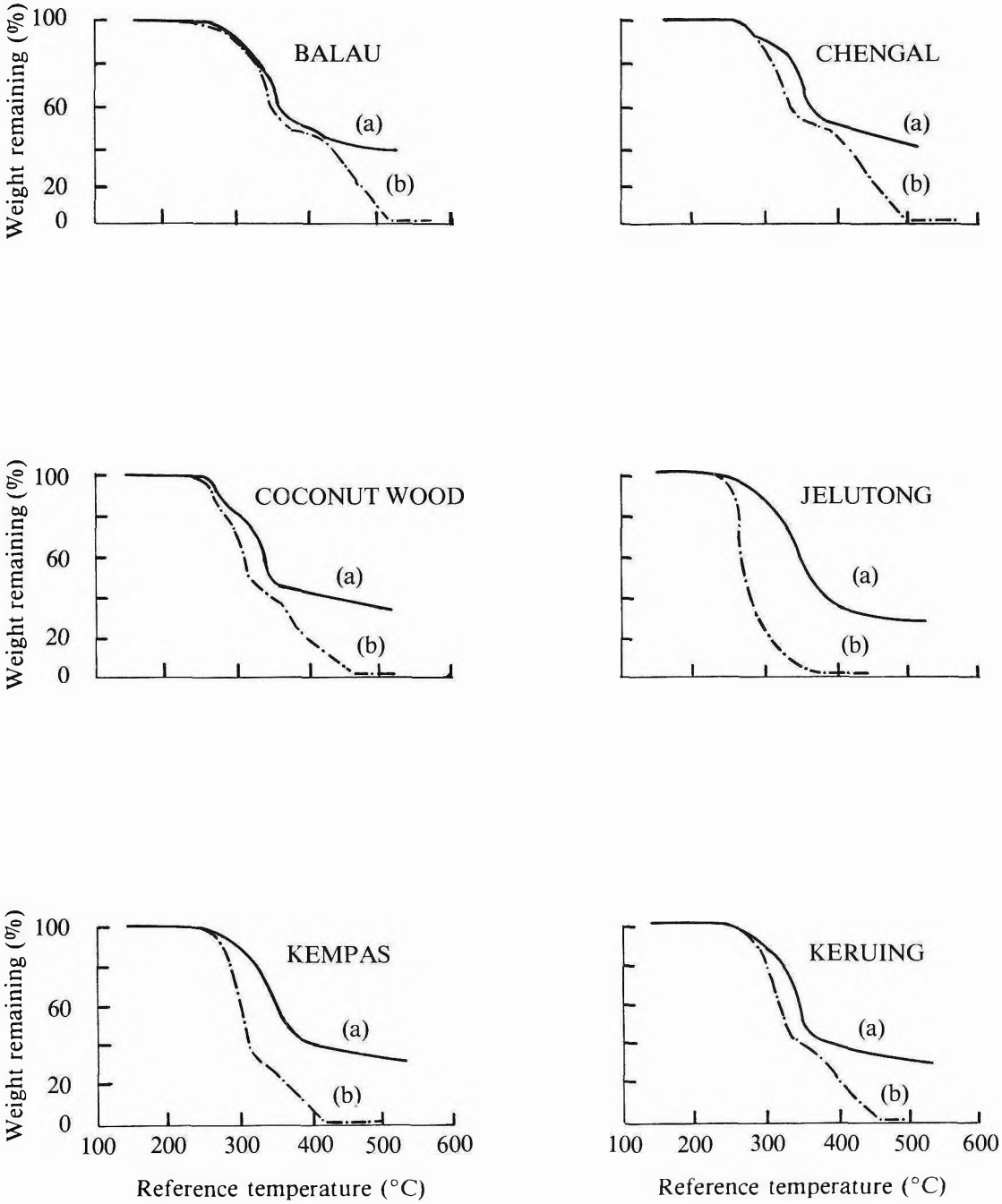

APPENDIX B (CONTD)

THERMOGRAVIMETRY CURVES OF SOME MALAYSIAN WOOD SPECIES:
(a) IN NITROGEN GAS AND (b) IN AIR

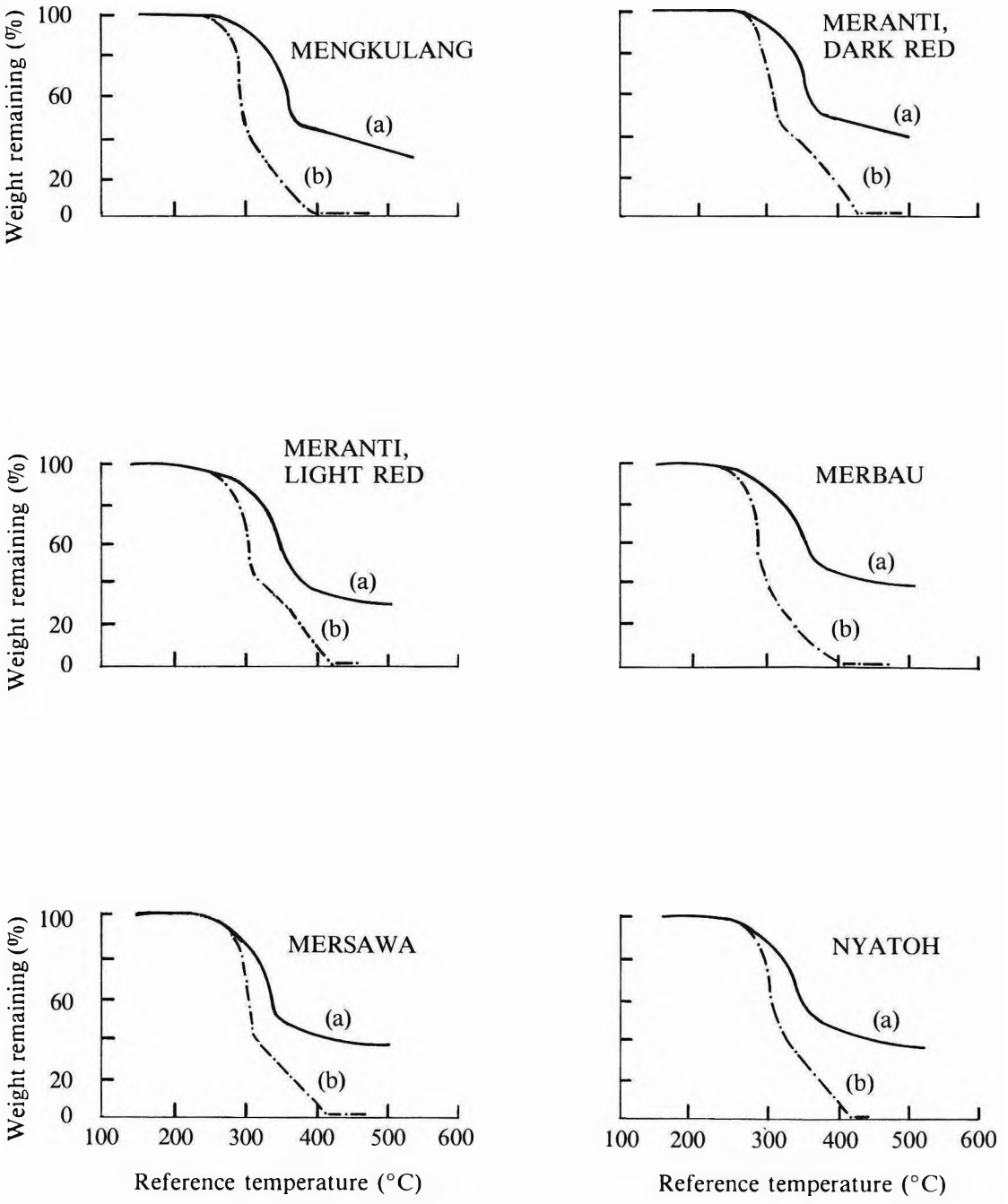

APPENDIX B (CONTD)

THERMOGRAVIMETRY CURVES OF SOME MALAYSIAN WOOD SPECIES:
(a) IN NITROGEN GAS AND (b) IN AIR

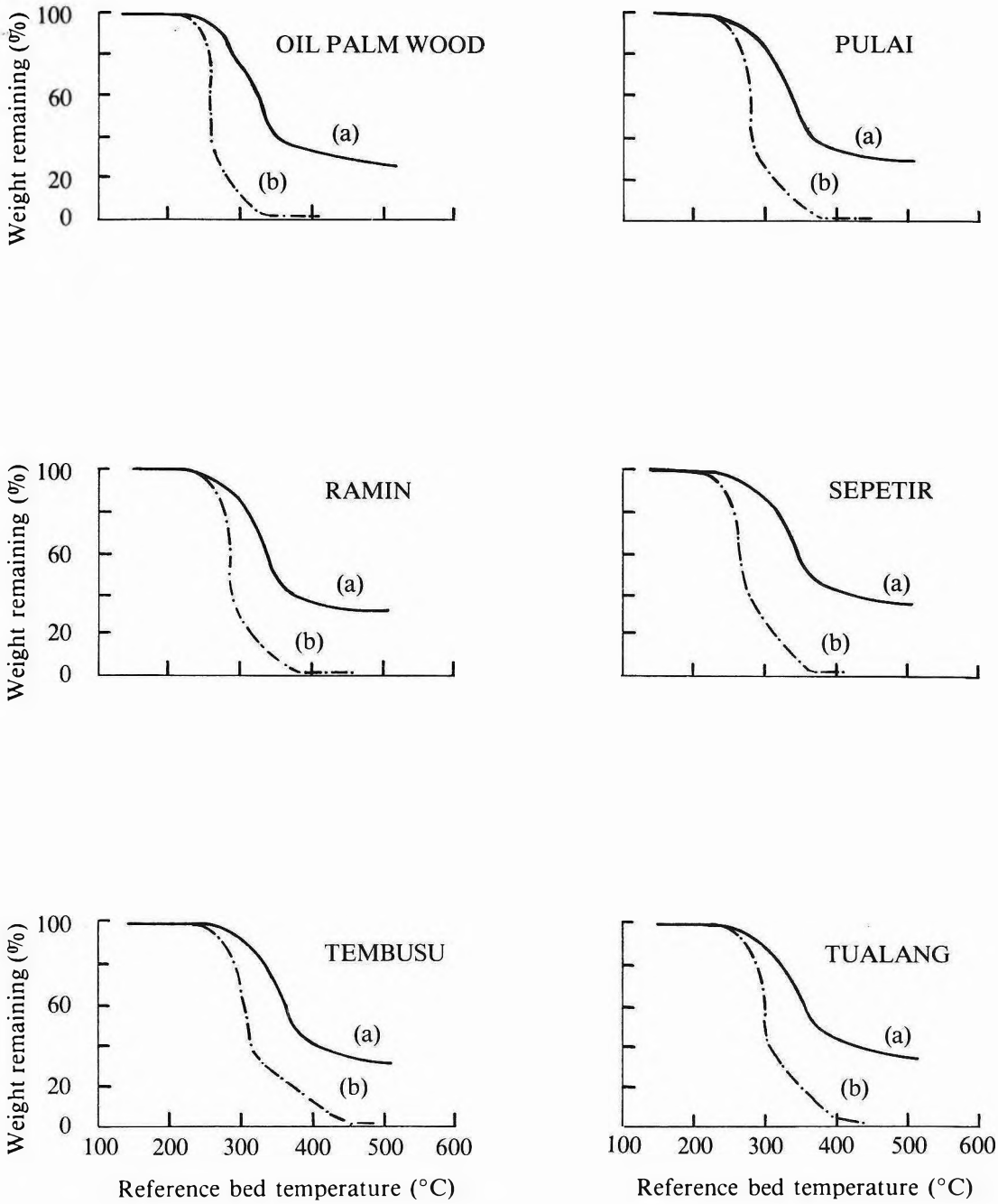

J. nat. Rubb. Res., **2(1)**, 46-54

Correlation Studies on Photosynthetic Rates, Girth and Yield in Hevea brasiliensis

Z. SAMSUDDIN*, H. TAN* AND P.K. YOON*

Correlation studies were carried out using photosynthetic rates (PR) of two-whorl buddings raised from budded stumps in a controlled growth chamber and yield and growth parameters of mature buddings from field trials. Positive correlations between PR and yield over five years (MY) were found. No correlations were, however, detected between PR and mature growth parameters i.e. *girth at opening (GO), girth at fifth year of tapping (GC) and girth increment (GI).*

The correlations between MY and GI or GC were negative and significant. Among the growth parameters, significant positive correlations were found between GO and GC, GC and GI but there was no correlation between GO and GI.

Multiple regression studies of PR on MY, GO, GC or GI suggest that MY was the only dominant and significant variable accounting for 22% of the variation in PR. Growth parameters do not appear to give significant positive predictive power for PR. When MY was used as the dependent variable, with GO, GC and GI as the independent variables, the coefficients of multiple determination (R^2) varied from 0.31 to 0.57. PR showed some additional contribution (significant at $P < 0.1$) when considered together with growth parameters to account for MY.

The significance of these results is discussed in relation to the usage of PR in early selection for yield in Hevea.

Photosynthetic rates (PR) of *Hevea brasiliensis* have been shown to be significantly different in seedlings[1] and in clones[2]. However, there is conclusive evidence available on the relationship between PR and productivity. Samsuddin *et al.*[3] studied PR in a hand pollinated seedling population produced through the breeding programme of the Rubber Research Institute of Malaysia and found significant variation in PR, nursery yield (early test-tapping) and growth parameters among individual seedlings and families. However, there was no significant correlation between PR and nursery yield. Only when combined with other growth characters, did PR show some contribution to variation in nursery yields. This paper extends the study using buddings of clones of known field performance but planted in a controlled environment chamber. It deals with the variations and inter-relationships of PR of buddings and their mature yields and growth performance. It also discusses the potentials of PR as an additional criterion for early culling in rubber breeding.

MATERIALS AND METHODS

Budded stumps of uniform sizes were prepared in Malaysia and despatched to Belgium. They were planted in polybags (25 × 55 cm, lay-flat measurement). These plants were raised in a Weiss controlled growth chamber (at the Department of Biology, Universitaire Instelling Antwerpen, Belgium) having day temperature of 27°C, relative humidity (R.H.) 70% and irradiance 480 $\mu Em^{-2}s^{-1}$ measured at plant height. At night (12 h) the temperature was 25°C and R.H. 90%. At one-whorl leaf stage

*Rubber Research Institute of Malaysia, P.O. Box 10150, 50908 Kuala Lumpur, Malaysia

the leaves were sprayed with a mixture of foliar feed and a zinc-based contact fungicides. Compound fertiliser containing NPK was given when they reached the two-whorl stage. Micro-elements were supplied weekly through nutrient solution following that of Hoagland's[4], but water was given daily.

Photosynthetic rates of the clones were measured on mature[5] intact leaves of the second whorl. A leaf was placed in an assimilation chamber (Sirigor, Siemens, West Germany) that had a constant temperature of 27°C and R.H. of 70%. This chamber was arranged in an open pneumatic circuit to a differential infra-red gas analyser (Maihak, UNOR, West Germany). Air having *circa* 340 $cm^3\ m^{-3}$ CO_2 from outside the laboratory was sucked into a 1 m^3 plastic container before passing through the chamber. Three high pressure sodium lamps (giving irradiance up to 1500 $\mu Em^{-2}\,s^{-1}$ in the 400–700 nm bands) placed at a height of 1.5 m above the chamber were used as the irradiance source. To reduce the heat load from the lamps reaching the chamber, a 5-cm water filter was placed at a distance of 15 cm below the lamps.

Irradiance was measured using a quantum sensor (Lambda Instrument, USA). The PR of interest were at saturated irradiance ($> 1000\ \mu Em^{-2}s^{-1}$)[6]. The course of PR under this irradiance saturated condition was monitored by an analogue recorder. Once equilibrium was attained, the data were printed out by digital data logger connected in parallel to the infrared gas analyser. Leaf area was measured using a portable leaf area meter (Lambda Instrument, USA). Five to ten plants were used for PR measurements. Three to five leaves were measured from each of these plants.

Photosynthetic rates were calculated following:

$$PR = [(C_i - C_o)\, f]/\dot{A}$$

where C_i and C_o are the concentrations of CO_2 (mg dm^{-3}) going into and coming out of the chamber, respectively; f is the air flow rate (dm^3s^{-1}) into the chamber and A is the leaf area (m^2).

Yield and girth data of the clones were obtained from records of large-scale clone trials (LSCT) conducted in various locations and environments in Peninsular Malaysia. Tapping of these trees commenced when 50% or more of the trees reached a circumference of 50 cm at the height of 1.5 m from the union. The half-spiral alternate daily (½S d/2) tapping system was used. Yield was measured once a month. Girth measurements (circumference of trunks) were made at a height of 1.5 m from the union. Girth at the opening of tapping (GO) was measured just before tapping commenced and GC was the girth at the fifth year of tapping. Girth increment (GI), was calculated as the difference between GC and GO. Yield (MY) was calculated as yearly means in grammes per tree per tapping for five years. The means of the variables (MY, GO, GC and GI) of the clones planted in various environmental conditions were calculated and used in the present study. As mature yield and growth performance of clones were derived from LSCT which were planted in various environments, it is assumed that the average values from these trials would be reasonable estimates for their genetic expressions. The trials from which mean performances were calculated are shown in *Table 1.*

Means ($\bar{x}$), standard deviations (s) and simple correlations among the parameters were calculated. Step-wise regression studies were also carried out to determine the contributions of various parameters, singly or in combinations, to variations in PR and MY. For graphical representation, the various classes of the parameters referring to low, $<(\bar{x} - s)$, below average $\bar{x}$ to $(\bar{x} + s)$, and high, $>(\bar{x} + s)$ were used. The upper limits of the low and above average classes are presented in *Figure 1;* thus, forming the boundaries of the carpets and the boxes in the *XY* and *YZ* planes, respectively.

For comparison of the common clones based on groupings of PR and MY, the five classifications considered were: $\bar{x} + 2s$, $\bar{x} + 1s$, $\bar{x}$, $\bar{x} - 1s$ and $\bar{x} - 2s$.

RESULTS

Means and Variations

The means of the parameters studied are shown in *Table 1.* MY has means that range

TABLE 1. MEANS AND STANDARD DEVIATION FOR LEAF PHOTOSYNTHETIC RATES, MATURE YIELD AND GIRTH PARAMETERS OF *HEVEA* CLONES

Clone	Photo-synthetic rate (mg Co_2 $m^{-2}s^{-1}$)	Range	No. of trials	Large-scale clone trial							
				Mean yield (g/tree) tapping)	Range	Girth at opening (cm)	Range	Girth after 5 years of tapping (cm)	Range	Girth increment (cm)	Range
RRIM 600	0.538	0.455–0.609	13	35.1	29.7–60.1	48.1	40.1–56.9	67.1	54.3–80.1	19.0	13.0–20.2
PB 28/59	0.526	0.426–0.572	9	39.0	26.7–51.1	48.8	41.2–54.2	61.2	59.4–64.6	12.4	9.1–13.9
PB 235	0.454	0.334–0.573	4	39.8	37.8–43.1	58.7	57.0–60.1	72.3	72.0–72.7	13.6	12.2–15.7
RRIM 703	0.490	0.471–0.521	8	38.7	31.9–44.4	49.8	47.2–52.4	64.4	62.7–67.6	14.7	12.4–15.7
RRIM 701	0.473	0.380–0.524	9	28.1	21.8–32.9	53.7	50.9–58.6	68.8	68.1–71.2	15.1	12.4–16.1
PB 260	0.452	0.360–0.518	4	39.8	33.7–54.2	52.2	50.9–55.0	66.9	66.6–69.8	14.7	12.2–17.7
RRIM 712	0.445	0.301–0.511	5	38.6	34.7–43.7	47.3	46.7–48.8	61.1	59.4–63.6	13.8	11.5–15.1
AVROS 2037	0.428	0.375–0.474	6	24.3	18.1–36.1	55.8	47.2–66.1	74.8	71.2–84.8	19.0	17.8–21.1
PR 255	0.424	0.328–0.462	7	5.4	28.8–43.0	50.8	44.5–57.2	68.0	65.3–72.7	17.2	13.4–19.2
PB 255	0.420	0.319–0.494	5	38.8	34.4–42.6	52.9	51.1–56.1	67.1	66.3–69.9	14.2	13.1–15.2
PB 217	0.414	0.303–0.506	7	25.5	18.1–27.0	49.5	45.8–51.8	69.2	66.2–72.0	19.7	16.5–20.4
RRIM 628	0.411	0.365–0.443	8	38.3	32.4–44.1	50.0	43.3–62.1	62.3	54.8–65.1	12.3	11.5–19.1
RRIM 623	0.411	0.373–0.440	8	29.0	25.4–41.0	55.1	49.7–60.6	73.3	66.1–78.0	18.2	15.2–20.0
RRIM 527	0.405	0.396–0.413	3	31.3	28.4–35.5	47.8	47.4–48.6	63.5	60.4–65.1	15.7	13.0–17.5
Ch 30	0.403	0.340–0.461	5	18.5	15.2–22.4	50.3	45.3–55.2	70.4	63.8–72.7	20.1	17.0–22.7
PB 5/51	0.395	0.303–0.540	5	29.0	25.5–38.1	49.4	43.0–53.4	65.3	61.8–67.1	15.7	12.9–16.5
RRIM 725	0.391	0.313–0.421	8	31.9	29.9–36.0	48.5	42.5–51.4	64.2	58.0–70.0	15.7	12.8–18.6
RRIM 501	0.381	0.303–0.461	9	33.2	28.7–42.1	50.6	39.6–55.4	62.0	51.0–68.2	11.5	7.0–13.7
PB 242	0.373	0.358–0.446	3	32.1	30.1–34.8	53.3	52.8–53.6	69.6	69.6–71.8	16.3	13.8–18.2
GT 1	0.365	0.320–0.422	8	25.5	21.4–31.8	51.7	47.6–59.3	68.8	62.6–77.1	17.1	12.8–17.8
RRIC 6	0.340	0.319–0.359	6	27.6	23.3–32.7	48.6	45.2–54.2	64.7	59.5–71.5	16.2	12.8–22.7
RRIM 612	0.337	0.329–0.351	6	19.7	15.0–27.6	52.0	49.5–57.3	74.1	70.5–78.9	22.1	19.1–25.4
PR 261	0.312	0.301–0.359	6	34.5	30.2–41.6	47.7	40.7–53.0	65.5	60.1–71.2	17.8	13.7–19.1
Mean	0.417			31.9		51.0		67.2		16.18	
S.D.	0.056			6.42		2.92		4.05		2.71	

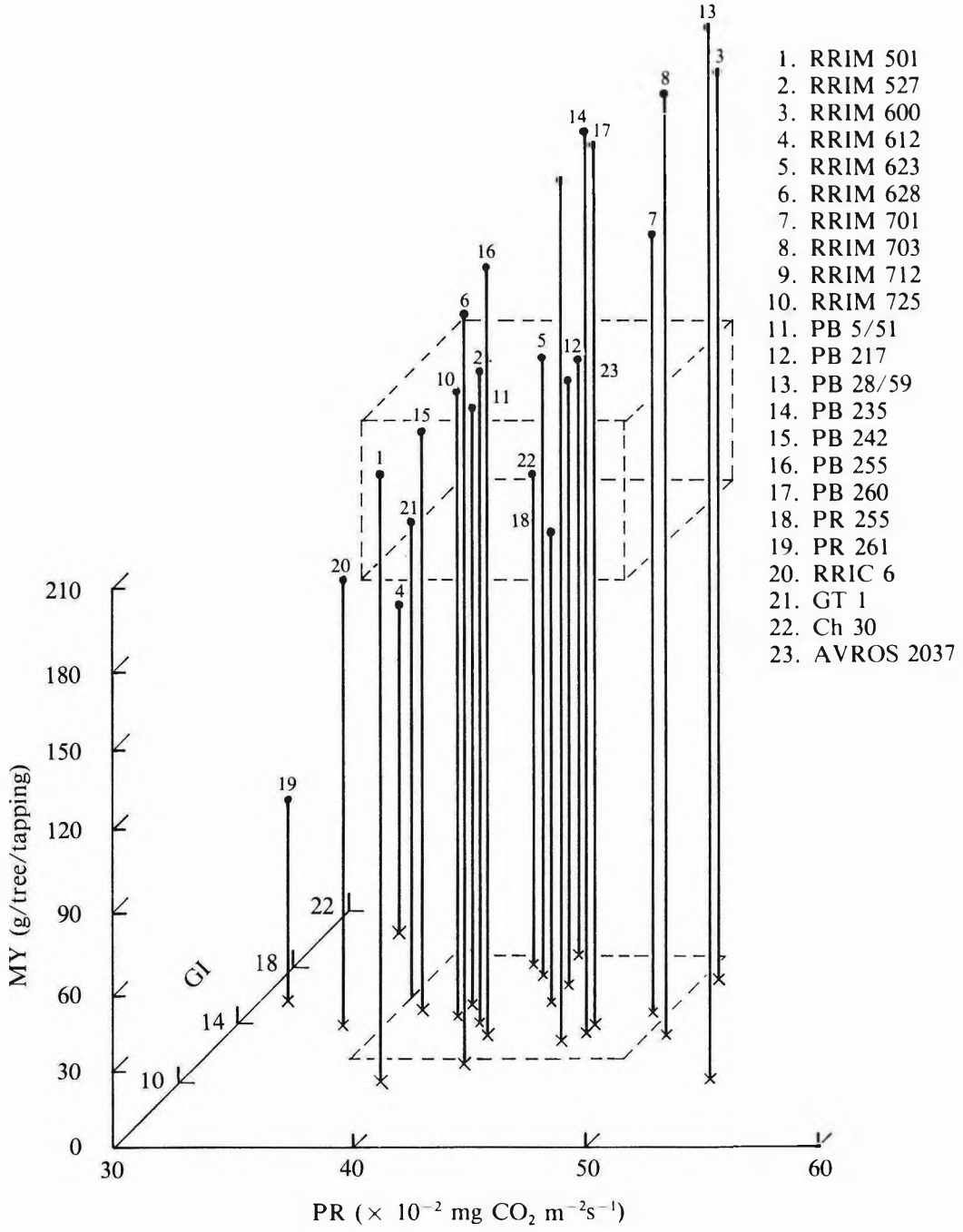

Figure 1. Relationship among leaf photosynthetic rates (PR), mean girth increment over five years (GI) and mean mature yield over five years (MY).

from 18.5 g per tree per tapping to 39.8 g per tree per tapping and shows the highest coefficient of variation (C.V.) (20.1%). The second highest C.V. is shown by GI (16.9%) that has means that range between 11.5 cm to 22.1 cm. This is followed by PR having C.V. of 13.4% and means that range between 0.312 mg CO_2 $m^{-2}s^{-1}$ to 0.538 mg CO_2 $m^{-2}s^{-1}$. GO and GC show low C.V. of 5.7% and 6% and have means that range between 47.7 cm to 58.7 cm and 61.1 cm to 74.8 cm, respectively. The C.V. suggest that the yield and the girth increment during tapping among the clones studied have higher variations than their girth at opening or at the fifth year of tapping. PR were also fairly variable among the clones studied.

Relationship Studies

Simple correlations. The simple correlation coefficients among the characters studied are shown in *Table 2.* The correlation coefficient between PR and MY is positive and significant but those between PR and GC and GI are negative and not significant. The correlation coefficient between PR and GO is, however, positive but not significant. The highly significant negative correlation between GI and MY (-0.754^{***}, d.f. = 21) probably demonstrates the phenomenon of competition for the common assimilates[7]. It is evident that tapping has created a bigger sink compared to that of dry matter accumulation as reflected by the girth increment.

Multiple regression. Two sets of multiple regressions were made *(Table 3).* One uses PR as the dependent variable to see how much the biomass (reflected by girth parameters[8]) and partition (reflected by yield of rubber) explain the variation of PR. The other uses MY as the dependent variable to see the contribution of PR in addition to the growth parameters.

In *Equations 1, 2* and *3* of the step-wise multiple regressions where PR is the dependent variable, MY accounts for 22.0% of the variation in PR. The addition of GC and GO did not contribute significantly in accounting for the variation in PR.

In *Equations 4, 5* and *6* where MY is the dependent variable, the growth parameters GO and GC jointly or GI singly was able to account for MY variation by about 57%. Inclusion of PR as an independent variable together with the growth parameters improve the predictive power for MY to some extent. An increase of about 7% to 13% in coefficients of determination was noted in the step-wise multiple regressions, suggesting that PR does play some part in determining MY.

Photosynthetic rates, girth increment and yield. A graphical presentation of the relation-

TABLE 2. SIMPLE CORRELATIONS AMONG LEAF PHOTOSYNTHETIC RATES, MATURE YIELD AND GIRTH PARAMETERS

Character	Correlation coefficient			
	MY	GO	GC	GI
Leaf photosynthetic rates (PR)	0.469*	0.061NS	−0.152NS	−0.293NS
Mean yield over 5 years (MY)		−0.070NS	−0.557*	−0.754***
Girth at opening (GO)			0.746***	0.038NS
Girth after 5 years of tapping (GC)				0.694**

Degrees of freedom = 21

*, **, *** = P < 0.05, 0.01, 0.001 respectively

NS = Not significant at P < 0.05

GI = Girth increment over five years of tapping

TABLE 3. STEPWISE MULTIPLE REGRESSIONS OF LEAF PHOTOSYNTHETIC RATES AND MATURE YIELD ON OTHER CHARACTERS STUDIED

Equation	Dependent variable	Independent variable	Intercept	R^2
1	PR	0.004*MY (0.002)	0.286	0.220
		0.005*MY + 0.002^{NS} GC (0.002) (0.003)	0.114	0.237
		0.005*MY + 0.003^{NS} GC − 0.001^{NS} GC (0.003) (0.006) (0.007)	0.108	0.238
2	PR	0.004*MY (0.002)	0.286	0.220
		0.004*MY + 0.002^{NS} GO (0.002) (0.004)	0.189	0.229
		0.005*MY + 0.002^{NS} GO + 0.003^{NS} GI (0.003) (0.004) (0.006)	0.108	0.238
3	PR	0.004*MY (0.002)	0.286	0.220
		0.005*MY + 0.002^{NS} GC (0.002) (0.003)	0.114	0.237
		0.005*MY + 0.002^{NS} GC + 0.001^{NS} GI (0.003) (0.004) (0.007)	0.108	0.238
4	MY	−0.881**GC (0.287)	91.088	0.310
		−1.786***GC + 1.685** GO (0.348) (0.483)	65.947	0.571
		−1.592**GC + 1.447** GO + $31.527^{\#}$ PR (0.342) (0.471) (16.491)	51.903	0.640
5	MY	−1.790***GI (16.123)	60.855	0.569
		−1.602***GI + $30.933^{\#}$ PR (0.335) (16.123)	44.913	0.636
		−1.447***GI + $31.527^{\#}$ PR − 0.145^{NS} GC (0.471) (16.491) (0.304)	51.903	0.640
6	MY	−1.790***GI (0.340)	60.855	0.569
		−1.602**GI + $30.933^{\#}$ PR (0.335) (16.123)	44.913	0.797
		−1.592***GI + $31.527^{\#}$ PR − 1.450^{NS} GO (0.342) (16.491) (0.304)	51.903	0.800

PR = Leaf photosynthetic rates
MY = Mean yield over five years
GO = Girth at opening
GC = Girth after five years of tapping
GI = Girth increment over five years
NS = Not significant at $P < 0.05$
# = $P < 0.01$; * = $P < 0.05$; ** = $P < 0.01$; *** = $P < 0.001$
Figures within brackets are the standard error of respective partial regression coefficients.

ships among PR and the means of GI and MY over five years of tapping is given in *Figure 1*. The box forms the boundaries for below average PR, GI and MY. The carpet is the projection of the lower surface of the box that encompasses clones with below average to above average PR and GI. Clones falling to the right of the box or the carpet have high PR. Clones that stand outside the carpet but to the distal boundary have high GI, whilst those outside the frontal boundary have low GI. In general, a good proportion of clones having high PR show high MY whilst those having low PR show low MY. For example, clones RRIM 703, PB 28/59 and RRIM 600 had high PR, average to above average mean girth increment over five years (GI) and high mean yield over five years (MY). On the other hand, clones RRIM 501, PR 261 and RRIC 6 that had low PR showed average to above average GI but low MY. Clones having PR that ranged between average to above average showed GI within the same limits but depending on their positions within the limits had MY that ranged between average to high. The phenomenon of competition between dry matter accumulation (as expressed by GI) and rubber yield that was apparent in the simple correlation study *(Table 2)* is also demonstrated in this graphical presentation.

Photosynthetic rates as selection criteria. The significant and positive though low correlation (r = 0.469) between PR and MY gives an indication that PR may be usefully used as a culling criterion. To assess this possibility, comparison of common clones on different groupings between PR and MY was carried out. PR and MY were ranked and the number of common clones falling into the corresponding groups (fractions) were scored and expressed as the percentage of the number of clones in the PR groupings *(Table 4)*. When means of clones greater than the general mean were taken as the point of cut-off for the top fraction, the percentage of common clones was 80%. However, when the means of clones less than the general mean were taken as the point of cut-off for the bottom fraction, the percentage of common clones was 84.6%.

TABLE 4. NUMBER AND PERCENTAGE OF COMMON CLONES SELECTED OR CULLED USING PHOTOSYNTHETIC RATES AND MATURE YIELD

No. selected in fraction	No. of common clones	
	Top fraction	Bottom fraction
3	2 (66.7)	1 (33.2)
5	3 (60.0)	2 (40.8)
10	8 (80.0)	6 (60.0)
13	9 (69.2)	11 (84.6)

Top 10 is having $\bar{x}$ > means of clones.

Figures within brackets indicate percentage of selected common clones.

DISCUSSION

For a character to be genetically manipulated, it must have a sufficient degree of variation. Photosynthetic rates satisfy this condition. The broad sense heritability for PR in this study has a value of 44%[9], suggesting that this character has sufficient genetic variability and is, therefore, amendable for genetic manipulation.

The significant but low correlation between PR and MY is of interest in this study. Samsuddin *et al.*[3] who studied the correlations between PR and nursery yield (NY) and other nursery growth parameters *i.e.* girth at two years after field nursery planting (NGO), girth after the completion of nursery test-tapping (NGC) and girth increment during test-tapping (NGI) reported no significant correlation between PR and other nursery characters. The approach in these two studies is essentially similar. However, the main differences are that in the previous study PR data were collected on single plants and correlations were made between PR, test-tapping yield and growth parameters of young seedlings grown in field nursery, while the present results were obtained from multiple buddings grown in a controlled environment. Though the magnitude of PR collected in the field and the laboratory is of the same order, the measurement errors can be expected to be greater in the field due to environmental influence and the lack of replicates of the plants. Further, the correlation between NY and mature yield ranges from low to moderate[10]. It is, therefore, possible that the correlation between PR and NY was not

demonstrable because of the limitations of the technique even though some positive association may exist between them.

The significant correlation between PR and MY found here may be due to the better expression of PR in terms of total canopy photosynthates input as the leaf area index (LAI) of *Hevea* clones is similar in mature stand[11]. This is not the case in nursery plants. As the plants in the nursery were young and planted at inter-plant distance of 1.8 × 1.8 m, giving a planting density of 3086 plants per hectare, the expression of the crown photosynthates input and its partitioning may not primarily be influenced by PR but confounded with the crown characteristics and inter-plant competition in the stand.

Leong[12] showed that the LAI of certain *Hevea* clones' canopies remained fairly constant after the fifth year of planting. Templeton[11] also showed that the LAI of a three-year-old AVROS 50 was 4.9 which was comparable to that of a seven-year-old RRIM 501. From these studies, it could be inferred that the LAI of *Hevea* canopies are fairly similar. Thus, it would appear that PR may play a positive role in determining yield of mature *Hevea* plants. Though the associations between PR and partition would be critical, they have yet to be ascertained.

Recognising the important role played by the canopy in mature stands, it would be advantageous if *Hevea* clones with good canopy architecture that effects maximum irradiance interception, thus resulting in a higher total photosynthetic inputs are identified. Conceptually, a good canopy should have leaves with ideal angles of display[13] to capture maximum irradiance and low leaf area density especially at the lower stratum to minimise mutual shading. Satheesan *et al.*[14] showed that due to mutual shading, the middle and lower strata of a *Hevea* canopy intercepted 13% and 6% of the total irradiance, respectively.

The high percentage of common clones falling into both corresponding groups of PR and MY is noteworthy. These results suggest that PR might be useful as a nursery culling criterion. However, this finding has to be treated with caution because of the following limitations. First, the clones used for this study were not selected at random and the sample size was small. Second, the plots from where the yield data were collected were not specially designed for this study, thus the data may not be sufficiently precise. Hence, this study should only be considered as preliminary. Further work using random and larger samples would be necessary to confirm the above findings.

A character to be measured for screening purposes should satisfy the following criteria. It should be cheap, fast and reliable. Whilst PR measurements can be rapidly done using relatively inexpensive instruments, the plants used in this study were raised in a highly sophisticated growth chamber. This factor may be a limitation. One could construct suitable growth chambers at relatively low cost so that large number of young seedling or buddings could be screened in a relatively short time for selection. However, this may not be feasible if one deals with a large population. Alternatively, if the plants to be measured can be replicated (such a technique is now available)[15] to minimise experimental error and/or confounding effect, it should reduce this limitation and PR measurement in field nursery would be worthwhile for inclusion as an additional early selection criterion.

CONCLUSION

Yield in *Hevea* is determined by many factors. This study shows that one of these factors is PR. The positive and significant but low correlation between PR and MY and the fair proportion of agreement of clones from the PR and MY groups are interesting. While this observation does not allow selection of good performers, it nevertheless suggests the possibility of using PR as a criterion for early culling of low yielders. This will effectively cut down the number of progeny to be tested, thus saving land, cost and effort. The speed and relative ease of screening for PR suggests that the use of this parameter may be practical if it is better than or complementary to nursery test-tapping yield that is currently used as one of the

important early selection criteria. However, further work to confirm this relationship should be carried out before the full potential of using PR in the rubber breeding programme can be determined.

ACKNOWLEDGEMENT

The authors are grateful to the Director of the Rubber Research Institute of Malaysia for his permission to publish this paper. Thanks are due to Prof. I. Impens for kindly allowing the PR measurements to be carried out in his laboratory, to the Breeding Group for making available the data from the large-scale clone trials for this study, to Encik-Encik Ku San and P. Kandaswamy for extracting the data from the Breeding Group's records and to Puan Phun for processing the data.

REFERENCES

1. SAMSUDDIN, Z. AND IMPENS, I. (1978) Water Vapour and Carbon Dioxide Diffusion Resistances of Four *Hevea* Clonal Seedlings. *Exptl. Agric.*, **14,** 173.

2. SAMSUDDIN, Z. AND IMPENS, I. (1979) Photosynthetic Rates and Diffusion Resistances of Seven *Hevea brasiliensis* Muell. Arg. Clones. *Biol. Plant.*, **21(2)),** 184.

3. SAMSUDDIN, Z., TAN, H. AND YOON, P.K. (1985) Variations, Heritabilities and Correlations of Photosynthetic Rate, Yield and Vigour in Young *Hevea* Seedling Progenies. *Proc. Int. Rubb. Conf. 1985 Kuala Lumpur,* **3,** 137.

4. HOAGLAND, D.R. (1948) *Lectures on the Inorganic Nutrition of Plants.* pp. 48–71. Walton, Mass., USA: Chronica Botanica Co.

5. SAMSUDDIN, Z., MOHD. KHIR ABD. RAHMAN AND IMPENS, I. (1978) Development of Leaf Blade Class Concept for the Characterisation of *Hevea brasiliensis* Muell. Arg. Leaf Age. *J. Rubb. Res. Inst. Malaysia,* **26(1),** 1.

6. SAMSUDDIN, Z. (1978) Laboratory Study of Leaf Gas Exchange Characteristics of *Hevea brasiliensis* Muell. Arg. and Their Relationships to Field Performance Data. Doctor of Science Thesis, Universitaire Instelling Antwerpen, Belgium.

7. TEMPLETON, J.K. (1969) Partition of Assimilates. *J. Rubb. Res. Inst. Malaya,* **21(3),** 259.

8. SHORROCKS, V.M., TEMPLETON, J.K. AND IYER, G.C. (1965) Mineral Nutrition, Growth and Nutrient Cycle of *Hevea brasiliensis.* III. The Relationships Between Girth and Shoot Dry Weight. *J. Rubb. Res. Inst. Malaya,* **19(2),** 85.

9. TAN, H. AND SAMSUDDIN, Z. (1985) Unpublished date. Rubber Research Institute of Malaysia.

10. TAN, H. (1987) Current Status and Strategy in *Hevea* Breeding. *Improvement of Vegetatively Propagated Plants (Abbott, A.J. and Atkin, R.K. ed).* London: Academic Press.

11. TEMPLETON, J.K. (1968) Growth Studies in *Hevea brasiliensis.* I. Growth Analysis up to Seven Years after Budgrafting. *J. Rubb. Res. Inst. Malaya,* **20(3),** 136.

12. LEONG, W. (1980) Canopy Modification and Its Effects on the Growth and Yield of *Hevea brasiliensis* Muell. Arg. Doctor of Agricultural Science Thesis, University of Ghent.

13. CAMPBELL, G.S. (1977) *An Introduction to Environmental Physics.* New York: Springer-Verlag Inc.

14. SATHEESAN, K.V., GURURAJA RAO, G., SETHURAJ, M.R. AND RAGHAVENDRA, A.S. (1983) Canopy Photosynthesis in Rubber *Hevea brasiliensis.* Characteristics of Leaves in Relation to Light Interception. *VI Int. Congr. Photosynthesis Brussels 1983.*

15. YOON, P.K. (1985) Unpublished data. Rubber Research Institute of Malaysia.

J. nat. Rubb. Res., **2(1)**, 55–65

Flow of Rubber in an Internal Mixer

MOHAMAD BIN HAMZAH*

Visualisation studies of the dynamics of flow of rubber were undertaken using a laboratory-scale Banbury mixer with a transparent chamber. This technique was developed at the Institute of Polymer Technology, University of Technology, Loughborough under the guidance of Mr P.K. Freakley. The method proved to be very informative; the flow pattern could be recorded and its complexity identified. By measuring pressure and the rheological properties of rubber, the stress distribution inside the mixing chamber could be calculated.

From the flow pattern and stress distribution, the modes of mixing inside the chamber could be identified as follows. Dispersive mixing occurs in the region at and immediately in front of the rotor tips while distributive mixing occurs at the S-shaped and bridge regions. There are also voids in the chamber where no mixing occurs, but the formation of these voids helps to enhance distributive mixing.

Since the 1950s a considerable amount of progress has been made in establishing fundamental concepts of the mixing process[1–3]. Though applications of these concepts have not yet been widely accepted, they provide some framework for the study of flow patterns and shearing characteristics of several widely used mixing devices[1]. In those studies the flow patterns were analysed based on the mathematical models of various workers[4–7] who made several simplifying assumptions on both material properties and rotor geometry.

It is generally known that the present understanding of flow patterns in rubber mixing is still inadequate to fulfil the requirement of the processor whose primary aim is to identify the optimum mixing conditions. The fundamental problems are the complexity of the rheological behaviour of rubber and the intentionally imposed 'disorder' of flow in the internal mixer. Boundary conditions and justifiable assumptions are difficult to determine due to non-steady state conditions.

In respond to the above problems a series of mixing programmes were drawn up at Loughborough University specifically to study the mixing behaviour of rubber in an internal mixer. In this work, an attempt was made to study the flow pattern of rubber in the mixing chamber by means of flow visualisation. By this method the difficulties of boundary conditions and simplifying assumptions could be largely eliminated and the true phenomena of the mechanics of flow could then be observed.

EXPERIMENTAL PROCEDURE

The experiment was carried out using a laboratory-scale midget Banbury with a transparent chamber[8].

Flow Pattern between Rotor and Chamber Wall

The aim of this experiment is to establish the flow pattern of the material between the rotor and chamber wall of the internal mixer.

Small cubes (about 1 mm^3) of coloured vulcanised rubber were incorporated into silicone rubber to act as markers. They were then introduced into the mixing chamber *via* the throat of the mixer. The ram was then applied and the mixer was operated at equilibrium ram pressure. (The equilibrium ram pressure was defined as being the condition when upward

*Rubber Research Institute of Malaysia, P.O. Box 10150, 50908 Kuala Lumpur, Malaysia

and downward forces on the ram were practically equal, and only a small amount of ram movement occurred due to transient differences between these forces.) When the machine was switched on, the movement of the markers was recorded using a polaroid polarvision cine cinema placed directly at the side of the mixer. The resulting films were studied using a polarvision viewer having four different speeds and capable of running frame by frame. The flow paths of the marker movement were traced at short intervals on a transparent sheet which was placed on the viewing screen. The experiment was carried out on the left hand rotor at 0.7 r.p.m. fill-factor and 16.7 r.p.m. rotor speed (20 r.p.m. on the fast rotor).

Pressure Measurement

The pressure in the mixing chamber was recorded by means of a Dynisco pressure transducer located in the wall of the mixing chamber. The pressure measuring diaphragm of the transducer was adjusted until it was just flashed out of the inner chamber wall.

Since the speed ratio between the slow (left) and fast (right) rotors was 1:1.2, there were five and six revolutions of the slow and fast rotor respectively in one complete cycle. The experiment was carried out for 0.5, 0.7, 0.9 and 1.0 fill-factors and 10, 15, 20, 25 and 30 r.p.m. rotor speeds (fast rotor) for at least three cycles.

RESULTS AND DISCUSSION

Definition of Regions in the Mixing Chamber

Figures 1 and *2* show the various regions inside the mixing chamber.

Region A : A sickle-shaped region, in front of the rotor wings, formed by the relative motion of the curve surface of the rotor and the cylindrical wall of the mixing chamber.

Region B : A void region situated directly behind the rotor tips which is essentially empty, but could contain fractured loose bits of rubber not adhering to the bulk of the coherent mass.

Region C : A circumferential *S*-shaped region, around the end of the two rotor

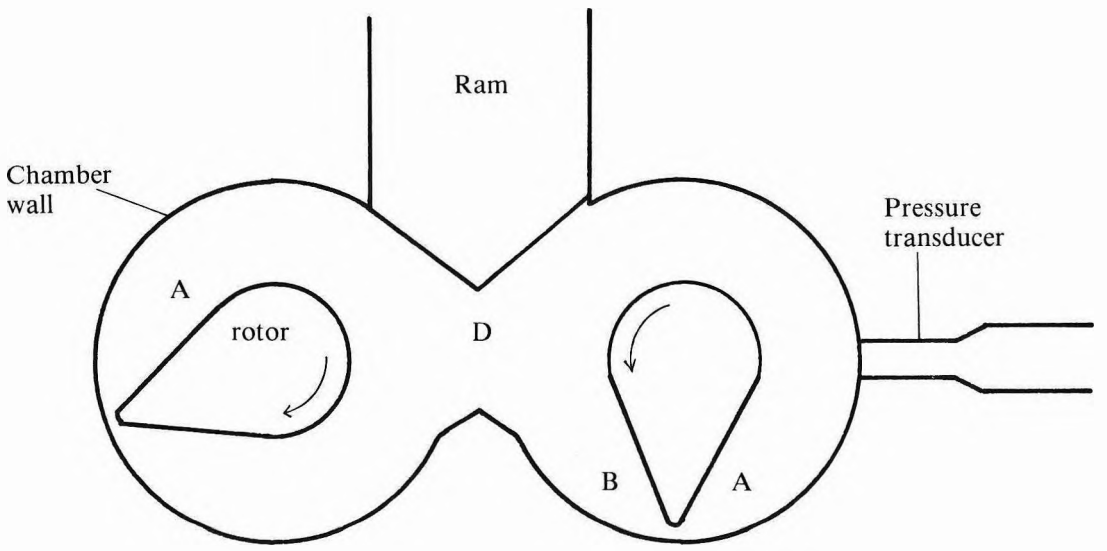

Figure 1. Cross-section view of Banbury visualisation rig. (Letters refer to various regions identified in the discussion.)

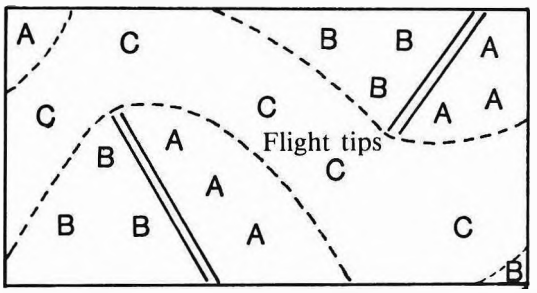

Figure 2. Development of the periphery of the rotor. (Letters refer to various regions identified in the discussion.)

wings, caused by the action of the two flights being situated opposite to each other.

Region D : A region in between the two rotors where transference of material between the two lobes of mixing chamber takes place or sometimes known as the bridge region.

Flow Pattern between Rotor and Chamber Wall

Sickle-shaped region (Region A). *Region A* is sickel-shaped in areas well away from the bridge. The sickel shape is formed by the curve surface of the rotor and the cylindrical wall of the mixing chamber. Due to the motion of the rotor this region is constantly filled with material when the fill-factor is greater than 0.7.

Figure 3 shows the general flow pattern of the markers flowing between the rotor and the chamber wall observed using the polarvision viewer. Each line represents the flow path of a marker. In order to see the overall flow pattern, the path of the markers was plotted on the same axis, although these were taken from different revolutions. The rotor was assumed to be stationary. From this plot, it is apparent that the markers flow at an angle to the direction of rotation or in the direction about normal to the helix angle.

Since *Region A* is always filled with material, a streamlined flow will occur, due to both pressure and drag flow. The pressure flow is caused by the converging effect of the rotor and chamber wall, while the drag flow is caused by the motion of the rotor relative to the chamber wall.

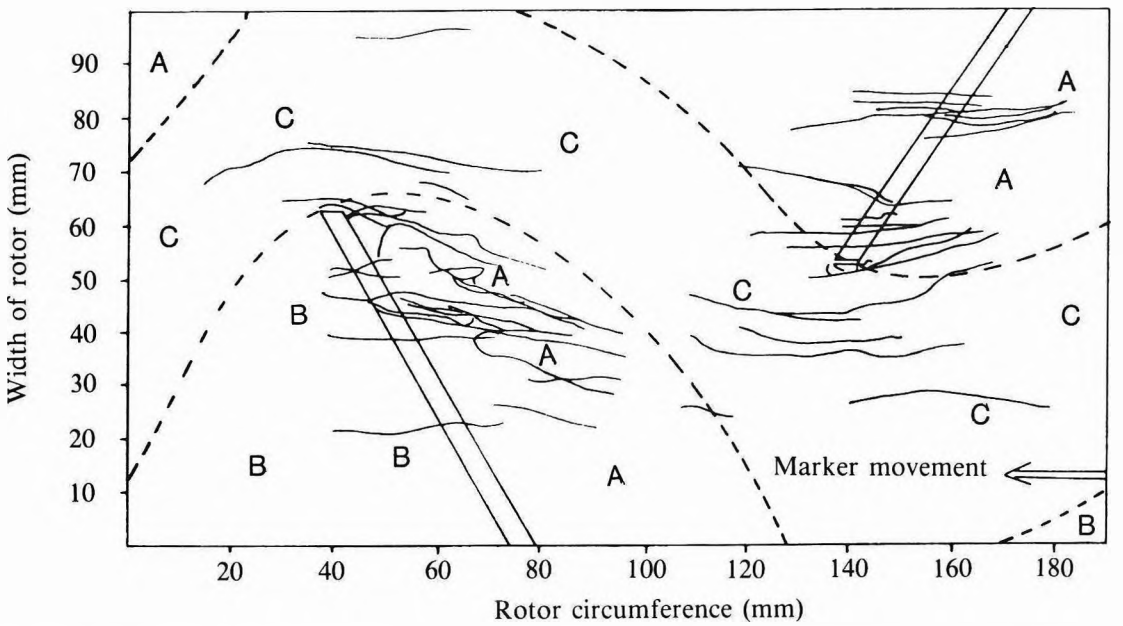

Figure 3. Flow pattern between rotor and chamber wall as observed from the movement of markers.

Figure 3 also shows that some of the markers move upstream in relation to the stationary rotor. This indicates that there are some markers moving faster than the rotor itself. The wide range of velocities at this region is also due to the narrow gap between the rotor and the chamber wall. As a result of this, a small change in the position in the radial direction can cause a tremendous change in the circumferential and lateral movement. The differential in velocities provides a high rate of deformation which is important for dispersive mixing. This phenomenon was also observed by Wan Idris[9] in a Brabender plastograph.

Adjacent to the sickle-shaped region is the tip region. This region is very small and it is less important as far as distributive mixing is concerned. The flow over the tip has been described as being equivalent to the leakage flow occurring over the flight tip in an extruder.

Void region (Region B). *Region B* covers the void positions which are situated directly behind the rotor tips. The formation of voids is one of the significant phenomenon during the mixing of rubber in an internal mixer. They are always formed as long as the fill-factor is less than unity. The size of the voids is inversely proportional to the fill-factor. *Figure 4* shows a schematic diagram of the region inside the mixing chamber where the voids are likely to form. The voids can be considered to stretch from just behind the flight tip down to the flow front.

Depending on the fill-factor and rotor speed the silicone rubber inside the void region may be fractured, thus the flow of material in this region may not be continuous. In the void region itself, there is not much mixing; however, the presence of voids is important for creating disorder in the flow pattern which contributes to effective distributive mixing.

S-shaped region (Region C). The reason for calling this region *S*-shaped is that the markers seem to move in the *S*-shaped pattern relative to the stationary rotor. *Figure 2* shows that this region occurs along the strip of dotted lines. It lies between the flow front and the sickle-shaped region. The *S*-shaped pattern is caused by the action of the two flights situated on the opposite ends of the rotor. Thus, this region provides an ideal transfer of material in the axial direction, *i.e.* from front to back and *vice versa* of the same rotor. From visual observation it was found that this region is normally filled

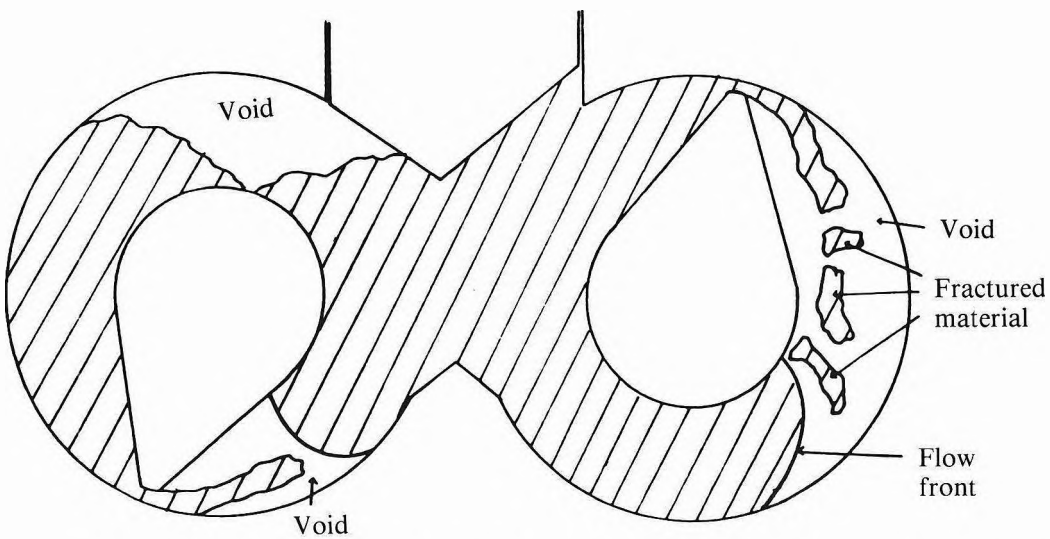

Figure 4. Schematic diagram showing distribution of voids inside mixing chamber.

with material (at 0.7 fill-factor and above), therefore the flow of material in this region is continuous.

Since the gap between the rotor and chamber wall in the region is large, the shear rate will be low, thus the magnitude of shear stress is substantially lower in comparison to shear stress in *Region A* and the tip region. Most researchers assume that this region provides little importance for dispersive mixing. However, with large gaps existing between the rotor and chamber wall, the extent of shear deformation of material is large and conducive for distributive mixing.

Flow Pattern between the Two Rotors

Bridge region (Region D). One of the primary functions of the flow of material in this region is to facilitate the exchange of material between the two lobes of the mixing chamber. The markers in this region can either move to the right or left lobe in one revolution, indicating the transfer of material into both lobes at the same time. The relative rotor position is one of the prime factors that control the transfer of material from the bridge position to either the left or right lobe. However, the markers which are situated adjacent to the front or back wall of the mixing chamber do not move significantly from their original positions, indicating that very little movement occurs around these positions.

Interaction between the two rotors. Figure 5 shows the interaction of the flow pattern occurring in between the two rotors with respect to the relative rotor position. This was shown by the air bubbles formed during the mixing operation. For ease of explanation these interactions are divided into three categories:

Condition 1: When both flights are moving towards the bridge position.

Condition 2: When one flight is moving towards the bridge position, while the other is moving away.

Condition 3: When both flights are moving away from the bridge position.

For *Condition 1,* high pressures will develop around the bridge region. Depending on which flight is nearer to the bridge region, the flow pattern profile will be skewed towards the opposite side. *Positions 3, 8* and *9* show that the flight of the left hand rotor is nearer to the bridge region. Thus the flow pattern profile is skewed to the right, while at *Position 19* the situation is opposite. It was also found that if the distance between the bridge region to either flight is about the same, the flow profile is symmetrical, as shown by *Positions 13* and *14.* It is expected that when the rotors are at these positions, the flow of material at that particular location will be limited.

For *Condition 2,* high pressures will develop on the side where the flight is moving to the bridge region. Thus, the flow pattern profile is skewed to the opposite side where low pressure region occurs. *Positions 1, 2, 4, 7, 18, 20, 21, 23, 24, 25, 26, 27, 28* and *29* all show the same pattern. In general, at *Condition 2,* the maximum transfer of material from one lobe to the other occurs. This is because a void may occur just after the bridge position immediately behind the tip of the rotor. This will create an empty space, ready to be filled with material carried in front of the flight of the opposite rotor.

For *Condition 3,* a low pressure region will develop around the bridge region. It was also found that the skewness of the flow pattern at this condition is less compared with the other two conditions. However, from *Positions 10, 11, 12, 16, 17, 22* and *30,* it was found that the flow pattern at *Condition 3* is rather complex. The complexity is caused by the disordered flow occurring behind the rotor tip (void region).

Another significant phenomenon that occurs at the bridge region is vortex flow due to the interaction of the material coming from each lobe. This interaction is important as far as distributive mixing is concerned because the material from two different lobes will combine here and, depending on the flow profile, it can either be transferred to the left or right lobe.

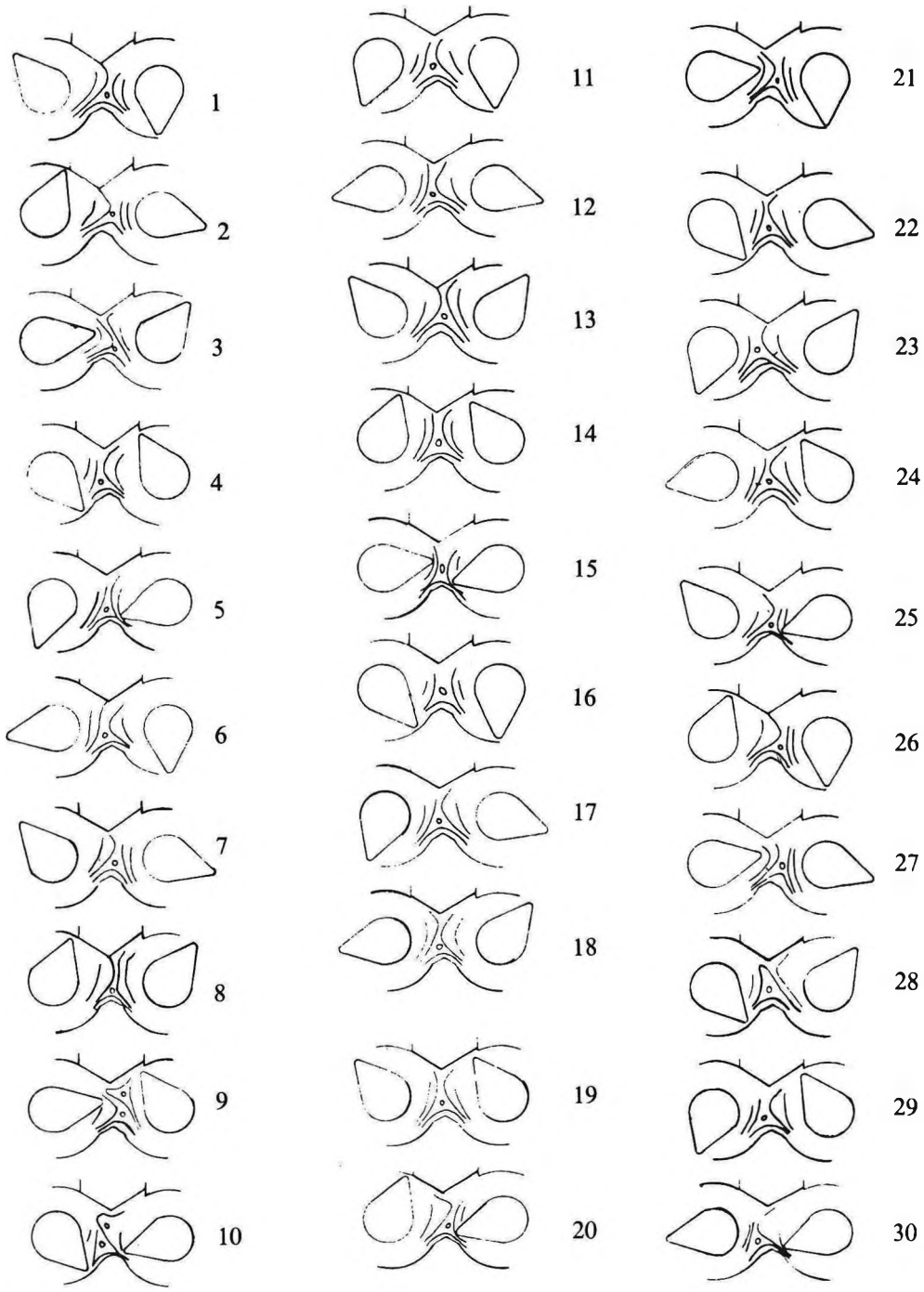

Figure 5. Flow pattern at the bridge region at different rotor positions.

Pressure Variation in Mixing Chamber

Figure 6 shows typical pressure traces for one revolution at different fill-factors (FF) and rotor speeds (revolution per minute, r.p.m.). The origins of the graphs correspond to the tip of the rotor. The pressure drops drastically to zero as the rotor tip passes the pressure transducer. This indicates that there is no material at the position of the pressure transducer, *i.e.* void is formed. Immediately after the void region the pressure starts to develop again. It increases progressively as the flight moves towards the pressure transducer and drops again after passing through the peak to make one complete revolution. The peak pressure occurs at about 10 mm in front of the tip measured from the centre of the flight tip. This signifies that drag flow and pressure flow at the tip region are in the same direction.

Figure 6 also shows that the shape of the trace seems to be asymmetric, tailing towards the left. Another phenomenon is the development of the secondary peak occurring between the void region and the primary peak. It was observed that the secondary peak occurs when the opposite flight is just about to pass beside the pressure transducer. This suggests that there is axial flow around this region. After the secondary peak the pressure trace passes through an inflection, indicating that the axial flow is reduced. The inflection occurs when the opposite flight passes over the pressure transducer. These two phenomena are directly related to the *S*-shaped pattern. After the inflection the pressure increases dramatically. This corresponds to the sickle-shaped region. The high pressure in this region indicates that the flow of material is continuous.

As expected, the pressure profiles increase with increase in fill-factor *(Figure 6A)*. However, there is little change in the pressure profile with respect to rotor speed, especially at low fill-factors (*i.e.* below 0.7) *(Figure 6B)*, except at the peak pressure where it seems to decrease as the rotor speed increases. There seems to be a marginal increase in pressure with respect to increase in rotor speed at high fill-factors (*i.e.* above 0.8) *(Figure 6C)*.

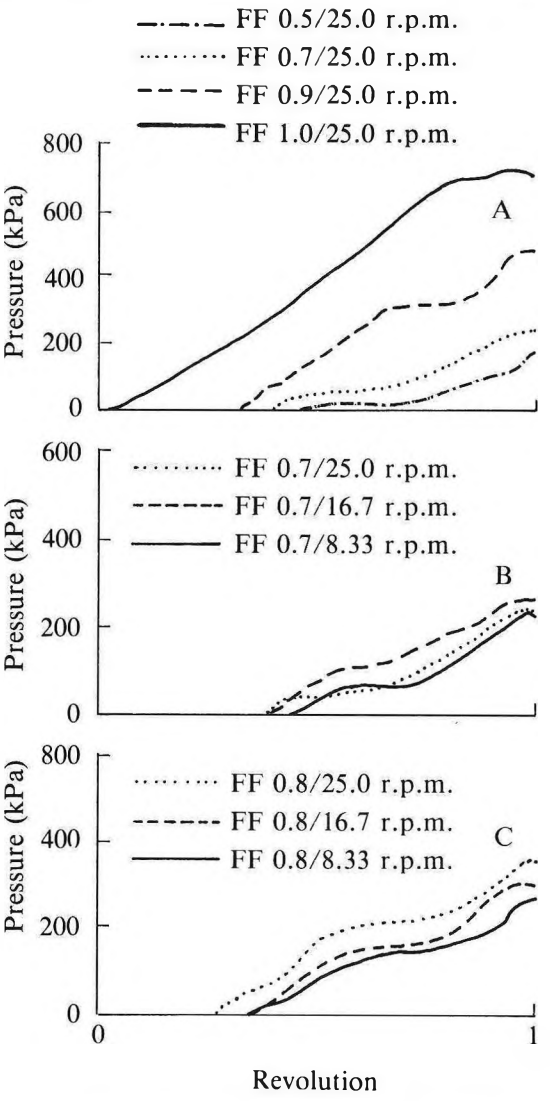

Figure 6. Pressure traces inside mixing chamber for one revolution.

At high fill-factors, pressure development is caused by both pressure wave and material transfer. It is expected that at high rotor speed the pressure wave will be greater, thus causing pressure inside the mixing chamber to be increased. Also at high fill-factors the rate of material transfer is less as compared to low fill-factors because the free space is relatively limited. Thus, the predominant factor in

pressure development at high fill-factors will be pressure waves.

Stress Distribution Inside the Mixing Chamber

In the analysis of stress distribution in the mixing chamber, the following four arbitrary points were chosen:

- *Point 1* corresponds to the region at the rotor tip.
- *Point 2* corresponds to the region around the end of the flight.
- *Point 3* corresponds to the *S*-shaped region.
- *Point 4* corresponds to the region in front of the flight tip or the sickle-shaped region.

By assuming that the ratio between the radius of the rotor and the radial distance between the rotor and chamber wall is sufficiently large, the assumption of the flow between parallel plates could be made. Using the lubrication approximation in one dimension, the velocity profile for pressure flow can be calculated with *Equation 1*[7].

$$V_p(y) = \frac{n}{n+1}\left(\frac{1}{\eta_o}\frac{dp}{dL}\right)^{1/n}\left(\frac{H}{2}\right)\left(\frac{n+1}{n}\right)\left[\left(\frac{2y}{H}\right)\left(\frac{n+1}{n}\right)-1\right] \quad ...1$$

where: V_p = pressure velocity

η_o = reference viscosity

n = power law index

y = the clearance gap size at the point of measurement (ranging from $\frac{H}{2}$ to 0)

$\frac{dp}{dL}$ = pressure gradient at each point

H = radial distance between rotor surface and chamber wall.

The velocity profile for drag flow can be calculated by using *Equation 2* and assuming that the rotor is stationary and the chamber wall is moving.

$$Vd = \omega (R - H) \quad ...2$$

where: Vd = drag velocity

ω = angular velocity

R = radius of the chamber.

From the pressure and drag flow profiles the resultant flow profiles can be calculated by means of vector addition of drag and pressure velocities. From the resultant velocity profiles the shear rate at particular points along the radial distance *(y)* can be calculated using *Equation 3*.

$$\gamma = \frac{dv}{dy} \quad ...3$$

The shear stress can be calculated using *Equation 4* assuming that material obeys power low relationship.

$$\tau = \eta_o \gamma^n \quad ...4$$

Using the TMS rheometer the values of η_o and n for the silicone rubber used were determined to be 25.7 kPa.s and 0.29, respectively[8].

Factors Affecting Stress Distribution in the Mixing Chamber

Figure 7 shows the stress distribution taken at four points inside the mixing chamber at different fill-factors and rotor speeds. As expected, high stress occurs at the tip region *(Point 1)*, followed by the sickle-shaped region *(Point 4)*, the *S*-shaped region *(Point 3)* and the region around the end of the flight *(Point 2)*.

In general, the magnitude of the stress is inversely proportional to the clearance between the rotor and the chamber wall; however, it appears that the stress is not constant across the gap. It was also found that on average the difference in the shear stress between the tip region and the sickle-shaped region is of the order of about 30%. However, the average stress at *Points 2* and *3* is much lower than that at the tip region, *i.e.* of the order of 60% lower. Therefore, it is reasonable to suggest that in the *S*-shaped region and in the region around the end of the flight only distributive mixing is taking place. The average shear stresses at the four points are shown in *Tables 1* and *2*.

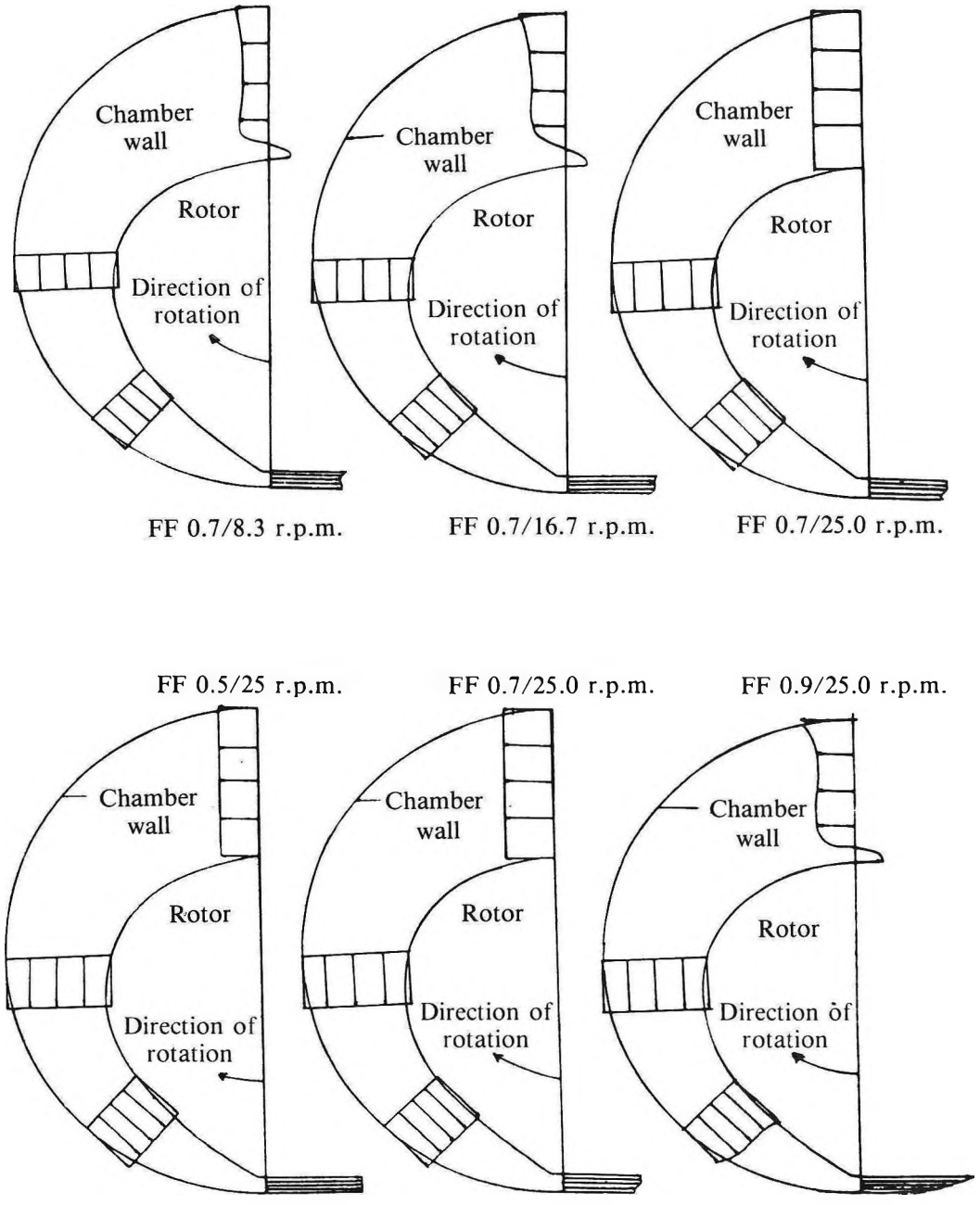

Figure 7. The stress distribution profile across the clearance inside the mixing chamber (1 mm = 3.2 kPa).

TABLE 1. AVERAGE SHEAR STRESS AT CONSTANT ROTOR SPEED[a]

Fill-factor	Shear stress (kPa)			
	Point 1	Point 2	Point 3	Point 4
0.5	74.6	29.5	39.5	66.6
0.7	64.0	35.4	39.4	44.6
0.9	60.8	24.0	39.6	44.6

[a]25 r.p.m.

TABLE 2. AVERAGE SHEAR STRESS AT CONSTANT FILL-FACTOR[a]

Rotor speed (r.p.m.)	Shear stress (kPa)			
	Point 1	Point 2	Point 3	Point 4
8.3	46.4	17.0	29.0	33.4
16.7	66.8	21.8	35.0	39.6
25.0	64.0	35.4	39.4	44.6

[a]0.7

Table 1 shows the influence of fill-factor on stress taken at 25 r.p.m. rotor speed and 0.5, 0.7 and 0.9 fill-factors respectively. In general, an increase in fill-factor will increase the stress occurring at the tip and sickle-shaped regions. However, fill-factor seems to have no effect on the stress distribution at the other two points. This indicates that increasing the fill-factor does not help to improve the dispersive mixing at the *S*-shaped region and the region around the end of the flight.

Table 2 shows the influence of the rotor speed on stress distribution taken at 0.7 fill-factor and 8.3, 16.7 and 25 r.p.m. rotor speed respectively. It was found that, in all cases, an increase in rotor speed will increase the shear stress. However, the relationship between the increase in rotor speed and shear stress is not linear.

CONCLUSION

The study of flow mechanisms of rubber inside a mixing chamber requires a systematic analysis of flow in various regions inside the mixing chamber. Flow visualisation has proved to be a good means for this purpose. It is important that in mathematical modelling of an internal mixer, the mode of action has to be considered separately in each region during the mixing operation. The flow pattern, which influences the rate of distributive mixing, is different in each of these regions.

The most complex flow patterns occur at the bridge and in the *S*-shaped regions. Due to the lower stress levels at these two regions, little dispersive mixing can take place here, therefore these regions are largely responsible for distributive mixing. The void region, where no mixing occurs, however, contributes to the enhancement of distributive mixing.

The high stress levels which occur at the tip and in the region just ahead of it are mainly responsible for dispersive mixing. The flow pattern in these two regions is not very complex, thus little distributive mixing can take place here.

It was also found that dispersive and distributive mixing are complementary to each other. However, these two modes of mixing have entirely different mechanisms. Distributive mixing depends on the extent of deformation and the flow pattern while dispersive mixing depends on the magnitude of the stresses. In most cases, the region which is good for distributive mixing will not be good for dispersive mixing and *vice-versa*. Thus, an important factor in mixer design is to obtain a balance between dispersive and distributive mixing to achieve the most efficient condition for the process as a whole.

REFERENCES

1. BORGEN, J. (1959) Mixing and Dispersing Process. *Processing of Thermoplastic Materials (Bernhardt, E. ed)*. New York: Reinhold.

2. LACEY, P. (1954) Developments in the Theory of Particle Mixing. *J. Appl. Chem. (Lond.)*, **4(5)**, 257.

3. SPENCER, R. AND WILEY, R. (1951) *J. Colloid Sci.*, **6(2)**, 133.

4. BOLEN, W. AND COLWELL, R. (1958) *SPE ANTEC Tech. Papers*, **14**, 1004.

5. GUBER, R. (1966) *Sov. Rubb. Tech.*, **25(9)**, 30.

6. GUBER, F. (1967) *Sov. Rubb. Tech.*, **26(1)**, 23.

7. MICKELVEY, J. (1962) *Polymer Processing*. New York: Wiley.

8. MOHAMAD BIN HAMZAH (1984) Master of Philosophy Thesis, Loughborough University of Technology.

9. WAN IDRIS, W.Y. (1978) Ph.D. Thesis, Loughborough University of Technology.

ORDER FORM
JOURNAL OF NATURAL RUBBER RESEARCH

Name: _____
(Please print)

Address: _____

_____

_____

_____

No. of copies: _____

Volume/Issue: _____

_____

_____

_____

Form of Remittance: Cheque/Bank Draft/Postal Order/Money Order
(Please include postage charges)

Amount: M$/US$ _____

Signature: _____ Date: _____

Journal Price

Overseas rate		Local rate	
Per issue	Per volume (4 issues)	Per issue	Per volume (4 issues)
US$15	US$50	M$30	M$100

Postage

By sea		By air	
Per issue	Per volume (4 issues)	Per issue	Per volume (4 issues)
US$1	US$4	US$5	US$20

JOURNAL OF NATURAL RUBBER RESEARCH

Submission of Articles

General. Manuscripts should be typewritten double-spaced throughout on one side only of A4 (21.0 × 29.5 cm) paper and conform to the style and format of the **Journal of Natural Rubber Research.** Contributions, to be submitted in four copies (the original and three copies) should be no longer than approximately ten printed pages (about twenty double-spaced typewritten pages). Intending contributors will be given, on request, a copy of the journal specifications for submission of papers.

Title. The title should be concise and descriptive and preferably not exceed fifteen words. Unless absolutely necessary, scientific names and formulae should be excluded in the title.

Address. The author's name, academic or professional affiliation, and full address should be included on the first page. All correspondence will be only with the first author, including any on editorial decisions.

Abstract. The abstract should precede the article and in approximately 150–200 words outline briefly the objectives and main conclusions of the paper.

Introduction. The introduction should describe briefly the area of study and may give an outline of previous studies with supporting references and indicate clearly the objectives of the paper.

Materials and Methods. The materials used, the procedures followed with special reference to experimental design and analysis of data should be included.

Results. Data of significant interest should be included.

Figures. These should be submitted together with each copy of the manuscript. Line drawings (including graphs) should be drawn in black ink on white drawing paper. Alternatively sharp photoprints may be provided. The lettering should be clear. Half-tone illustrations may be included. They should be submitted as clear black-and-white prints on glossy paper. The figures should be individually identified lightly in pencil on the back. All legends should be brief and typed on a separate sheet.

Tables. These should have short descriptive titles, be self-explanatory and typed on separate sheets. They should be as concise as possible and not larger than a **Journal** page.

Values in tables should include as few digits as possible. In most cases, more than two digits after the decimal point are unnecessary. Units of measurements should be metric or SI units. Unnecessary abbreviations should be avoided and as few horizontal lines as possible should be used. Information given in tables should not be repeated in graphs and *vice versa.*

Discussion. The contribution of the work to the overall knowledge of the subject could be shown. Further studies may also be projected.

Acknowledgements. These can be included if they are due.

References. References in the text should be numbered consecutively by superscript Arabic numerals. At the end of the paper, references cited in the text should be listed as completely as possible and numbered consecutively in the order in which they appear in the text. No reference should be listed if it is not cited in the text.

Abbreviations of titles of Journals should follow the **World List of Scientific Periodicals.**

Reprints. Twenty-five copies of Reprints will be given free to each author. Authors who require more reprints may obtain them at cost provided the Chairman or Secretary, Editorial Committee is informed at the time of submission of the manuscript.

Correspondence

All enquiries regarding the **Journal of Natural Rubber Research** including subscriptions to it should be addressed to the Secretary, Editorial Committee, Journal of Natural Rubber Research, Rubber Research Institute of Malaysia, P.O. Box 10150, 50908 Kuala Lumpur, Malaysia.


INSTITUT PENYELIDIKAN GETAH MALAYSIA
RUBBER RESEARCH INSTITUTE OF MALAYSIA